DEVELOPMENT OF A MODEL FOR TEMPERATURE IN A GRINDING MILL

Edgar Kapakyulu

MSc

2007

DEVELOPMENT OF A MODEL FOR TEMPERATURE IN A GRINDING MILL

Edgar Kapakyulu

A dissertation submitted to the Faculty of Engineering and the Built Environment, University of the Witwatersrand, Johannesburg, in fulfillment of the requirements for the degree of Master of Science in Engineering.

Johannesburg, January 2007

Declaration

I declare that this dissertation is my own, unaided work. It is being submitted for the Degree of Master of Science in the University of the Witwatersrand, Johannesburg. This thesis, to the best of my knowledge, has not been submitted before for any degree or examination in any other University.

_____

Edgar Kapakyulu

_____ day of _____ , _____

Abstract

Grinding mills are generally very inefficient, difficult to control and costly, in terms of both power and steel consumption. Improved understanding of temperature behaviour in milling circuits can be used in the model-based control of milling circuits. The loss of energy to the environment from the grinding mill is significant hence the need for adequate modeling.

The main objectives of this work are to quantify the various rates of energy loss from the grinding mill so that a reliable model for temperature behaviour in a mill could be developed. Firstly models of temperature behaviour in a grinding mill are developed followed by the development of a model for the overall heat transfer coefficient for the grinding mill as a function of the load volume, mill speed and the design of the liners and mill shell using the energy balances in order to model energy loss from the mill. The energy loss via convection through the mill shell is accounted for by quantifying the overall heat transfer coefficient of the shell.

Batch tests with balls only were conducted. The practical aspect of the work involved the measurement of the temperatures of the mill load, air above the load, the liners, mill shell and the environmental temperature. Other measurements were: mill power and sound energy from the mill. Energy balances are performed around the entire mill.

A model that can predict the overall heat transfer coefficient over a broad range of operating conditions was obtained. It was found that the overall heat transfer coefficient for the grinding mill is a function of the individual heat transfer coefficients inside the mill and outside the mill shell as well as the design of the liners and shell. It was also found that inside heat transfer coefficients are affected by the load volume and mill speed. The external heat transfer coefficient is affected by the speed of the mill. The values for the overall heat transfer coefficient obtained in this work ranged from 14.4 – 21W/m^{2}K.

List of Publications

The author has published the following papers based on the contents of this dissertation as follows:

Published conference abstract

Kapakyulu, E., and Moys, M.H., 2005. Modelling of energy loss to the environment from the grinding mill, Proceedings of the Mineral Processing 2005' Conference, *SAIMM*, Cape Town, South Africa, 4-5 Aug. pp 65-66 - SP03

Research Papers: Accepted for publication and currently in press in Minerals Engineering:

Kapakyulu, E., and Moys, M.H., 2006. Modelling of energy loss to the environment from a grinding mill, Part I: Motivation, Literature Survey and Pilot Plant Measurements, (*Currently in press in Minerals Engineering*)

Kapakyulu, E., and Moys, M.H., 2006. Modelling of energy loss to the environment from a grinding mill, Part II: Modeling the overall heat transfer coefficient, (*Currently in press in Minerals Engineering*)

To the loving memory of my late Grandmother, Mrs Belita Kalenge Yengayenga

Acknowledgements

I would like to extend my gratitude to the following people and institutions that made it possible for me to complete this dissertation.

- Professor Michael Moys, for his role as supervisor and mentor throughout the execution of this work
- Dr. Hongjung Dong for his assistance with the instrumentation
- Mr. Godfrey Monama for providing many useful suggestions which enhanced the quality of this work.
- Mr. Theo Prassinos, the workshop manager for the assistance received from the work shop
- Eskom, Anglogold Ashanti and NRF (National Research Foundation) for their financial assistance and support
- I would also like to thank my family for the moral and spiritual support during my studies.
- Finally, I would like to thank the Almighty God my creator, for strength and comfort and also for this opportunity and ability to pursue this research work.

Table of Contents

DECLARATION ii

ABSTRACT iii

LIST OF PUBLICATIONS iv

ACKNOWLEDGEMENTS vi

TABLE OF CONTENTS vii

LIST OF FIGURES xii

LIST OF TABLES xvii

NOMENCLATURE xix

CHAPTER 1: INTRODUCTION **1**

1.1 Importance of milling 2
1.2 Model-based mill control 3
1.3 Research objectives 6
1.4 Summary of the dissertation 7

CHAPTER 2: LITERATURE REVIEW **9**

2.1 Introduction 10
2.2 Energy Balances and review of work in the energy balances 10
2.3 Mill power 11
2.3.1 Theory of mill power 11
2.3.2 Effect of speed on mill power 14
2.3.3 Effect of mill filling on mill power 15

2.4 Energy and temperature in milling 16
2.5 Energy consumed in milling 19
2.6 The discrete element method 20
2.7 Energy losses in a milling system 22
2.8 Analysis of conduction and convection heat transfer 23
2.8.1 Conduction Heat Transfer 23
2.8.2 Convection Heat Transfer 24
2.8.3 The Practical Significance of the Overall Heat Transfer Coefficient 31
2.8.4 Estimation of parameters- Least squares filtering 32

2.9 Conclusions 33

CHAPTER 3: DEVELOPMENT OF A MATHEMATICAL MODEL 35

3.1 Introduction: Principles of mathematical modeling 36
3.1.1 The energy balance 37
3.1.2 Assumptions made in deriving the model 38
3.1.3 Model derivation 39
3.2 Energy balance models for the mill temperature 41
3.3 A model for the overall energy loss as a function of load volume and mill speed 44
3.3.1 Modeling of two parallel paths 44
3.4 Dynamic and steady state models 47
3.4.1 Steady state models 50
3.5 Conclusions 51

CHAPTER 4: EXPERIMENTAL APPARATUS, METHODOLOGY, MEASUREMENTS AND DATA ACQUISITION 52

4.1 Introduction – Experimental setup 53

4.1.1 Description of the milling setup 53

4.2 Measurements 54
4.3 Temperature probes 55
4.3.1 Choice of probe and material of construction 57
4.3.2 Expected temperature range 57
4.3.3 Insertion points 58
4.4 Temperature probe calibration 60
4.4.1 Calibration curves for the temperature probes 61
4.5 Torque measurement 63
4.5.1 Torque calibration 63
4.6 Measurement of Sound Energy 64
4.7 Experimental Procedure 65
4.8 Difficulties encountered 66
4.9 Summary and Conclusions 67

CHAPTER 5: ANALYSIS OF THE MILL TEMPERATURE DATA 68

5.1 Introduction 69
5.2 Results of the milling process 69
5.3 Analysis of temperature probe data 73
5.4 Variation of process temperatures with speed and load volume 74
5.5 Transient behaviour of grinding mill temperature with time 74
5.6 Effect of sudden water addition to mill on temperature and power 76
5.7 Effect of change of ambient conditions on mill temperature 77
5.8 Conclusions 78

CHAPTER 6: RESULTS OF POWER AND SOUND ENERGY DATA 80

6.1 Results of the Torque data 81
6.2 Results of the Sound energy data 83
6.3 Conclusions 84

CHAPTER 7: APPLICATION OF THE TEMPERATURE MODELS TO ESTIMATE AND QUANTIFY PARAMETERS 85

7.1 Introduction: Analysis of steady state results 86
7.2 Analysis of steady state temperature 88
7.3 Quantifying the Overall Heat Transfer Coefficient 88
7.3.1 Model Validation 88
7.3.2 Determination of the ball to air and ball to metal surface heat transfer coefficient 89
7.3.3 Validation of the Overall Heat Transfer Model 105
7.4 Conclusions 106

CHAPTER 8: CONCLUSIONS AND RECOMMENDATIONS 108

8.1 Introduction 109

8.2 Summary 109

8.3 Overall findings 109

8.4 Recommendations 110

REFERENCES 112

APPENDICES 116

APPENDIX A - Calibration of the Temperature probes: Calibration Equations and Constants 117

APPENDIX B - Torque calibration 122

APPENDIX C - Specific Heat Capacities, density and thermal conductivities of Steel balls, air mild steel and cast steel 124

APPENDIX D – General Procedure for analytical solution for dynamic model 125

APPENDIX E – Determination of the sound energy from the sound measurements 131

APPENDIX F – Summary of steady state temperature data 133

List of Figures

Chapter 1

Figure 1.1: The Sump energy balance output compared with the mass balance and manual samples 4

Chapter 2

Figure 2.1 Illustration of forces of friction and gravity for turning moment about the center of a ball mill (Austin et al., 1984) 13

Figure 2.2 The effect of critical speed on mill power 15

Figure 2.3 DEM contact force law diagram 21

Figure 2.4 Temperature profile in a grinding mill 26

Chapter 3

Figure 3.1 Batch grinding mill: energy balance measurements 38

Figure 3.2 Schematic diagram of the orientation of the load, air above the load, liner and mill shell 42

Chapter 4

Figure 4.1 The schematic representation of the experimental mill set up 54

Figure 4.2 Electric circuit diagram for the thermistor 56

Figure 4.3 Measurement of the temperatures of the load and the air above the load inside the mill grinding chamber 59

Figure 4.4 Measurement of the liner and shell temperatures 59

Figure 4.5 Laboratory temperature probe calibration 61

Figure 4.6 Calibration of the torque load beam 64

Chapter 5

Figure 5.1 (a) Variation of mill power, mill process temperatures and ambient temperature with time at a mill filling of 20% and speed of 65% 69

Figure 5.1 (b) Variation of mill power, mill process temperatures and ambient temperature with time at a mill filling of 20% and speed of 75% 69

Figure 5.1 (c) Variation of mill power, mill process temperatures and ambient temperature with time at a mill filling of 20% and speed of 95% 70

Figure 5.1 (d) Variation of mill power, mill process temperatures and ambient temperature with time at a mill filling of 20% and speed of 105% 70

Figure 5.2 (a) Variation of mill power, mill process temperatures and ambient temperature with time at a mill filling of 25% and speed of 75% 70

Figure 5.2 (b) Variation of mill power, mill process temperatures and ambient temperature with time at a mill filling of 25% and speed of 95% 70

Figure 5.3 (a) Variation of mill power, mill process temperatures and ambient temperature with time at a mill filling of 30% and speed of 30% 71

Figure 5.3 (b) Variation of mill power, mill process temperatures and ambient temperature with time at a mill filling of 30% and speed of 50% 71

Figure 5.3 (c) Variation of mill power, mill process temperatures and ambient temperature with time at a mill filling of 30% and speed of 80% 71

Figure 5.3 (d) Variation of mill power, mill process temperatures and ambient temperature with time at a mill filling of 30% and speed of 120% 71

Figure 5.4 (a) Variation of mill power, mill process temperatures and ambient temperature with time at a mill filling of 40% and speed of 75% 72

Figure 5.4 (b) Variation of mill power, mill process temperatures and ambient temperature with time at a mill filling of 40% and speed of 95% 72

Figure 5.4 (c) Variation of mill power, mill process temperature and ambient temperature with time at a mill filling of 40% and speed of 105% 72

Figure 5.5 Transient variations of mill process temperatures with time 75

Figure 5.6 Effect of water addition on mill power and process temperatures 77

Figure 5.7 Effect of ambient temperature on mill process temperatures 78

Chapter 6

Figure 6.1 Variation of mill power with mill speed at a mill filling of 20% 82

Figure 6.2 Variation of mill power with mill speed: load volume 30% 83

Chapter 7

Figure 7.1 Temperature profiles of the grinding mill at different mill speed at a constant mill filling of 20% 86

Figure 7.2: Temperature profiles of the grinding mill at different mill speed at a constant mill filling of 25% 87

Figure 7.3: Mill Power and Steady state mill process temperature distribution, J=30%, N=80% and t=3 hours 88

Figure7.4: Variation of ball temperature with time for ball with thermistor covered in pile of heated balls and for ball swung in air at various velocities 90

Figure 7.5: Ball to air heat transfer determination: Variation of $h_{Ball\text{-}Air}$ with velocity 92

Figures 7.6: Load behaviour from DEM simulations at varying mil speeds and load volumes 94

Figure 7.7: Profile of a cataracting ball in a grinding mill 96

Figure 7.8: Variation of model and experimental values of $hA_{(LD-L)}$ with mill speed 101

Figure 7.9: Variation of model and experimental values of $hA_{(LD-AIR)}$ with mill speed 102

Figure 7.10: Variation of model and experimental values of $hA_{(AIR-L)}$ with mill speed 102

Figure 7.11: Variation of model and experimental values of h_{ext} with mill speed 103

Figure 7.12: Variation of model with measured various rates of energy loss from the grinding mill 104

Figure 7.13: Variation of measured with model steady state temperature values 104

Figure 7.14: Variation of the model and experimental values of the overall heat transfer coefficient with mill speed at various mill fillings 106

List of Tables

Chapter 4

Table 4.1 Calibration of the temperature probes: Table of temperature and voltage for the probes for the liner, shell, load and air above the load 62

Table 4.2 Table of temperature and voltage for the ambient thermistor calibration and values from the manufacturers 62

Chapter 6

Table 6.1 Variation of sound intensity from the mill with the mill speed 84

Chapter 7

Table 7.1: Table of DEM velocities and the corresponding values of the heat transfer coefficients from the ball to the air at various mill conditions 96

Table 7.2: Number of balls in contact with the air and liner surface form DEM simulations at varying mill conditions 97

Table 7.3: Approximate total number of balls in a 2D and 3D Mill 97

Table 7.4: Experimental and model values of $hA_{(LD-AIR)}$, $hA_{(AIR-L)}$, $hA_{(LD-L)}$, h_{ext} and U_{ext} at various mill conditions 99

Appendix A

Table A1: Temperature versus Resistance values for the Bead Thermistor 118

Table A2: Resistance-Temperature characteristics for the thermistors from manufacturer's data 119

Table A3: Calculation of Power applied to the thermistor and the thermistor self heat 121

Appendix B

Table B1: Calibration of the Torque load beam 122

Appendix C

Table C1: Thermal properties of substances 124

Table F1: Summary of temperature results at steady state at various mill conditions 133

Nomenclature

General:

P = Mill power draw (W)

T = Torque (N.m)

Nc = Critical speed of the mill

N = Mill speed (Fractional of the mill speed)

J = Load volume (fraction of the mill volume)

f = Fractional mill speed $\left(f = \frac{N}{Nc} \right)$

t = Milling time (s)

D = inside lining mill diameter (m)

L = interior mill length (m)

Pr = Prandtl number (Dimensionless)

Q = Rate of energy loss (J/s or W)

$h_{LD\text{-}L}$ = heat-transfer coefficient between the load and the liners ($W/m^2.K$)

$h_{LD\text{-}A}$ = heat-transfer coefficient between the load and the air above the load ($W/m^2.K$)

$h_{A\text{-}L}$ = heat-transfer coefficient between the air above the load and the liners ($W/m^2.K$)

h_{ext} = heat-transfer coefficient between the shell and the environment ($W/m^2.K$)

U = Overall heat transfer coefficients ($W/m^2\ ^oK$)

C_{Pair} = specific heat capacity of the air above the load at constant pressure (J/kg.K)

C_{pLD} = specific heat capacity of the load (steel balls) at constant pressure (J/kg.K)

C_{pL} = specific heat capacity of the liners (cast steel) at constant pressure (J/kg.K)

C_{pS} = specific-heat capacity of the shell (mild steel) at constant pressure (J/kg.K)

Kg = thermal conductivity of the air (W/m.K)

k_S = thermal conductivity of the shell (W/m.K)

k_L = thermal conductivity of the lifter (W/m.K)

μ = viscosity of the fluid (Kg/m.s or Pa.s)

T_{LD} = Temperature of the load (grinding media) (^oC)

T_{AIR} = Temperature of the air above the load (^oC)

T_L = Temperature of the lifter/liner (^oC)

T_{L1} = Lifter temperature at surface 1 (^oC)

T_{L2} = Lifter temperature at surface 2 (^oC)

T_S = Temperature of the shell (^oC)

T_{S1} = Shell temperature at surface 1 (^{o}C)

T_{S2} = Shell temperature at surface 2 (^{o}C)

T_A = Ambient temperature (^{o}C)

m_{LD} = Mass of the load (Kg)

m_S = Mass of the shell (Kg)

m_L = Mass of the liners (Kg)

A = Surface area (m^2)

U = Overall heat transfer coefficients (W/m^{o}K)

v = Velocity (m/s)

Chapter 1

Introduction

1.1 Importance of milling

Milling is an important and indispensable part of mineral processing. Rotary grinding mills are used in mineral processing for particle size reduction. A ball mill is a system composed of a number of interacting and interdependent elements working together to accomplish the grinding or breakage of ore (Radziszewski, 1999). The elements necessary in a ball mill are the cylindrical mill, the mill liners, the ball charge, the ore to be ground as well as the control system needed to govern the ore feed and water rates and the mill speed. These consist of a rotating cylindrical shell of length usually greater than the diameter. These elements interact in such a way as to continually lift the ball charge which then falls and breaks the ore nipped between the balls. Lifter bars and sacrificial plates are bolted to the inside of the mill shell. Rock generally arrives from the crusher or perhaps a semi-autogenous (SAG) mill depending on the design of the milling circuit and the mineral being processed and enters the feed end of the mill. Grinding media consisting of steel balls are present in the mill along with any rock that has not yet overflowed through the discharge end. Comminution or size reduction is effected by ore-to-ore, ore-to-media and ore-to-mill wall interaction.

The importance of milling in mineral processing is to liberate or release the valuable minerals from the host rock or ore, to a size suitable for subsequent metallurgical processes. In mineral processing it is normally done wet and the resulting slurry is immediately passed on to the subsequent material separation stage. This is very often froth flotation, and grinding and flotation are then carried out in one combined section of the concentrator. Dry grinding is also widely applied in mineral processing and power generation.

The milling process however is very inefficient, difficult to control and costly, in terms of both steel and power consumption. A typical comminution plant accounts for a significant proportion of the total operational costs. It is an indispensable operation of mineral processing and size reduction circuits expend significant amounts of energy (Stamboliadis, 2002). Fuerstenau (1999) reported that

comminution consumes up to 70% of all energy required in a typical mineral processing plant.

It is also generally recognized that the actual energy required to reduce the particle size of a brittle material is a small percentage, about 4% or less, (Tavares and King, 1998) of the total energy consumed by grinding equipment. Stairmand (1975) indicated that about 99% of the energy supplied to an industrial grinding system appears as heat and there is very little evidence that any appreciable proportion is locked up as surface energy or strain energy. The loss of energy to the environment is significant and needs to be adequately modeled. These factors amplify the need to assess, control and improve the efficiency of milling circuits. The behaviour of temperature in milling circuits can be obtained from an energy balance methodology. Model-based control of milling circuits using temperature measurements could then provide substantial benefits. An example of a model-based control process is given in section 1.2.

1.2 The Model-Based Mill Control

The energy balance models thus provide a tool for the computation of the heat transfer coefficients, the overall heat transfer coefficient and therefore estimates of the thermal energy loss from the grinding mill to the environment. The use of temperature measurements in the milling process may lead to improved understanding of temperature behaviour and can be used to control milling circuits.

One method used to control grinding circuits involves continuous online matching of a dynamic model for the process to the measurements that are made on the process (Herbst et al, 1989). This is usually done using a Kalmin Filter. This allows the estimation of variables which cannot be measured, eg rate of grinding of solids in the mill, percent solids in the mill discharge, etc. This should enable more precise control of the milling circuit.

Briefly, a dynamic model of the process is formulated; based on certain assumptions, eg perfect mixing in each compartment of a 2-compartment model of the mill, perfect mixing in the discharge sump, first-order rate of grinding, three size classes, etc. Generally it is a substantially simpler model than is used for steady-state simulation of the process. Very accurate temperature measurements (±0.01°C) are made on key streams entering and leaving the mill in addition to all the other conventional measurements that are normally made. Since temperature measurements can be made far more accurately than other process measurements such as flowrate and density, much more precise knowledge of process behaviour becomes available. By applying laws of energy conservation it becomes possible to estimate several variables relating to mill load behaviour which have not been available before.

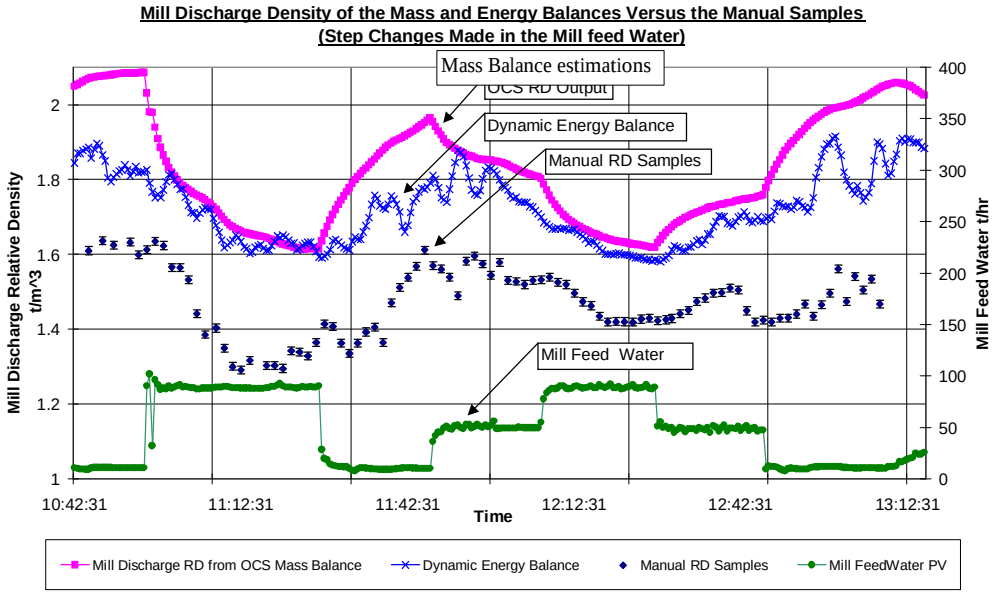

Figure 1.1: The Sump Energy Balance Output compared with the Mass Balance and Manual Samples

Van Drunick and Moys (2002) applied this technique to the estimation of mill discharge percent solids. They used mass and energy balances around the mill discharge sump in order to estimate the flowrate and percent solids in the discharge from the mill. Their results are illustrated in Figure 1.1, which shows the variation of relative density (RD) as the rate of feed water addition to the mill is changed. The output of their estimator is labelled “Dynamic Energy Balance”

and the experimentally measured values are labelled “Manual RD samples”. These are compared to that produced by the similar algorithm based on mass balances only (labelled “Mass Balance estimations”) and produced a substantially better fit, partly because of the accuracy of the temperature measurements and partly because the mass balance estimator is based on the assumption that the mill is perfectly mixed, which is by no means correct.

It is estimated conservatively that more accurate control of the load behaviour will lead to substantial improvements in milling efficiency (eg a 3 - 5 % reduction in kWh/ton) and/or a greater stability in the circuit product size distribution leading to an average increase of 3-5 percent –75 micron material (for a gold ore example). If desired, it should be possible to increase circuit capacity by a similar order of magnitude. Any of these improvements will lead to project pay-backs of the order of months.

The model-based approach is becoming advantageous for several reasons. Firstly, modern processing plants are highly integrated with respect to the flow of both material and energy (Serbog et al., 1989). This integration makes plant operation more difficult. Secondly, there are economic incentives for operating plants closer to limiting constraints to maximize profitability while satisfying safety and environmental restrictions. There are a number of major steps involved in designing and installing a control system using the model-based approach. The first step involves formulation of the control objectives. In formulating the control objectives, process constraints must also be considered.

After the control objectives have been formulated, a dynamic model of the process is developed. The process can have a theoretical basis, for example, physical and chemical principles such as conservation laws and rates of heat transfer, or the model can be developed empirically from experimental data. The model development usually involves computer simulation.

The next step in the control system design is to devise an appropriate control strategy that will meet the control objectives while satisfying process constraints. Computer simulation of the controlled process is used to screen alternative control

strategies and to determine preliminary estimates of suitable controller settings. Finally, the control system hardware is selected, ordered, and installed in the plant. Then the controllers are tuned in the plant using the preliminary estimates from the design step as a starting point. Controller tuning usually involves trial and error procedures. Controller self-tuning techniques are also available.

The use of models for on-line decision making represents the next logical step in mineral processing control system design. The key elements required for model-based control are good on-line models and accurate estimation procedures based on precise measurements. Models can be used in various ways in a control strategy as showed by Herbst et al, 1992. When the objective is to minimize the variance of the outputs of a process, then the dynamic models of the process can be used to find the optimal inputs. When the objective is to find the operating conditions that maximize profit or minimize cost, then from steady state models the desired level of process outputs is found. In both cases it is up to the control system to ensure that the set points provided by the model are achieved; the models act as a supervisor for the control system. The model can be used to estimate variables too costly or difficult to measure. In other words, a model contains missing information about the process. By building in such a model, "well informed" responses to disturbances can be made and, ultimately, truly 'optimal' control performance can be achieved.

1.3 Research objectives

The main issue in this research is the development of mathematical models of temperature behaviour in the grinding mill. The model is derived from the energy balance methodology and is based on a horizontal batch grinding mill. Due to difficulties in direct estimation of heat transfer coefficients in milling, considerable effort is made on modeling temperature in grinding mills.

The objective of this research is to quantify the various rates of energy loss from the mill under a wide range of conditions, so that a reliable model for temperature

behaviour in a mill could be developed. The project is also aimed at developing a model for energy loss from the mill to the environment as a function of important mill operating parameters such as mill speed, load volume and mill shell/liner design from the energy balances.

By using the models, important operating variables such as load volume, flow rate (as in continuous mills), % solids, etc, can be controlled and optimized and this would lead to improved control of a milling process.

1.4 Summary of the Dissertation

This dissertation is organized into 8 chapters which includes the introduction. The first chapter presents an introduction to the project and most importantly the background and the objectives of this research. Chapter 2 provides a review of published literature on energy balances, mill power and temperature in milling, as well as related work in this field of study.

Chapter 3 forms the core of this project, the development of mathematical models for temperature behaviour in a grinding mill. The chapter involves the development of a model for the overall heat transfer coefficient in terms of the individual heat transfer coefficients and the mill liner and shell design using the energy balances so as to model energy loss from the mill.

Chapter 4 introduces the reader to the experimental equipment, instrumentation, data acquisition and methodology employed in this project. The analysis of data collected in this chapter is described in chapter 5 with particular emphasis on temperature data.

In chapter 6, the analysis of data on torque and sound energy from the mill is done. Due to limited data on sound from the mill, not much analysis was done. Moreover, the energy converted into sound was found to be negligible compared to other forms of energy. In this chapter though, the analysis of torque data is

much more important as it was considered to be the only source of energy input to the mill.

The analysis of steady state results are reported in chapter 7. This analysis involves evaluating such important parameters as the overall heat transfer coefficient of the mill shell as well as application or validation of the model for the overall heat transfer coefficient. Most of the analysis of the work done is presented in this chapter.

Chapter 8 completes the thesis by summarizing the main conclusions, the overall findings and makes recommendations for further research.

Chapter 2

Literature Review

2.1 Introduction

This chapter is concerned with review of energy balances and their applicability to the milling system. Milling is a very inefficient process and a lot of effort has been made on improving the current state of operation of milling systems. The energy balance methodology could prove to be a competent tool in the optimization of mill control and operation as compared to other balances such as the mass balance. A lot of work has been done on mass balances in milling circuits with important measurements being the flow rate and density.

What follows is a review of literature on published work on the energy balances as well as related and earlier work done on the energy balances. With particular emphasis is the application of the energy balances to the milling system.

2.2 Energy Balances and a review of work done with energy balances

Energy can be defined as the capacity to do work. Energy assumes many forms. It can assume the form of mechanical energy, chemical energy, electrical energy, heat energy, atomic energy, sound energy and many others. Energy can be converted form one form into another, but its total amount within a system remains the same, as *energy can neither be created nor destroyed*.

The subjects of thermodynamics and energy transfer are highly complementary. The subject of heat transfer treats the rate at which heat is transferred and therefore can be viewed as an extension of thermodynamics (Incropera and Dewitt, 2002). Conversely, for many heat transfer problems, the first law of thermodynamics (the law of conservation of energy) provides a useful, often essential, tool.

According to the time basis, first law formulations that are well suited for heat transfer analysis may be stated over a time interval (Δt) as follows:

The amount of thermal energy and mechanical energy that enters a control volume, plus the amount of thermal energy that is generated within the control volume, minus the amount of thermal energy and mechanical energy that leaves the control volume must equal the increase in the amount of energy stored in the control volume (Incropera and Dewitt, op. cit).

In recent work done in the milling system, the energy balance has been found to have advantages over the mass balance (Van Drunick and Moys, 2002). The energy balance relies on temperature data which can be obtained to a higher degree of accuracy than the flow data required by the mass balance. In addition to that, the temperature probes are quite cheap and affordable and this adds to the advantages.

Since the initial results were published from the earlier work by Van Drunick and Moys (2002), it has now been decided to further develop the modeling techniques in order to focus on balancing the energy around the entire mill**.** Van Drunick and Moys (2003) developed the modeling techniques in order to focus on balancing the energy around the entire mill circuit. The energy balance around a mill is given by:

Energy into the mill=Rate of energy loss from mill+Rate of energy accumulation in mill

The equation above can be expanded as follows:

$$E\ in = E\ out(shell) + E\ out(discharge) + E\ accumulated \qquad (2.1)$$

2.3 Mill Power

2.3.1 The Theory of Mill Power for Tumbling Mills

Austin et al. (1984) from data given by numerous investigators (White, 1904; Davis, 1919; Rose and Sullivan, 1958; Hogg and Fuerstenau, 1972) pointed out

that there are two main approaches in the derivation of equations describing the power required to drive tumbling mills. One approach calculates the paths of balls tumbling in the mill and integrates the energy required to raise the balls over all possible paths. The other approach (Hogg and Fuerstenau, 1972) treats the ball-powder aggregate as shown in Figure 2.1, assuming that the turning moment of the frictional force must balance the turning moment of the centre of gravity of the bed around the mill center. The frictional force presumably arises from between the case and the bed plus friction of ball-on-ball as balls move up through the bed. In both cases, the energy used to turn a well-balanced empty mill is small since it consists only of bearing friction.

In their approach Hogg and Fuerstenau (op. cit.) considered only the rate at which potential energy was gained by particles as they rose up the mill in a locked manner. Once they reach the upper-most point of their upward motion they were assumed to roll down the inclined charge surface and re-enter the charge lower down. By integrating the rate of potential energy gain over all paths they obtained the following equation:

$$Power = K \sin a \sin^3 q f r L D^{2.5} \qquad (2.2)$$

where: K = constant, Φ = fraction of critical speed, L = interior mill length, D = interior mill diameter , α = charge angle of repose, θ = angle related to mill filling and ρ = mean bulk density of the charge

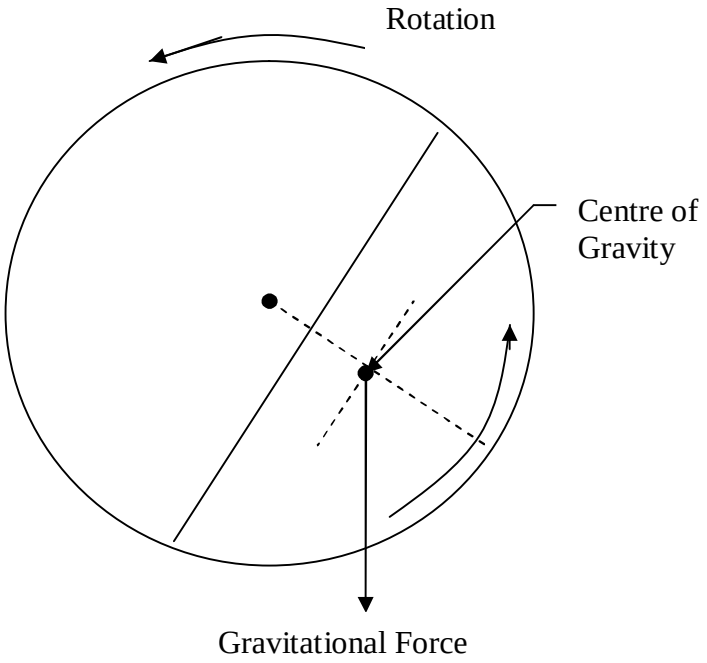

Figure 2.1: Illustration of forces of friction and gravity for turning moment about the center of a ball mill (Austin et al., 1984)

Austin et al. (1984) also pointed out that the relation for net power for a grinding mill as given by Rose and Sullivan (1958) for dry grinding is:

$$m_p = (2.8)(10^{-4})(LD^{2.5} r_b)(\Phi_c)(1 + 0.4sU / r_b)FJ \text{ , kW} \qquad (2.3)$$

where the empirically determined constant $(2.8)(10^{-4})$ is for units of ball density ρ_b in lb/tf^3 and L and D in feet. For L and D in meters and ρ_b in kg/m^3, the constant is $(1.12)(10^{-3})$. In this equation, it is assumed that the power to the mill is proportional to ϕ_c, from $\phi_c = 0$ to 0.8, so that the equation should not be extrapolated beyond $\phi_c = 0.8$.

Liddell and Moys (1988) reported that an equation for mill power which is in common use was developed by Bond, who based it on the torque principle and modified it by the use of empirical results:

$$P = 12.262\, r_b f LD^{2.3} J(1 - 0.937J)(1 - 0.1/2^{9-10f}) \qquad (2.4)$$

where J is the fractional filling of the load.

2.3.2 Effect of speed on mill power

Power consumption in a milling process generally increases with increasing mill speed within operating limits (Taggart, 1927). The higher the speed the more power transmitted and therefore the more energy transfer to the load. He also showed that power consumption increases with increase in ball load until the load reaches a point at or slightly above the axis, after which further loading by ore or balls results in the decrease of power.

The power drawn by the mill is a function of mill speed. At very low mill speeds, the charge (slurry & balls) moves over one another in concentric layers resulting in poor grinding. As the speed increases, the power draw increases, but it then decreases at supercritical speeds due to centrifuging. Critical speed is the speed at which the mill charge will centrifuge. *Nc* indicates fraction of critical speed. It is expressed as:

$$Nc = 42.3/\sqrt{D} \qquad \text{rpm} \qquad (2.5)$$

where: D = mill diameter (m)

For optimum charge movement, mills should operate at a narrow range of about 75-95% of critical speed. This is represented by the relationship between power drawn and %critical speed shown in Figure 2.2.

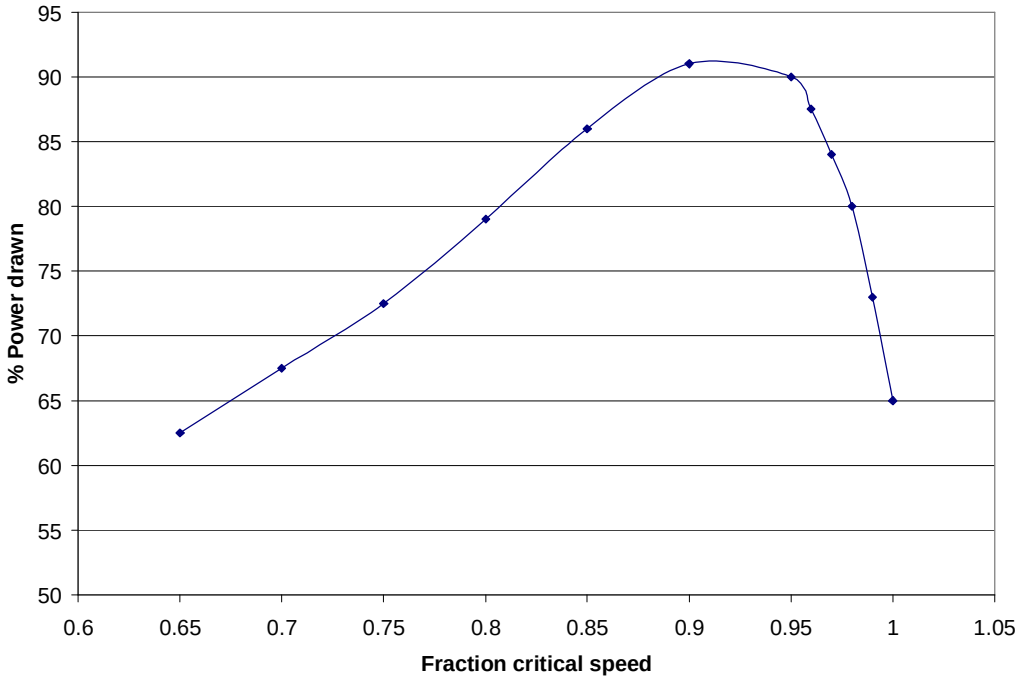

Figure 2.2: The effect of critical speed on power drawn

2.3.3 Effect of mill filling on mill power

Power drawn by the mill is a function of load volume. As the volume (and hence mass) of the load increases, the power draw increases, but it then decreases again after a certain point. This occurs when load volume exceeds 45-50%. Power draw also decreases when some of the load components begin to centrifuge, thereby reducing the active mass of the load and reducing the effective diameter of the mill. The charge volume has a significant effect on the power drawn by the mill. Thus, it is feasible to operate the mill as full as possible between 30 - 45%, since at this filling the power drawn is maximized.

2.4 Energy and Temperature in milling

Grinding is directly related to energy absorbed in the mill chamber. Simply, the more energy you can input into a batch, the more grinding action is achieved. During milling for liberation of minerals the power drawn by the mill at any time is a direct index of the lifting action on the balls at the instant of time, and the rate of breakage is expected to be directly proportional to the lifting action (with all other variables constant).

The power to the mill is used to produce the mechanical action, so the total efficiency involves (Austin et al, 1984):

1 Efficient conversion of input energy to mechanical action
2 Efficient transfer of the mechanical action to the particles
3 Matching the stress produced by the mechanical action to the failure stress of the particles

For example, if a tumbling mill is operated with too small a loading of particles, the impact will be of steel balls and part 2 will clearly be very inefficient. Again, if the ball density, ball size, and mill diameter are all low and if the particles are large and strong, the mill might not break the particles at all (except by slow abrasion) and part 3 will be inefficient (Austin et al, op cit.).

The energy input to mills is obviously linked to the specific energy of grinding, which is defined from a given feed size distribution to a desired product size distribution (Austin et al., op. cit.).

Much of the power consumed in ball milling is transformed into heat and becomes apparent in rise of temperature of the load (i.e. raising the mill discharge temperature) as it passes through the mill (Taggart, op. cit). The mill speed, milling time and mill filling affect this temperature increase.

Mill process temperatures are affected by mill conditions critical to mill operation, namely, mill speed and load volume. At higher mill speeds, more lift is imparted

to the load and therefore more cataracting, which means more energy generation due to friction and impacts. This will lead to higher mill temperatures than at lower speeds.

At supercritical speed, the outermost layers of the balls are centrifuged, which results in a decrease in mill diameter and reduction in the active mass of the load; this produces a rapid loss of power as mill speed increases (Moys and Skorupa, 1992). At the speed at which the load centrifuges completely, no power is drawn by the mill. This loss of thermal energy increases due to the increase in the overall heat transfer coefficient (which increases with mill speed) on the outside of the mill. Only when there is substantial slip between the load and liner will there be power increase and therefore temperature rise.

It has been noted that liner design determine speed of the mill at which cataracting and centrifuging occur. If higher lifter bars are employed, centrifuging will occur at relatively lower mill speeds. Generally, load behaviour of rotary grinding mills determines the level of temperatures attained and is obviously fundamental to mill efficiency.

Mill temperature is also a function of milling time. Longer milling times will result in more energy being transferred to the load and this will lead to higher mill temperatures. This situation applies only for a batch mill. At steady state, when there is no further increase in mill temperature with time, power supplied to the mill will be equal to the rate of energy loss from the mill.

Viscosity, particularly in wet mills, is affected by temperature. The viscosity or percentage of solids in the mill affects most of the parameters within the mill, and also has a large effect on the dynamic behaviour of the load. Variations in temperature affect the slurry viscosity by affecting the viscosity of the water in the slurry (Kawatra and Eisele, 1998). An increase in temperature decreases the viscosity of the carrier fluid and thus the viscosity of the slurry.

Small changes in temperature of the slurry in the mill, however, would not produce dramatic changes in the slurry rheology. Large variations in pulp

temperatures are needed to observe significant changes in slurry rheology. In view of this, it can be said that temperature has little effect on the milling process in particular on the rheology of the slurry. Changes in particle size and percent change in solids produce far more significant changes in the slurry rheology and such changes in these variables are more realistic than large changes in pulp temperature.

The viscosity of the slurry affects load behaviour and density. It also has a strong influence on the grinding performance of the mill media. An excessively high viscosity implies thick slurry inside the mill. The slurry effectively separates the grinding media such that the grinding performance decreases. On the other hand, when the viscosity is too low, the grinding media are allowed to come into direct contact and this results in excessive wear of grinding media. Therefore any shift from the operating mill temperature will affect the viscosity and therefore mill load behaviour. However it is worth stating that the effect of temperature on slurry viscosity may not be significant compared to the effect of percent solids.

Van Nierop and Moys (2001) showed that the temperature in a 1.3MW gold mill increases from the feed end to the discharge end. They showed that the temperature difference along the length of the mill was approximately 5.5°C. This indicated that the mill is not perfectly mixed. When there is no flow through the mill the temperature of the middle of the mill stayed warmer than both the feed and discharge probe temperatures. This is because of a lower rate of energy transfer from the middle of the mill (as expected) than at the two ends of the mill. Energy is lost through the ends of the mill as well as through the shell. Van Nierop and Moys (1997) investigated the changes of temperatures in the mill in relation to other variables, principally mass and power. It was indicated that when the solids feed is switched off and the mass decreases, then the temperature increases, tending towards a steady state. The absence of new cold feed no longer keeps the temperature in the mill down. Where the feed is switched on, the mill load mass increases, and the temperature initially decreases, due to the cold feed, and then increases to a new steady state. When the mill is stopped, the temperature slowly decreases. This investigation showed that load temperature measurement,

together with other temperatures and flows, makes the calculation of the axial mixing coefficient possible. The amount of material present in a mill at a particular time and the magnitude of in and out-flows thus influences temperature in the mill. The higher the mill filling, the higher the temperature of the milling system. Mill filling is an important parameter in the control of temperature rise in the grinding mill.

2.5 Energy consumed in milling

Grinding is a very inefficient process and it is important to use energy as efficiently as possible. Unfortunately, it is not easy to calculate the minimum energy required for a given size reduction process, but some theories have been advanced which are useful.

Austin *et al* (1984) from data given by Rose (1967), showed by careful measurement of the energy balance in a mill, that the surface energy is only a very small fraction of the energy input to the mill. Within the limits of experimental error, he found that all energy to the mill appears as heat, sound, or the energy of phase transformation.

Austin *et al* (1984) from data reported by Austin and Klimpel (1964) discussed the fracture process from the point of view of the utilization of energy in creating new surface. In any fracture process the solid must be raised to a state of strain to initiate the propagation of fracture cracks. Creation of this state of strain requires energy, greater than or equal to the stored strain energy. Whether fracture initiates at low strain energy or at high strain energy depends on a number of factors in addition to the value of the specific surface energy of the material. This includes:

(i) The presence of pre-existing cracks or flaws; (ii) Whether plastic flow can occur in the solid or whether it is completely brittle; and (iii) The geometry and rate of stress application.

This picture applied to compressive or impact fracture in a milling machine immediately explains why the input energy appears primarily as heat. In a tumbling ball mill, for example, the mill energy is used to raise balls against the force of gravity, and when the balls fall the energy is converted to kinetic energy. The balls strike particles, nipping them between balls, and the kinetic energy is converted to strain energy in the particles. If the impact force is sufficient, a particle is rapidly stressed to the fracture point and it breaks via propagating branching fractures, giving rise to a suite of fragments. Each fragment converts the remainder of its stored strain energy to heat after fracture (Austin *et al*, *op cit*).

The fraction of mill energy not converted to heat is very small. As additional confirmation, it is known that the heat rise of a material flowing in a continuous mill can be calculated quite accurately by direct conversion of the energy input rate to the mill to the sensible heat content of the material. It follows that the utilization of energy in a mill is extremely inefficient.

Fuerstenau and Abouzeid (2002) reported, with regard to energy of comminution, that the well-known laws of comminution given by Kick and Bond have been the basis for assessing comminution energy, and indirectly, comminution efficiency for ball mills only. Rittinger considered that the required energy for comminution is proportional to the new surface produced. Kick considered that energy for comminution is determined by the energy required to stress the particle to failure.

Fuestenau and Abouzeid, (*op cit*), defined the comminution efficiency as the ratio of the energy of the new surface created during size reduction to the mechanical energy supplied to the machine performing the size reduction. In terms of this concept, the energy efficiency of the tumbling mill is as low as 1%, or less.

2.6 The Discrete Element Method

The Discrete Element Method (DEM) is a numerical method that is used to track the motion of individual balls in grinding mills. The DEM simulations can be used

to model the behaviour of both fluids and contacting particles. The simulations have wide applications in both mining and mineral processing (Zhang and Whiten, 1996). The discrete element method simulates the mechanical response of the systems by using discrete elements. In this method, the forces between assumed discrete components are calculated and used to determine the motion of discrete components thus giving a dynamic simulation. During the simulation process, the simulation time is discretized into small time steps. The motion of each particle boundary is calculated. The positions of these particles and boundaries are updated at each time step.

There are a number of possible contact force models available in the literature that approximate collision dynamic. Cleary (2001) used the linear spring-dashpot model shown in Figure 2.3 below.

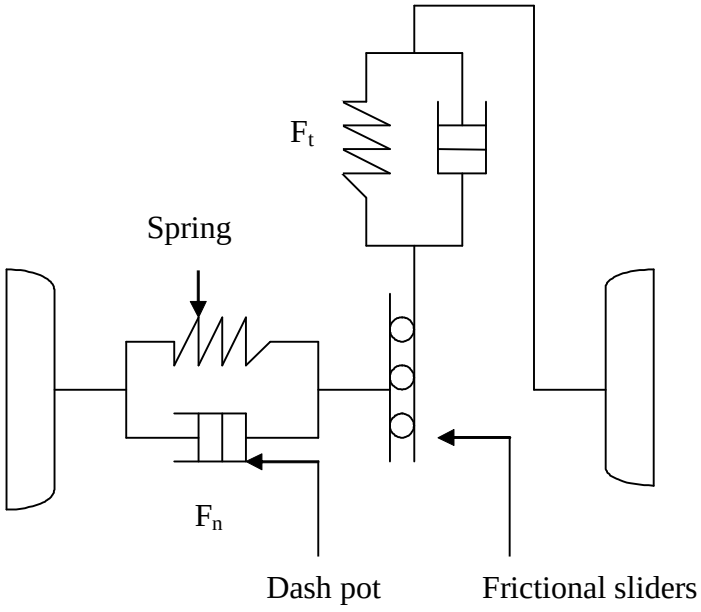

Figure 2.3: Contact force law consisting of springs, dashpots and frictional sliders used for evaluating forces between interacting particles and boundaries

"Soft Particle" contact model

Δx is the particle overlap, k_n and k_t are the normal and tangential spring constants, v_n and v_t are the normal and tangential velocities, C_n and C_t are the normal and tangential damping coefficients, and m is the friction.

Normal Force: $F_n = -k_n \Delta x + C_n v_n$

Tangential Force $F_t = \min\left(mF_n, k_t \int v_t dt + C_t v_t\right)$

Cleary (op. cit.) suggested that the normal force consists of a linear spring to provide the repulsive force and a dashpot to dissipate a proportion of the relative kinetic energy. The maximum overlap between particles is determined by the stiffness k_n of the spring in the normal direction. In the case of a tangential force, the force vector F_t and velocity v_t are defined in the plane tangent to the surface at the contact point. The integral represents an incremental spring that stores energy from the relative tangential motion and models the elastic deformation of the contacting surfaces, while the dashpot dissipates energy from the tangential motion and models the tangential plastic deformation of the contact (Cleary, op. cit.).

This DEM code has been used extensively for studying load behaviour in grinding mills. It can provide information on velocity profiles of each ball. It can be used to simulate load behaviour and therefore energy transfer in the grinding mill. In this study the DEM has been used to provide ball velocities and estimates of the number of balls in contact with the liners as well as the number of balls in contact with the air that is above the load.

2.7 Energy losses in a milling system

There are considerable energy losses in any practical milling processing of which some of the most important are as follows (Stairmand, 1975):

(i) Energy converted into sound, heat lost in the motor and mechanical losses in the mill bearings and gear box.

(ii) The actual mechanical efficiency of energy transmission to the grinding elements (e.g. the balls or beaters in a mill) will be less than 100%; losses are likely in the motors and in the transmission system.

(iii) Some energy is used to wear the liners by impact and abrasion due to friction and some is lost in inter-particle friction.

(iv) Not all of the energy transmitted to the grinding elements will reach the particles; a considerable part may be lost in inter-particle friction in the grinding zone.

(v) Not all of the energy reaching the particles will be usefully employed in comminution. In a ball-mill, for example, the balls may be so small that they possess insufficient energy to break the particles to be comminuted, or so large that part of their energy is wasted in re-aggregating crushed particles.

(vi) The conditions in the mill may be such that stresses are not applied in the most efficient manner e.g. stressing of semi-plastic materials may be too slow, so that energy is lost in plastic deformation.

(vii) Auxiliaries such as air-sweeping systems and classifiers may be employed, in attempts to improve grinding conditions in the mill; while no doubt these will increase the actual grinding efficiency, they consume power, which must be debited to the process.

2.8 Analysis of conduction and convective heat transfer

2.8.1 Conduction Heat Transfer

Consideration is now given to the analysis of conduction heat transfer in solids and fluids. The general theoretical analysis of conduction-heat-transfer problems involves (1) the use of (a) the fundamental first law of thermal dynamics and (b) the Fourier law of conduction (particular law) in the development of a

mathematical formulation that represents the energy transfer in the system; and (2) the solution of the resulting system of equations for the temperature distribution. Once the temperature distribution is known, the rate of heat transfer is obtained by use of Fourier law of heat conduction (Thomas, 1980).

A simple practical approach to the analysis of basic steady state conduction-energy-transfer problems has been developed which involves the use of an equation developed from the fundamental and particular laws. This practical equation for conduction heat transfer takes the form:

$$q = \frac{kA}{L}(T_1 - T_2) \tag{2.6}$$

Where q is the rate of heat conducted from a surface at temperature T_1 to a surface at temperature T_2, A is the heat transfer area and L is the thickness of a surface. The practical approach to the analysis of conduction-heat-transfer will be developed for multidimensional systems as in a mill under consideration in the following sections.

2.8.2 Convection Heat Transfer

Convection is the transfer of heat from a surface to a moving fluid or vice versa. The conduction heat transfer mechanism plays a primary role in convection. In addition, the thermal radiation-heat transfer mechanism is also sometimes a factor. The theoretical analysis of convection requires that the fundamental laws of mass, momentum, and energy and the particular laws of viscous shear and conduction be utilized in the development of mathematical formulations for the fluid flow and energy transfer. The solution of these provides predictions for the velocity and temperature distributions within the fluid, after which predictions are developed for the rate of heat transfer into the fluid by the use of Fourier law of conduction. The practical approach to the analysis of convection heat transfer from surfaces has been developed which employs an equation of the form:

$$q = hA_s(T_s - T_F) \tag{2.7}$$

Where q is the rate of heat transferred from a surface at uniform temperature T_s to a fluid with reference temperature T_F, A_s is the surface area, and h is the mean coefficient of heat transfer.

Equations (2.6) and (2.7) will be useful in the next section and in the derivation of the steady state temperature models.

The most important aspect to this study is the energy loss through the mill shell. This loss of energy is a function of mill speed, mill filling and the liner/lifter design. Most of the energy is lost from the mill in the form of thermal energy through the mill shell by conduction, convection and radiation, and also as sound energy (noise) from the mill. Energy lost in the form of heat can be modeled as a combined form of energy transfer in most cases by conduction and convection, and also radiation. Energy loss by radiation is applied where higher temperatures are involved and therefore is not considered in this Dissertation. Figure 2.4 below describes the physical situation.

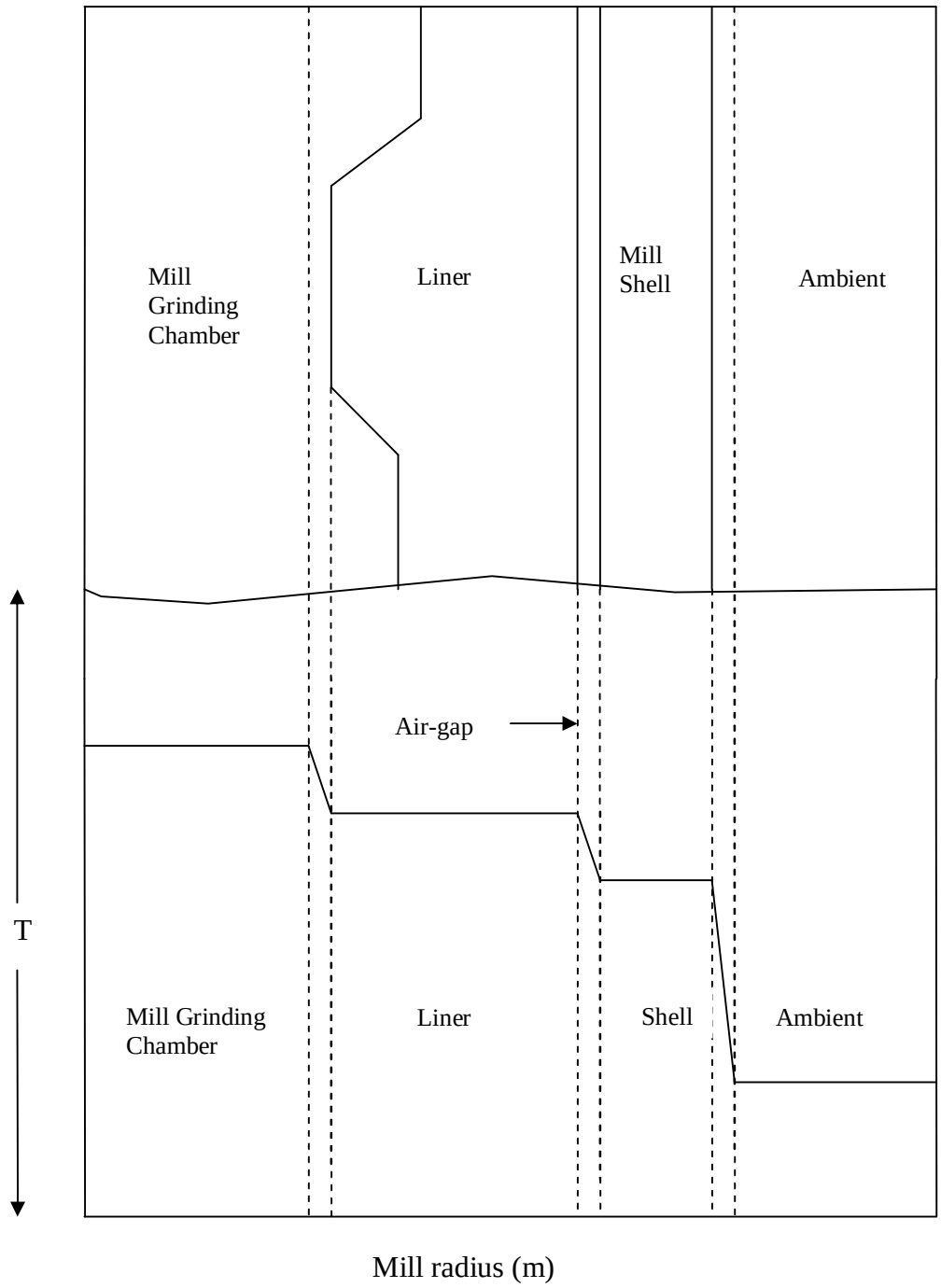

Figure 2.4: Temperature profile in a grinding mill.

The temperature profile on a liner with a lifter will be generally different from the temperature profile on liner position. The energy lost through the liner position of the mill lining would encounter a resistance due to the inside resistance, flat metal sheet lining, air gap (or cork), mill shell and the resistance from the air around the

mill shell. It has however been found that the temperature of the shell behind the lifter and that of the shell behind the liner were the same.

The energy lost through a liner with a lifter encounters a load-lifter resistance, transfer across the mill liners, transfer across the air-gap under the liners, transfer across the mill shell and transfer across the air on the outside of the shell. These boundaries will provide resistance in series to the flow of energy. The total resistance is the sum of these resistances in series, which will be equal to the overall resistance and therefore an overall heat transfer coefficient for the mill wall and fluid boundary layers can be defined. The energy flow leaving the mill must be equal to the energy entering the environment, since steady state precludes energy storage. The thermal energy will flow radially through the mill wall.

On the outside shell of the mill, the energy transfer coefficient is influenced by the speed of the mill. Inside the mill, the thermal energy transfer coefficient is likely to be affected by the mill load mass or volume, the mill speed and the flow pattern of the air in the mill. The energy transfer is possibly also a function of the voidage which increases with increase in mill speed.

Figure 2.4 shows the expected temperature profile of a grinding mill at steady state. The temperature of the mill decreases with increasing mill radius.

For the entire boundary,

$Q = \frac{\Delta T}{R}$, where R is the total resistance and

$$R = R_{\text{par}} + R_2 + R_3 + R_4 + R_5 \tag{2.8}$$

R_{PAR}, R_L, R_g, R_S and R_{ext} are unequal as a result of differing conductivities and thickness; the ratio of the temperature difference across each layer to its resistance must be the same as the total temperature difference is to the total resistance, i.e.

$$Q = \frac{\Delta T}{R} = \frac{\Delta T_1}{R_{PAR}} = \frac{\Delta T_2}{R_L} = \frac{\Delta T_3}{R_g} = \frac{\Delta T_4}{R_S} = \frac{\Delta T_5}{R_{ext}} \tag{2.9}$$

The individual heat transfer coefficients are a function of a number of variables, such as the fluid velocity, density, viscosity, mill speed, the load volume and the flow pattern of the air inside the mill. On the outside of the mill shell however, the outside heat transfer coefficient is a function of the mill speed only. If the mill is not enclosed in a building, wind speed would also be a variable.

Generally, heat transfer by convection occurs as a result of the movement of fluid on a macroscopic scale in the form of circulating currents (Coulson and Richardson, 1999). If the currents arise from the heat transfer process itself, natural convection occurs. In forced convection, circulating currents are produced by an external agency such as an agitator in a reaction vessel or as a result of turbulent flow in a tube. In general, the magnitude of circulation in forced convection is greater, and higher rates of heat transfer are obtained than in natural convection. In most cases where convective heat transfer is taking place from a surface to a fluid, the circulating currents die out in the immediate vicinity of the surface and a film of fluid, free of turbulence, covers the surface (Coulson and Richardson, op. cit.). In this film, heat transfer is by conduction and, as the thermal conductivity of most fluids is low, the main resistance to transfer lies there. Thus an increase in the velocity of the fluid over the surface gives rise to improved heat transfer mainly because the thickness of the film is reduced. As a guide, the film coefficient increases as (fluid velocity)^n, where $0.6<n<0.8$, depending on the geometry. If the resistance to transfer is regarded as lying within the film covering the surface, the rate of heat transfer Q is given as:

$$Q = \frac{kA}{x}\Delta T \qquad (2.10)$$

The effective thickness x is not generally known and therefore the equation is usually rewritten in the form as given by:

$$Q = hA\Delta T \qquad (2.11)$$

where h is the heat transfer coefficient for the film and $\left(1/h\right)$ is the thermal resistance. Note that $h = k/x = Const.\left(v^n\right)$, and 0.6<n<0.8 as explained before.

So many factors influence the value of h that it is almost impossible to determine their individual effects by direct experimental methods. By arranging the variables in a series of dimensionless groups, however, the problem is made more manageable in that the number of groups is significantly less than the number of parameters. It is found that the heat transfer rate per unit area q is dependent on those physical properties which affect flow pattern (viscosity m and density r), the thermal properties of the fluid (the specific heat capacity Cp and thermal conductivity k) a linear dimension of the surface l, the velocity of flow u of the fluid over the surface, the temperature difference ΔT and a factor determining the natural circulation effect caused by the expansion of the fluid on heating (the product of the coefficient of cubical expansion b and the acceleration due to gravity g. Writing this as a functional relationship (Coulson and Richardson, 1999):

$$q = \Phi\left(u, l, r, m, Cp, \Delta T, bg, k\right) \tag{2.12}$$

The relationship in equation 2.12 can be written as:

$$\frac{ql}{k\Delta T} = \frac{hl}{k} = \Phi\left[\left(\frac{lur}{m}\right)\left(\frac{Cpm}{k}\right)\left(\frac{bg\Delta Tl^3 r^2}{m^2}\right)\right] \tag{2.13}$$

This general equation involves the use of four dimensionless groups. For design purposes, this is frequently simplified. From equation 2.13:

hl/k is known as the *Nusselt* group *Nu*,

lur/m the *Reynold's* group *Re*,

Cpm/k the *Prandtl* group *Pr*, and

$bg\Delta Tl^3 r^2/m^2$ the *Grashof* group *Gr*. For conditions in which only natural convection occurs, the velocity is dependent on the buoyancy effects alone, represented by the Grashof number and the Reynold's number may be omitted. When forced convection occurs the effects of natural convection are usually negligible and the Grashof number may be omitted. Thus:

For natural convection: $Nu = f(Gr, \mathrm{Pr})$, (2.14)

For forced convection: $Nu = f(\mathrm{Re}, \mathrm{Pr})$ (2.15)

For most gases over a wide range of temperature and pressure, the Prandtl group may be omitted as it is considered to be a constant. This simplifies the design equations for the calculation of film coefficients.

Based on the Sieder and Tate's work, (Richard and Coulson, op. cit.), the equation is:

$$Nu = 0.027\,\mathrm{Re}^{0.8}\,\mathrm{Pr}^{0.33}\left(\frac{m}{m_s}\right)^{0.14} \tag{2.16}$$

μ and μ_s are the viscosities of the fluid and the wall. When these equations are applied to heating or cooling of gases for which the Prandtl number group usually has a value of about 0.74, substitution of $\mathrm{Pr} = 0.74$ in equation (2.16) gives:

$$Nu = 0.020\,\mathrm{Re}^{0.8} \tag{2.17}$$

Many attempts have been made to correlate the convective heat transfer coefficient with gas flow rate and properties of the fluid and solid particles. Most often, such correlations seek empirical relationships between a Nusselt number (*Nu*) with the fluid Prandtl number (*Pr*) and a Reynolds number (*Re*). A typical example is a correlation presented by Vreedenberg (1958) for horizontal tubes:

$$Nu_t \equiv \frac{h_c D_t}{k_g} = 420\left(\frac{r_p}{r_g}\mathrm{Re}_t\right)^{0.3}\left(\frac{m_g^{\,2}}{g r_p^{\,2} d_p^{\,3}}\right)^{0.3}\left(\mathrm{Pr}_g\right)^{0.3} \tag{2.18}$$

for $\left(\frac{r_p}{r_g}\mathrm{Re}_t\right) > 2250$

where Re_t is the Reynold's number based on tube diameter, D_t, while k_g, ρ_p, ρ_g, μ_g, and d_p are the gas thermal conductivity, particle density, gas density, gas viscosity, and mean particle diameter, respectively.

One of the most reliable equations used to correlate the heat transfer coefficients as given by Coulson and Richardson (1991) was obtained from data given by Dow and Jakob. Their equation is:

$$\frac{hd_t}{k} = 0.55\left(\frac{d_t}{l}\right)^{0.65}\left(\frac{d_t}{d}\right)^{0.17}\left\{\frac{(1-e)r_s c_s}{erc_p}\right\}^{0.25}\left(\frac{u_c d_t r}{m}\right)^{0.80} \qquad (2.19)$$

where*: h* is the heat transfer coefficient, *k* is the thermal conductivity of the gas, *d* is the diameter of the particle, d_t is the diameter of the tube, *l* is the depth of the bed of solids in the tube, *e* is the voidage of the bed, ρ is the density of the gas, ρ_s is the density of the solids in the bed, c_s is the specific heat of the solid, c_p is the specific heat of the gas at constant pressure, μ is the viscosity of the gas, and μ_c is the superficial velocity based on the empty tube.

2.8.3 The Practical Significance of the Overall Heat Transfer Coefficient

The overall heat transfer coefficient, the total surface area of heat transfer and the temperature difference between the load temperature and the environment (ambient) will predict the rate of energy loss to the environment. The overall heat transfer coefficient, *U*, is a measure of heat conductivity for steady state heat transfer through the convective heat transfer coefficient on the inside of the mill, across the liners, through the small air gap between liner/lifter and the shell, across the mill shell and through the convective film of air on the outside of the shell. Knowledge of the overall heat transfer coefficient is as important for the examination of heat transfer processes, as is an understanding of the Ohm's Law for electrical engineering. It embraces all heat transmission processes through plane or slightly curved walls consisting of one or more layers (Schack, 1965).

The concept of the overall heat transfer coefficient is best understood by analogy with the components of electrical conductance. According to Ohm's Law, current intensity in a given cross-sectional area of a conductor is proportional to the potential and inversely proportional to the resistance. In the above statement, the resistance signifies the sum of the individual resistances. This relationship is analogous to the basic equation of heat transmission. The overall heat transfer coefficient is almost equal to the smallest heat transfer coefficient, *h*. The reason is purely numerical. The reciprocal of the largest *h* is smaller than that of the smallest *h*. The reciprocals are the heat transfer resistances.

2.9 Estimation of model parameters using parameter estimation (Least squares filtering)

The technique of "least squares filtering involves the use of measurements, together with model predictions of these values, to calculate the difference between what is measured and what is predicted. This difference is then squared, and the sum of the squared errors for each of the measurement-prediction pairs is then obtained. This total "sum of squared errors" is then minimized by manipulation of the variables. The minimization procedure is carried out until the desired convergence is achieved. The use of a computer in this application is essential. In particular, Microsoft®Excel is used to perform the sum of squares minimization. The solver function is employed to minimize the sum of squares, subject to constraints that are described below.

Parameter estimation is a common problem in many areas of process modeling, both in on-line applications such as real time optimization and in off-line applications such as the modeling of reaction kinetics and phase equilibrium. The goal is to determine values of model parameters that provide the best fit to measured data, generally based on some type of least squares filtering.

In this study, mathematical models of temperature behaviour in a batch-grinding mill have been developed. The parameters within the model are found which

minimize the sum of squares of the errors between the temperature predicted by the mathematical model and the measured temperatures.

The expression used for finding this minimum of errors is:

$$S = \sum_{i=1}^{n} (T_{\text{mod}} - T_{meas})^2 \qquad (2.20)$$

Where T_{mod} and T_{meas} are the steady state model and measured temperatures respectively. The parameters of the mathematical model for temperature are found such that "S" is minimized. In other words parameters are found by fitting the mathematical model. In this estimation the parameters estimated are heat transfer coefficient from which the overall heat transfer coefficient is evaluated. The other parameter such as power, sound, ambient temperature and initial temperature are taken from measurements.

2.11 Conclusions

The first law of thermodynamics encompasses the three fundamental laws; the conservation of energy, mass and momentum. The conservation of energy is fundamental in the study of energy systems in milling particularly when used together with Fourier's law of heat conduction. The energy balance could prove to be a competent tool in the optimization of mill control and operation. Mill power is an important variable in energy modeling in a grinding mill. The power transmitted to the mill is proportional to the lifting action. Load behaviour of rotary grinding mills determines the level of temperature attained and therefore is important as far as mill efficiency is concerned.

In conclusion, the energy going into the mill is used to lift the load, break the particles and creating new surfaces, raising the mill discharge temperature, and raising the temperature of the mill and the air in the mill. However, energy is also lost in the form of sound but mainly as heat. Some energy is used to wear the

liners by impact and abrasion due to friction. Losses are also likely to occur in the motor, gear box and bearings, and generally in the transmission system.

Chapter 3

Development of a Mathematical Model

3.1 Introduction: Principles of mathematical modeling

A mathematical model can be a very powerful tool in the development of new and existing metallurgical processes when in combination with careful experimental measurements (Szekely et. al, 1988). It is needed to describe how a process reacts to various inputs. However, it is not the only tool that the process engineer will need to employ in process analysis because a measurement program is normally necessary as well. These are measurement of concentration, temperature, and fluid flow or mixing (tracer tests) in an existing process. A mathematical model offers many advantages on the objectives of a study:

(i) It can increase understanding of a process in fundamental terms.
(ii) A model can be used for the purpose of process control and optimization.
(iii) It can be an invaluable aid in scale-up and design.
(iv) It can assist in the evaluation of results from in-plant trials, for example, the conversion of temperature measurements to heat fluxes as in this research.
(v) A model can assist in making decisions on trial conditions in an experimental campaign in-plant.

A mathematical model in general, is an equation or set of equations, algebraic or differential, together with initial and/or boundary conditions, that represents the important chemical and/or physical phenomena in a process. Mathematical models can be classified as Fundamental or Mechanistic, Empirical and Population-Balance models. Fundamental models are based on mechanisms involving transport phenomena and chemical reaction rates in a process. Chemical and physical laws are applied to obtain mathematical equations relating independent and dependent variables. Examples of the laws involved are conservation of mass, energy and momentum; Fourier's law (for conduction heat transfer), and Fick's law (for molecular diffusion). Frequently, empirical constants are required in the model to characterize phenomena that are very complicated and defy rigorous mathematical treatment. Empirical models rely on the determination of mathematical equations linking dependent and independent variables using

measurements of the variables in an operating plant. The fitting of the relationships is usually based on statistical analysis; but fundamental knowledge of the process may influence the form of the equations. However, unlike the fundamental model, the empirical model relies much less (often hardly at all) on an understanding of the mechanisms involved in the process. This type of model has been used extensively by mineral engineers to describe such processes as flotation, crushing and grinding. The population-balance model has been used extensively in the mineral-processing field in recent years. It has been developed to describe processes having distributed properties, such as particle size in a ball mill. In this study, fundamental or mechanistic models are employed to develop the mill temperature model.

3.1.1 The Energy Balance

The temperature profile within a body depends upon the rate of internal generation of energy, its capacity to store some of this energy, and its rate of thermal transfer by conduction and convection to its boundaries (where the heat is transferred to the surrounding environment). This can be written in the form of an energy balance as follows:

Rate of energy into reactor = rate of energy out of reactor + rate of energy accumulation in the reactor (3.1)

The behaviour of temperatures in a mill can be obtained from an energy balance methodology. The state variables of interest for the mill temperature model are the temperatures of the load, the air above the load, the liners and the shell. By definition a state variable is a variable that arises naturally in the accumulation term of a dynamic energy or material balance. It is a measurable quantity that defines the state of a system.

The overall energy balance model considers an energy balance problem wherein energy coming into the batch mill is only in the form of power, P transmitted to

the mill (refer to figure 3.1). This energy is transferred to the load at the load-liner interface. Due to the tumbling action (cataracting and cascading leading to impacts and collisions), the load gains thermal energy which is accompanied by heat dissipation to its environment through the mill wall and attains a temperature of *T(t)* after time *t*. Some of the energy is also converted to sound. The energy loss through the mill wall occurs following Fourier's theory of heat transfer with the temperature on the outer wall being cooled by air draft. Work is also done between the mill wall and the surrounding air due to friction. Some of the energy is also lost in the motor as well as mill bearings and gearbox. These energy losses are catered for in the no load power in section 4.5.1 of chapter 4 during load beam torque calibration. At steady state when there is no further increase in mill process temperatures, the energy input to the mill equals the energy loss from the mill. The temperatures become constant at steady state.

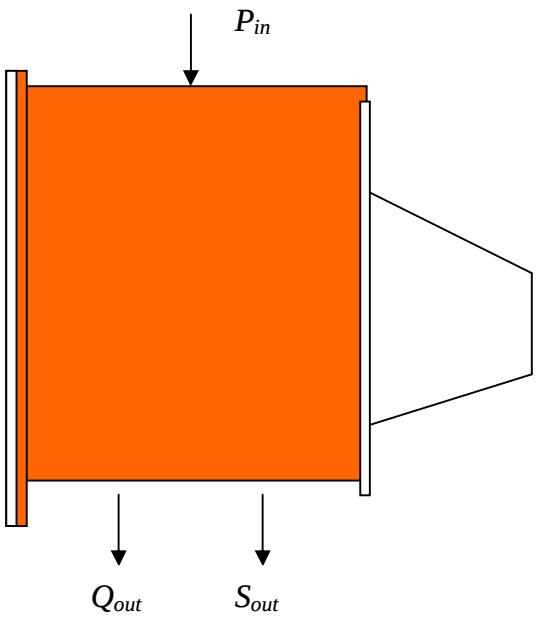

Figure 3.1: Batch grinding mill: Energy balance measurements

3.1.2 Assumptions made in the derivation of the model

The following assumptions were made in the derivation of the model:

(i) It is assumed that all the power P is transmitted to the load; ignoring the fact that some frictional energy is actually dissipated at the liner surface

(ii) The thickness of the mill wall, Δr, is small compared to the radius of the mill.

(iii) The process reaches steady state after milling for some time.

(iv) The overall heat transfer coefficient is constant at steady state and so are the individual heat transfer coefficients on the inside and out of the mill wall.

(v) Heat dissipation occurs through the mill wall by conduction and convection.

3.1.3 Model Derivation

The technique used in this study utilizes an energy balance that is applied to the load, the air above the load, liners and mill shell.

The temperature measurements made in the mill included the temperatures of the load inside the mill, the air above the load, the liners, the shell, and ambient temperature. These temperatures (with exception of the ambient as it is not a state variable in this case) are measured and modeled, and therefore estimates of the heat transfer coefficients, the overall heat transfer coefficient and an estimate of the rate of thermal energy losses from the mill can be quantified. The steady state temperature models are of value in this study as our design variable, the overall heat transfer coefficient, are evaluated at steady state temperature.

Another important measurement considered in this study is the power transmitted to the mill. This is considered as the only source of energy going into the mill. This is determined from the load beam calibrations as given in section 4.5.1 of chapter 4. The measurement of this variable is explained more in chapter 4.

The model is based on a horizontal batch grinding mill shown in Figure 3.1. The overall energy balance is constructed around the entire grinding mill as follows:

$$P(t) = Q(t) + S(t) + \frac{dE(t)}{dt} \tag{3.2}$$

Where:

Q is the rate of thermal energy loss through the mill wall

S is the rate of energy conversion into sound

P is the net power drawn by the mill and transmitted to the grinding media. This is the main term responsible for the temperature increase of the whole milling system.

$$P_{net} = P_{load} - P_{noload}$$

The no load power incorporates the energy lost in the motor, mill bearings and gear box, as well as work done due to friction between the mill and the air as discussed earlier. This is measured by running an empty mill and determining the power drawn by an empty mill.

$\frac{dE}{dt}$ and Q are functions of temperature, i.e,

$$\frac{dE}{dt} = \sum_{i=1}^{N} \frac{d\left[m_i C_{p_i}\left(T_i - T_{ref,i}\right)\right]}{dt} \tag{3.3}$$

Where: T_i is the temperature of the component under consideration, i.e., the temperature of the load (i=1), air-above lifter (i=2), liner (i=3) and shell (i=4). T_{ref} is the reference temperature and is taken to be zero. Equation (3.3) is a lumped model for all the mill components under consideration. These being: the load, air above the load, the liners and the shell. Therefore, the term mC_p incorporates the mass and specific heat capacity of the ore, balls, the air above the load, water (in the case of a wet mill), liners and the mill shell. In this project, dry balls only experiments are employed. Of interest was the modeling of energy loss to the environment and not the energy consumed in comminution.

3.2 Energy balance models for the mill temperature

The dynamic models are derived on the basis of Figure 3.2 below. The figure shows the schematic representation of the cross-section of the mill in a horizontal position. The presence of the air-gap between the liners and the shell offers resistance to the flow of energy and therefore a temperature drop exists.

The energy balances are performed between the active load, the air above the load, the liners and the environment. The objective is to determine a model for the overall heat transfer coefficient as a function of the load volume, mill speed and the design of the liners and shell so as to quantify energy loss from the mill. The heat transfer coefficients governing transfer between these phases and the overall heat transfer coefficient U was correlated with mill speed and load volume. The data gathered in the milling experiments together with an energy balance model for temperatures in the mill was used to obtain estimates of interphase heat transfer coefficients and the overall heat transfer coefficients. The energy loss via convection through the mill shell is accounted for by quantifying the overall heat transfer coefficient of the shell. The ambient temperature allows the model to account for convective loss. U increases with both load volume and mill speed.

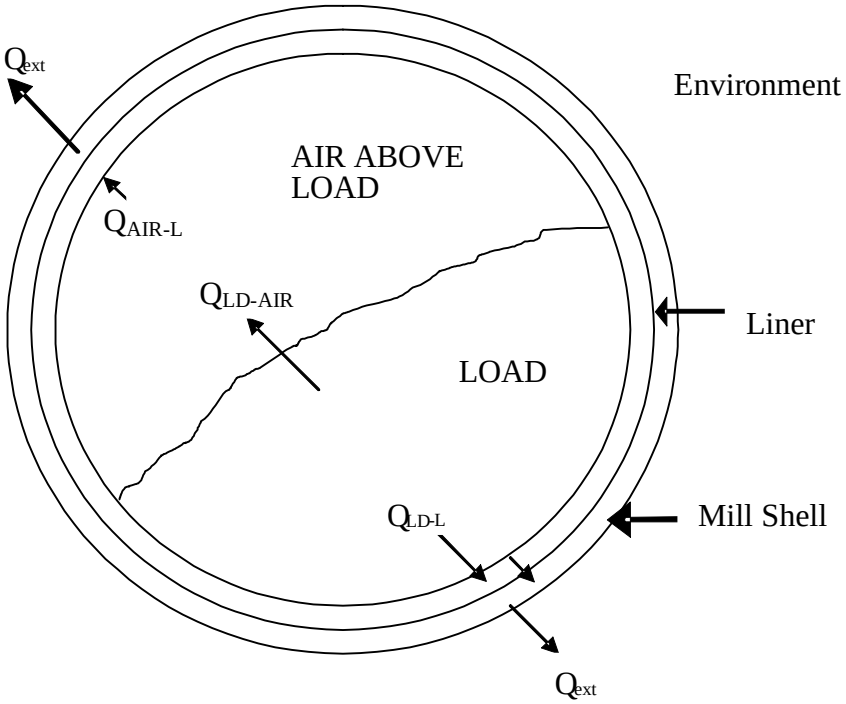

Figure 3.2: Schematic diagram of the orientation of the load, air above load, liner/lifters and mill shell.

From Figure 3.2, it can be observed that thermal energy leaving the mill follows two paths. The first path involves energy leaving the load and passing through the liners, air gap and mill shell to the environment. In the second path, the energy is transferred from the load to the air above the load. From the air above the load the energy enters the liners through the mill shell to the environment. In other words two parallel paths of energy transfer are established in this system. The modeling of the parallel path is performed in the following section. The following is the mechanism of energy transfer in the grinding mill.

(1) The direct transfer of energy from the load to the liner by convection and conduction. The model is given by:

$$Q_{LD-L} = hA_{(LD-L)}(T_{LD} - T_L) \tag{3.4}$$

(2) Thermal energy transfer from the load to the air above the load by convection:

$$Q_{LD-AIR} = hA_{(LD-AIR)}(T_{LD} - T_{AIR}) \quad (3.5)$$

(3) Transfer of energy from the air above the load to the liner by convection:

$$Q_{AIR-L} = hA_{(AIR-L)}(T_{AIR} - T_L) \quad (3.6)$$

(4) Transfer of thermal energy across the liner by conduction:

$$Q_L = \frac{k_L(T_{L1} - T_{L2})}{x_L} A_L \quad (3.7)$$

(5) Transfer of energy from the liner to the mill shell across an air-gap (or across a gasket between the liner and the shell) by conduction:

$$Q_g = \frac{k_g A_g (T_{L2} - T_{S1})}{x_g} \quad (3.8)$$

(6) Transfer of thermal energy across the mill shell:

$$Q_S = \frac{k_s A_s (T_{S1} - T_{S2})}{x_s} \quad (3.9)$$

(7) Transfer of thermal energy from the mill shell to the environment by forced convection:

$$Q_{ext} = hA_{(ext)}(T_{S2} - T_{Amb}) \quad (3.10)$$

It is assumed that the temperature of the shell T_{S2} is assumed to be constant for the entire shell. This will not hold in a continuous mill because the temperature will be changing from the feed end to the discharge end.

Since at steady state, $Q_L = Q_g = Q_s = Q_{ext}$ (3.11)

In terms of the overall heat transfer coefficient,

$$Q = UA_{(ext)}\left(T_{LD} - T_{Amb}\right) \tag{3.12}$$

3.3 Model for the overall heat transfer coefficient as a function of important variables: mill speed, load volume and mill liner /shell design

The overall heat transfer coefficient is a function of the individual heat transfer coefficient both in the inside of the mill as well as outside the mill shell. The heat transfer coefficient is influenced by a number of factors: these are: the speed of the mill, the load volume and the physical properties of the fluid involved. The heat transfer coefficient from the load to liner, load to air and air to liner is affected by the velocity of the air inside the mill as well as the mill load volume. On the outside of the mill shell, the heat transfer coefficient is a function of the peripheral velocity of the mill and the thermal physical properties of the air in contact with the outside of the mill shell.

It has been given in section 2.8 of chapter 2 that generally, the film heat transfer coefficient on a surface increases as (fluid velocity)^n, where $0.6<n<0.8$, depending on the geometry (Coulson and Richardson, 1999).

3.3.1 Modeling of parallel paths

The total thermal resistance in a grinding mill can be given by:

$$R_T = R_{par} + R_L + R_g + R_S + R_{ext} \tag{3.13}$$

where R_{par}, R_L, R_g, R_s, and R_{ext} are the resistances in parallel, due to the liners, air gap between liner and shell, mill shell and the outside of the mill shell respectively.

$$R_L = \frac{x_L}{k_L A_L}; R_g = \frac{x_g}{k_g A_g}; R_S = \frac{x_S}{k_S A_S}; \text{ and } R_{ext} = \frac{1}{hA_{(ext)}}$$

The resistances in parallel are the load to liner and air above the load to liner resistances. These can be expressed as:

$$R_1 = \frac{1}{hA_{(LD-L)}}, \text{ and } R_2 = \frac{1}{hA_{(LD-AIR)}} + \frac{1}{hA_{(AIR-L)}}$$

Therefore:

$$\frac{1}{R_{par}} = \frac{1}{R_1} + \frac{1}{R_2} \tag{3.14}$$

Solving for the parallel resistance we have:

$$R_{par} = \frac{R_1 R_2}{R_1 + R_2} \tag{3.15}$$

Thus, the overall heat transfer coefficient is governed by the individual heat transfer coefficients on the inside and outside of the mill wall as well as by the design of the mill shell and liners. The overall heat transfer coefficient, *U*, is a measure of heat conductivity for steady state heat transfer through the convective heat transfer coefficients on the inside of the mill, across the liners, through the small air gap between liners and the shell, across the mill shell and through the convective film of air on the outside of the shell. From equations (3.12) and (3.13), the overall resistance is therefore expressed as:

$$\frac{1}{UA_{(ext)}} = \frac{hA_{(LD-AIR)} + hA_{(AIR-L)}}{(hA_{(LD-L)} x hA_{(LD-AIR)}) + (hA_{(LD-L)} x hA_{(AIR-L)}) + (hA_{(AIR-L)} x hA_{(LD-AIR)})} + \frac{x_L}{k_L A_L} + \frac{x_g}{k_g A_g} + \frac{x_s}{k_s A_s} + \frac{1}{hA_{(ext)}}$$

(3.16)

The inside heat transfer coefficients can be represented as a product with the heat transfer areas and are assumed to be functions of the fractional mill speed f and load volume J. These can be written as:

$$hA_{(LD-AIR)} = k_1 f^a J^b \tag{3.17}$$

$$hA_{(AIR-L)} = k_2 f^c J^d \tag{3.18}$$

$$hA_{(LD-L)} = k_3 f^y J^z \tag{3.19}$$

If we had data for different mill sizes then these equations would more appropriately be written in terms of the appropriate dimensionless numbers e.g. Reynold's number (*Re*), Nusselt number (*Nu*) and the Prandtl number (*Pr*) in order to explore scale up of this data.

k_1, k_2, k_3, a, b, c, d, y and z are parameters and are estimated by fitting the model to the experimental data in a least squares sense. These are modeled individually and as a product with the heat transfer area. The fractional mill speed f is proportional to the peripheral speed of the mill and J is the volume of the load which is expressed as a fraction of the mill volume. Since A_{LD-L} is unknown, the heat transfer coefficients can be evaluated from the model only as a product with the heat transfer area. It is however possible to determine the heat transfer coefficient on the outside as a function of the mill velocity since A_{ext} is known. We assume

$$h_{ext} = \bar{h}_{ext} f^x \tag{3.20}$$

where x is determined by regression on measured data and peripheral velocity of the mill. The model for the overall heat transfer coefficient then becomes:

$$\frac{1}{UA_{(ext)}} = \frac{k_1 f^a J^b + k_2 f^c J^d}{\left(k_3 f^y J^z \times k_1 f^a J^b\right) + \left(k_3 f^y J^z \times k_2 f^c J^d\right) + \left(k_2 f^c J^d \times k_1 f^a J^b\right)} + \frac{1}{A_{ext}\ \bar{h}_{ext}\ f^x} + C \tag{3.21}$$

where C is a constant representing terms 2, 3 and 4 in equation (3.16).

From the model above, the individual heat transfer coefficients, the overall heat transfer coefficient and the thermal energy loss can be predicted at any given mill load volume and mill speed.

3.4 The dynamic and steady state model equations for the mill load, air above load, liner and mill shell

The mathematical models are based on the thermal physical properties and they require a detailed understanding of the heat transfer processes taking place in the grinding mill. The use of these models allows accurate prediction of the temperature distribution. In this work however, emphasis is on steady state temperature models. It is at steady state temperatures that such important variables as the individual heat transfer coefficients and therefore the overall heat transfer coefficient are evaluated.

On the basis of the energy transfer mechanisms described above, the model reads for the respective components (assuming all *P* is transmitted to the load; ignoring the fact that some friction is actually dissipated at the liner surface):

(1) Dynamic model for mill load

$$m_{LD} Cp_{LD} \frac{dT_{LD}}{dt} = P - Q_{LD-AIR} - Q_{LD-L} \tag{3.22}$$

Where:

m_{LD} and Cp_{LD} are the mass and specific heat capacity of the mill load

$T_{LD} = T_{\text{Load}}$, the temperature of the load at $t=0$

P is the power drawn by the mill and transferred to the load and it is the main term responsible for the temperature increase of the whole system. In other words it is assumed that all power is transmitted to the load ignoring the fact that some friction is actually dissipated at the liner surface. Equation (3.22) is the core of the model, and expresses the thermal energy balance for the mill load in the grinding chamber whose volume depends on the mill load considered.

At steady state, since $\frac{dT_{LD}}{dt} = 0$, equation (3.22) becomes:

$$P_{SS} = Q_{LD-AIR(SS)} + Q_{LD-L(SS)} = Q_{ext} \tag{3.23}$$

Alternatively, equation (3.23) can be written in terms of the measured temperatures and the heat transfer coefficients as:

$$P = hA_{(LD-AIR)}(T_{LD} - T_{AIR}) + hA_{(LD-L)}(T_{LD} - T_L) \tag{3.24}$$

This also applies to other components.

(2) Dynamic model of the air above the load

Similarly the dynamic equation modeling temperature behaviour in the air above the load can be given by:

$$m_{AIR}C_{pAIR}\frac{dT_{AIR}}{dt} = Q_{LD-AIR} - Q_{AIR-L} \tag{3.25}$$

At steady state, $Q_{LD-AIR(SS)} - Q_{AIR-L(SS)} = 0$ (3.26)

(3) Dynamic model for the liner

The dynamic equation of state modeling temperature behaviour in a liner can be given by:

$$m_L Cp_L \frac{dT_L}{dt} = Q_{LD-L} + Q_{L-AIR} - Q_g \tag{3.27}$$

Where:

m_L and Cp_L are the mass and specific heat capacity of the liner

At steady state, the equation becomes:

$$Q_{LD-L(SS)} + Q_{L-AIR(SS)} - Q_{g(SS)} = 0 \tag{3.28}$$

(4) Dynamic model for the shell

For the shell, the model reads:

$$m_S Cp_S \frac{dT_S}{dt} = Q_g - Q_{ext} \tag{3.29}$$

Where:

m_S and Cp_S is the mass and specific heat capacity of the shell

Again at steady state, the equation becomes:

$$Q_{g(SS)} - Q_{ext(SS)} = 0 \tag{3.30}$$

Also steady state,

$$Q_{LD-L} + Q_{AIR-L} = Q_L = Q_g = Q_S = Q_{ext} \tag{3.31}$$

And $Q_{LD-AIR} = Q_{AIR-L}$ (3.32)

3.4.1 Steady state models

The normal procedure is to design processes to operate at steady state conditions. This approach is based on the implicit assumption that some steady state system will generally correspond to the most profitable plant. By restricting our attention to steady state analysis we greatly simplify the design problem, for we need only consider sets of steady state relationships describing the process equipment. However this approach requires the assumption that all the inputs to the plant are constant, even though we know that some will vary with time.

It was very important in this study that steady state models for temperature be formulated in each of the regions of the grinding mill under consideration. This is because it is possible to evaluate the important parameters. These being: the heat transfer coefficients, the overall heat transfer coefficient and therefore estimates of energy loss to the environment. The system consists of a set of four steady state linear equations which can be solved simultaneously by matrix, namely Gaussian Elimination Method.

The steady state models in terms of the measured temperatures are as given below:

$$hA_{(LD-AIR)}(T_{LD} - T_{AIR}) + hA_{(LD-L)}(T_{LD} - T_L) = P \tag{3.33}$$

$$hA_{(LD-AIR)}(T_{LD} - T_{AIR}) - hA_{(AIR-L)}(T_{AIR} - T_L) = 0 \tag{3.34}$$

$$hA_{(LD-L)}(T_{LD} - T_L) + hA_{(L-AIR)}(T_{AIR} - T_L) - \frac{k_g A_g}{x_g}(T_L - T_S) = 0 \tag{3.35}$$

$$\frac{k_g A_g}{x_g}(T_L - T_S) - hA_{(ext)}(T_S - T_{Amb}) = 0 \tag{3.36}$$

3.5 Conclusions

A model that can predict energy loss from the mill is needed. Energy loss from the grinding mill to the environment is affected by a number of factors, namely, load volume, mill speed and design of the liners and mill shell. Knowledge of the overall heat transfer coefficient is important in order to have an estimate of energy loss form the grinding mill. The energy balance requires a number of measurements to be made to the system in order to be utilized. Energy balances are an important tool in estimating important variables critical to mill operation.

Chapter 4

Experimental apparatus, methodology, measurements and data acquisition

4.1 Introduction-Experimental apparatus

This chapter deals with the experimental program followed: These are: the experimental apparatus, methodology, measurements and data acquisition.

4.1.1 Description of the milling setup

The experiments were performed in a laboratory batch mill which was mounted on a milling rig to permit precise control and experimentation. The mill, shown in Figure 4.1, has an internal diameter of 0.54m and an internal length of 0.4m. The interior of the mill was lined with 12 trapezoidal liners with 45^{o} base angles. Because of the requirements of another project, halfway through the programme these liners were replaced by liners with 24 lifters having a height of 15mm. The end wall was made of steel plate while the front plate was made of a 12mm thick PVC sheet. The front plate and the back of the mill were insulated using polystyrene material to avoid energy losses through these positions. This is to ensure energy transfer in the radial direction only.

The front plate was firmly fastened to the mill with steel bolts for easy removal. In order to ensure that the mill was dust / particle proof, a rubber gasket was placed between the front plate and the mill shell. The rig was designed to drive any mill that can draw power less than 2.5KW. The mill had many features relevant to this project. The mill was mounted on a conical flange attached to the axle drive of the rig. The mill was flanged to an axle that both supported the mill and rotated it. The axle turned in large bearings (3) attached to the supporting frame. The motor and gear box were suspended in the cage below the mill by bearings (2). Power from the motor was transmitted to the axle via a drive chain. The mill's speed could be varied from 0-200% of the critical speed with minimum variations from the set speed. The grinding media employed in the experiments were 6, 10 and 20mm steel balls.

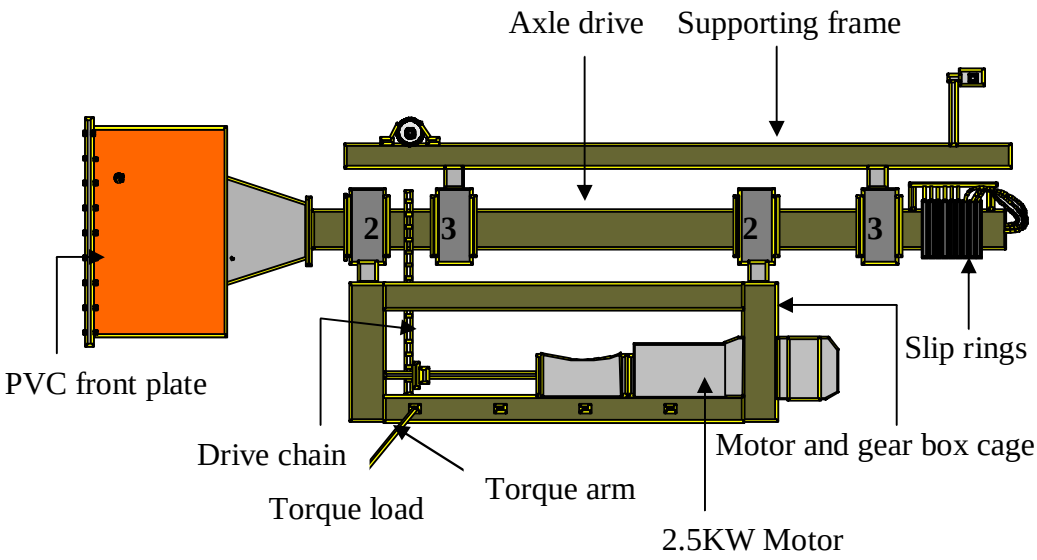

2- Motor Cage Bearing; 3-Axle Bearing

Figure 4.1: The schematic representation of the experimental mill set up

4.2 Measurements

Various measurements were made: These were: the temperatures of the load, air above the load, liner, shell, and the environment. Other measurements were power drawn by the mill and noise emanating from the grinding mill during the milling process. The methods of measurements and points of insertions of the probes are described in section 4.3.3. In the first experiments, only the temperature of the air above the load inside the mill was measured. It was assumed that the temperature of the air in the mill and the load were the same. However this was not the case. In actual fact, the temperature of the load was higher than the temperature of the air above the load from the measurement obtained using this arrangement. In view of this, another temperature measurement was introduced in the experiments in addition to the other temperature measurements: the temperature of the load. To measure the temperature of the load, a steel ball was drilled to a depth of half its diameter (This innovation was added halfway through the experimental programme in some experiments). A thermistor was inserted into the steel ball and

this was connected to an electrical circuit mounted on the mill by means of electrical wires. The electrical wires sending information from the load were inserted in a PVC tube to protect them from the motion of the grinding media in the mill and from coming in contact with the load. The steel ball under consideration was glued to the PVC tube to keep it in position and tight, and to protect it from being detached from the electrical wires. The electrical wires from the steel ball carrying temperature data of the load were passed through the hole in the centre of the front plate to the circuit outside. All information on mill process temperatures to the circuit are sent to the computer via slip rings mounted at the back of the mill.

4.3 Temperature probes

Probes employed to measure temperatures were thermistors (thermally sensitive-resistors) - bead type. These have a resistance of 10 kΩ at 25°C, whose resistance decreases with increasing temperature. By definition, a thermistor is a thermally sensitive resistor whose primary function is to exhibit a change in electrical resistance with a change in body temperature. The thermistors that we used were Negative Temperature Coefficient. This means that the temperature of the thermistor increases with decreasing resistance. Thermistors have a Standard Reference Temperature which is defined as a thermistor body temperature at which nominal zero-power resistance is specified (25^{o}C). The zero- power resistance is the DC resistance value of a thermistor measured at a specified temperature with a power dissipation by the thermistor low enough that any further decrease in power will result in not more than 0.1 percent (or 1/10 of the specified measurement tolerance, whichever is smaller) change in resistance. Thermistors are based on the temperature dependency of a semi-conductor's resistance, which is due to the variation in the number of available charge carriers. When the temperature increases, the number of charge carriers increases while the resistance decreases, yielding a negative temperature coefficient.

Thermistors are used in this application because of their precision and sensitivity to small temperature changes. In this project, the thermistors are connected to the voltage source of 12.6V and a very small current is allowed to pass through the thermistors so as to prevent self-heating of the thermistors. Since a thermistor is a resistor, passing a current through it generates some heat. The circuit designer must ensure that the pull-up resistor is large enough to prevent excessive self-heating, or the system will end up measuring the thermistor dissipation instead of the ambient or object temperature. To avoid self-heating of the thermistor, a 94 kΩ fixed resistor was connected in series with the thermistor to form a voltage divider as shown in Figure 4.2.

The circuit for the thermistors was enclosed in a circuit box which was mounted on the mill. The signals are sent from the thermistors to the computer via the slip rings which are mounted at the back of the mill rig. All variables, mill power and temperature data are collected from the laboratory PC computer.

Circuit Diagram for the thermistor

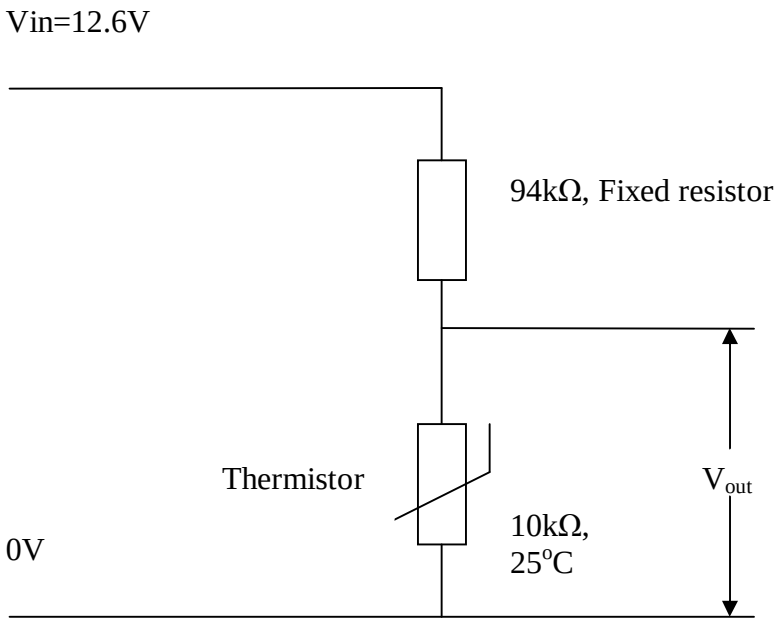

Figure 4.2: The electrical circuit diagram for the thermistor

From the circuit:

$$V_{out} = V_m \left(\frac{1}{1 + R/R_T} \right)$$

The average amount of self heating in the thermistor was found to be 0.08°C. This value is less than the tolerance value of 0.2°C. Calculation of thermistor self heating is given in Appendix A.

4.3.1 Choice of probe and material of construction

Thermistors are used in this application because of their precision and sensitivity to small temperature changes. Negative coefficient thermistors are made from sintered mixtures of the oxides of certain metals. The thermistors employed to measure the mill temperatures were the bead type. Measurement of ambient temperature was made using the disc type thermistor as the bead types were only sufficient for the measurement of the mill temperatures.

4.3.2 Expected temperature range

The thermistor tracks a specified curve to within +/-0.2°C over the temperature range of 20°C to 50°C or 0°C to 70°C. The best overall stability is achieved with exposure or storage temperatures lower than 105°C. The expected temperature range in this study is between 15 to 80°C. The Steinhart and Hart (1968) equation was used to relate temperatures to resistance for the thermistors:

$$T(^o K) = \left(a + b \log R + c (\log R)^3 \right)^{-1}$$

where *a*, *b* and *c* are constants which are estimated from three measurements of *R* at known temperatures in the range of interest. This was checked at other temperatures as well and the results were found to agree within +/-0.5^{o}C.

The thermistor dissipation constant is 1mW/^{o}C in still air and 8mW/^{o}C in stirred oil. The thermal time constant in still air is 10s and 1s in oil.

4.3.3 Insertion points

The holes were drilled on the grinding mill, namely on the liner; and shell as shown in Figure 4.4. The thermistors were then installed on the liner and shell. These gave the temperatures of the lifter/liner and shell.

The front plate was drilled and a steel pipe of diameter 20mm was inserted through it. The copper tube with a thermistor inserted through it was then put inside the steel pipe. The copper tube was glued inside the steel pipe. The thermistor suspended in the copper tube in the mill provided the temperature of the air above the load (Figure 4.3). Another temperature was suspended at the back of the mill rig and above it to record ambient temperature. The temperature of the load was measured by inserting a thermistor into a steel ball. This was held firm to the ball by means of a cable and wires twisted around it and connected to the front plate. The cable had electric wires inside it carrying information on the load temperature. The ball under consideration was suspended in the mill and allowed to tumble with the load.

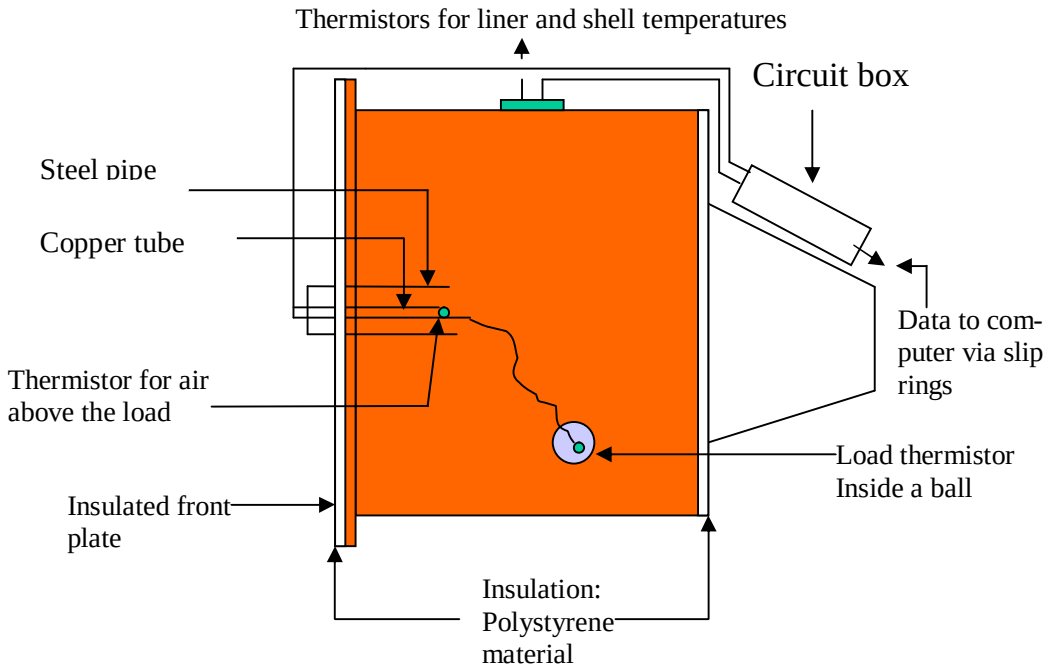

Figure 4.3: Measurement of the temperatures of the load and the air above the load inside the mill grinding chamber

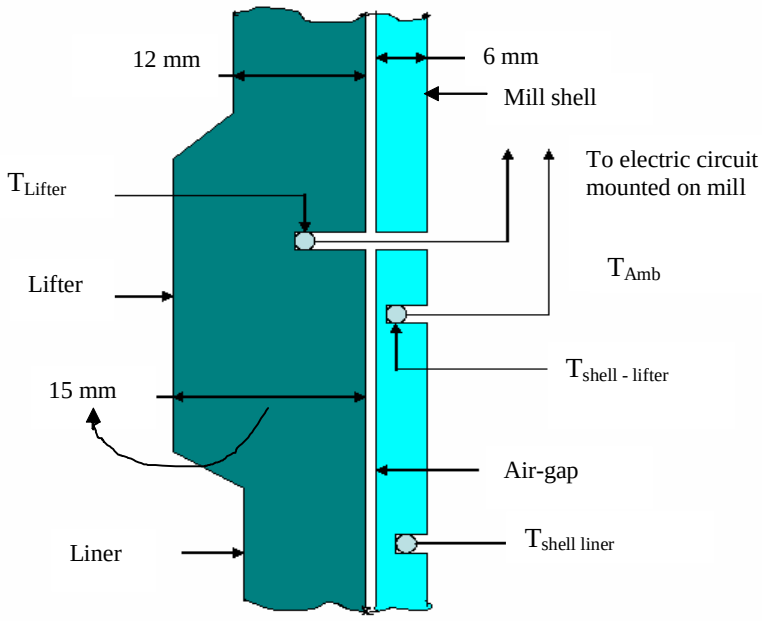

Figure 4.4: Section of mill wall for measurement of the liner and shell temperature

4.4 Temperature probe calibration

The very factors which make thermistors more useful than other temperature detectors, namely, small size, fast response, and high sensitivity, also present problems in their testing and calibration. In general, thermistors and assemblies should be calibrated in a well-circulated temperature-controlled liquid bath.

The thermistors were first calibrated electronically prior to installation so as to convert the electrical resistance of the thermistor to a temperature. Calibration of the thermistors also introduces measurement reliability in the form of accuracy and precision. Calibration was carried out by comparison with a mercury-in-glass thermometer. A voltage temperature characteristic was achieved in this calibration. Details of the calibration equations and constants are given in Appendix A.

The first calibration was carried out in the laboratory where the mercury thermometer and the thermistor were placed in the same constant temperature environment. The thermistors were wrapped in thin plastic sheets to avoid them getting wet. The mercury thermometer was used to measure the water bath temperature. The temperature was then coupled with the voltage output of the thermistor (read from the voltmeter) to give a temperature-voltage pair for the thermistor. The temperature of the calibrating bath was then changed and the process repeated. This was continued until the entire temperature range to be covered was completed. A similar procedure was followed when calibrating the thermistors on the mill except that the voltages were read from the laboratory PC computer via slip rings mounted on the mill rig. The experimental (calculated) data was compared with that measured from manufacturer's data as shown in Figure 4.5.

4.4.1 Calibration Curves for the Temperature Probes

(a) **Laboratory Calibration**

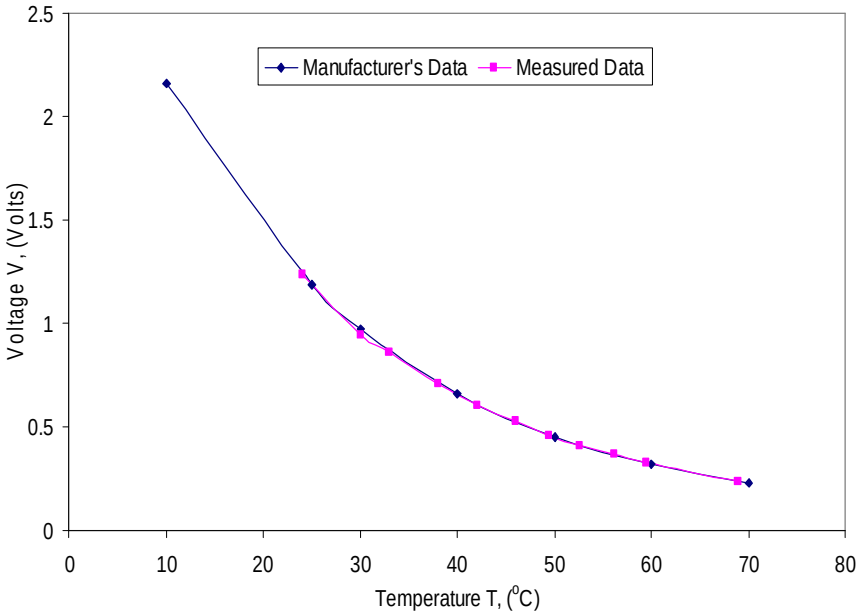

Figure 4.5: Laboratory temperature probe calibration

(b) **Calibration on the mill circuit for the Temperature Probes**

Table 4.1 shows the output voltages for the four thermistors and their variation with temperature during the calibration of the thermistors. The variation of temperature with voltage for the data from manufacturers has also been included in the table to compare with data from the calibration. The bead thermistor was used to measure the temperature of the load, air above the load, the liner and shell. The disc type thermistor was used to measure the environmental temperature. In both cases, calibration was done.

Table 4.1: Calibration of the temperature probes (Bead Type Thermistor): Table of temperature and voltage for the probes for the liner, shell, load and air above the load

	Output Voltages as read from PC computer				Manufacturer's data	
Calibration Temperature (^{o}C)	Liner (V)	Shell (V)	Load (V)	Air above load (V)	T	V
14.8	1.81	1.80	1.81	1.79	10	2.16
21	1.43	1.43	1.41	1.42	25	1.19
26.2	1.10	1.12	1.10	1.10	30	0.97
31	0.94	0.94	0.93	0.94	40	0.66
36.1	0.77	0.76	0.75	0.77	50	0.45
41	0.63	0.629	0.628	0.63	60	0.32
46	0.52	0.51	0.50	0.53	70	0.23
50.8	0.43	0.43	0.43	0.43		
56	0.37	0.375	0.374	0.375		
60.9	0.32	0.31	0.30	0.31		
65	0.282	0.28	0.28	0.282		
69	0.241	0.243	0.24	0.242		

Table 4.2: Table of temperature and voltage for the ambient thermistor calibration and values from the manufacturers (Disc Type Thermistor)

Manufacture's Data		Thermistor Calibration	
Temperature	Voltage	Temperature	Voltage
0	3.79	15.7	1.67
10	2.23	22	1.25
25	1.22	28	0.98
30	0.996	34.7	0.74
40	0.64	39.8	0.61
45	0.52	44.9	0.499
50	0.39	51.5	0.385
60	0.26	55.4	0.33

4.5 Torque measurement

The measurement of torque provided the data for the net power drawn by the mill. The torque was measured by use of a calibrated torque load beam.

4.5.1 Torque calibration

The torque-voltage relationship was achieved in this calibration. The torque was calibrated using a torque arm bar mounted at the back of the mill. Various loads of different masses were added on the bar. Before the masses could be added, a no load torque and that of the container holding the masses were determined. The no load torque was obtained at various speeds of interest. The mill was allowed to run after setting it to the mill setting of 1000 (41.5% of critical). For each load added, the voltage was recorded. The torque is then found by multiplying the force exerted by the weight of the load on the torque arm bar, and the perpendicular distance from the point of application of the force due to the weight of the load (on one end of the beam) to the center of the mill. The power is then computed from the relationship:

$$P = \frac{2pNT}{60},$$

Where:

N is the speed of the mill in revolutions per minute

T is the Torque

The following graph of Torque versus Voltage was obtained from the calibrations.

The data obtained in this experiment is given in Appendix B in Table B1.

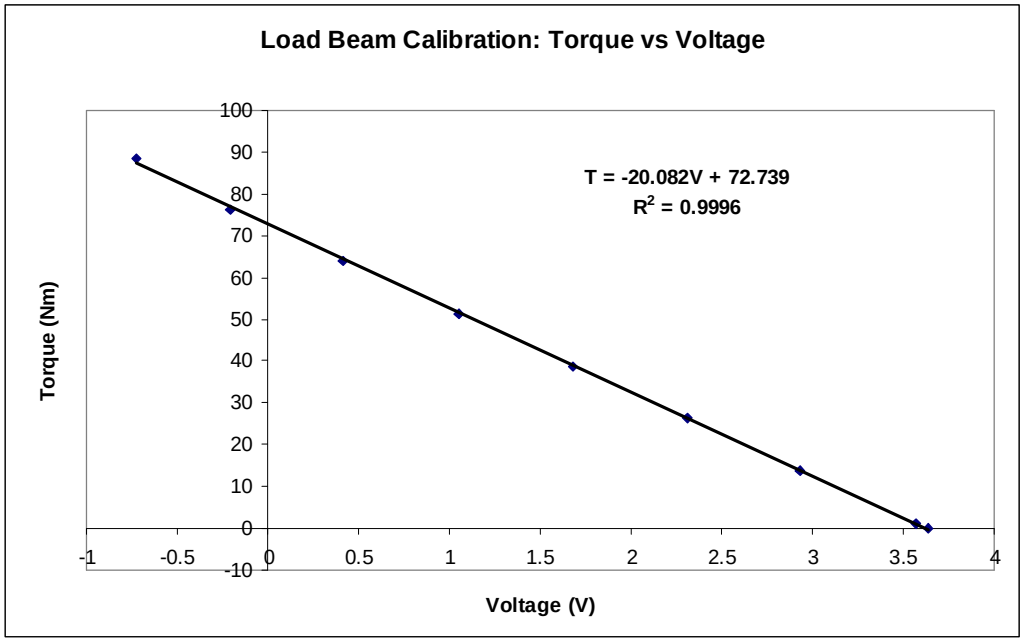

Figure 4.6: Calibration of the torque load beam: Variation of torque with voltage

4.6 Measurement of Sound energy

The Sound and Vibrations Analyzer was employed to measure energy dissipated into sound. This portable sound and vibration analyzer SVAN 912A has been dedicated for the signal measurement and analysis in the frequency band: 0.8 Hz – 22.6 kHz. The instrument is able to operate in the field using an internal battery. Depending on the selected operating mode, the SVAN 912A can be used as "Type 1" Sound Level Meter, "Type 1" Vibration Meter or Real-Time Signal Analyzer. In this study, the instrument was used as a Sound Level Meter.

After the power is switched on and the end of the "self test", the main menu control window is presented on the instrument's display. It contains four basic options: meter mode, analyzer mode, calibration and auxiliary functions. The Meter Mode provides the user with the standard functions of the Integrating Sound Level Meter and Vibration Meter. It is also possible to measure the RMS of the voltage in this mode. The Analyzer Mode provides the user with the standard functions of the Real Time Signal Analyzer. The Calibration provides the user

with the measurement channel. The Auxiliary functions provide the user with the rest of the instrument control options (e.g. the interface transmission speed, the polarization voltage of the condenser microphone, time and date setting e.t.c.) and the control of the battery condition.

For the sound measurement, the system configuration is as follows:

- Sound and vibrational analyzer SVAN 912A,
- ½" microphone SV 01A,
- Measurement microphone SV 02/C4
- And optionally, an SV 03A calibrator or any other compatible.

The data collected and results for sound energy measurement are presented in chapter 6. The calculation of the sound energy is presented in Appendix F of the Appendix section.

4.7 Experimental Procedure

The milling experiments involved varying the mill speed and mill filling. A number of mill speeds were employed: these were: 30, 50, 65, 75, 80, 85, 95, 105, and 120% of the critical speed. Mill fillings of 20%, 25%, 30% and 40% were employed in the experiments. For each mill filling, the mill was run at different mill speeds. The experiments were conducted with dry steel balls only. No ore was added to the mill as of interest was the thermal energy loss to the environment and not the energy used in comminution. The grinding media made of steel balls were first heated in an oven to a temperature of about 40-60^{o}C prior to the milling process. The steel balls while still hot were then introduced into the grinding mill. Milling was done for 4-hours to allow it to come to steady state. The grinding mill was allowed to come to steady state under one set of conditions. The initial temperatures of the load, air above the load, liners and shell were recorded for each experiment. It should be noted that it was not possible to measure the temperature of the load while in the oven. The oven did not have a provision for

direct temperature measurement. Therefore to measure the initial load temperature, a thermometer was inserted into the load prior to milling to provide an indication of the load temperature. Steel ball of size 6, 10 and 20mm ball size were employed as grinding media in the experiments. The 10mm ball size however constituted the bulk of the grinding media (about 80%).

All variables, power, sound and process temperatures (which include; load, air above load, liner, shell and ambient temperatures) were recorded. All variables were measured on-line during the entire duration of the experiments. Sound energy was also measured throughout the entire experiment by means of a separate external Sound and vibrations Analyzer circuit. The signal lines for power and temperature measurements were interfaced to a laboratory PC which was programmed to collect data continuously and to store 10-s averages of all variables on disk for subsequent processing. The raw data collected from the computer was transferred to a personal computer where all analysis was done.

4.8 Difficulties Encountered

In the experimental work, a number of difficulties were experienced. Some signal channels for temperature data on the laboratory PC were quite noisy. This could in a way affect some readings. This was kept to a minimum as calibrations were done prior to the experiments.

The equipment (oven) in which the steel balls were heated did not have a provision where the ball temperature could be read or determined. It was therefore difficult to determine the initial temperature of the balls right from the oven. This was only measured by a thermistor inserted in a ball after the hot balls have been removed from the oven. The initial temperature varied from experiment to experiment. The balls were heated for about 2 to 3 hours prior to the experiment. During this period of time, it was expected that the balls would be hot enough for the experiment. Overall the initial temperature of the balls varied between 40 to 60^{o}C.

4.9 Summary and Conclusion

The measurement of temperature in a grinding mill has been done. The experimental work conducted is rigorous and novel. The temperatures of the milling system so measured were the temperature of the load, the air above the load, the liners and the mill shell. Thermistors were employed in the measurement of temperature data as they were precise and sensitive. They are also cheap, readily available and easy to calibrate. The calibration of the thermistors was done for accuracy and precision in the measurements.

The Torque load beam was easily calibrated and this was used to provide the power input to the mill. Enough data was obtained from the sound analyzer which provided the sound energy data.

Chapter 5

Analysis of the mill temperature data

5.1 Introduction

The various measurements were made to the mill and data was obtained as is given in the following section. The measurements included the power transmitted to the mill, the mill process temperature and the environmental temperature. The figures below present the variation of mill temperature with mill speed and mill load volume. New Matimba liner profiles shown in Figure 4.4 were installed on the mill in these experiments.

5.2 Results of the milling process

The data presented in the following figures shows the variation of mill power, mill process temperatures and ambient temperature with time at various mill speeds. A moving average of 10 was used to plot these data.

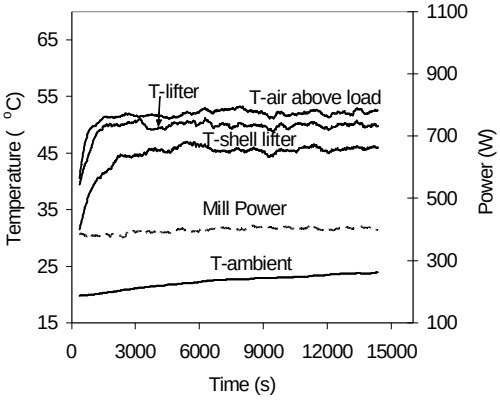

Figure 5.1 (a)

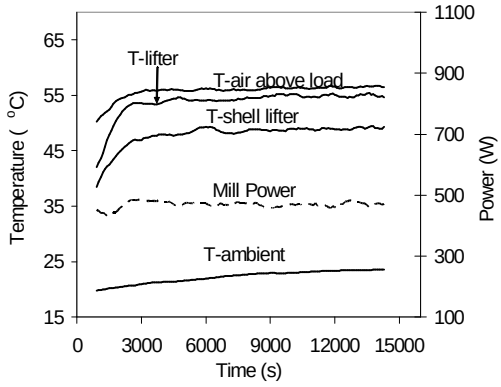

Figure 5.1 (b)

Variation of mill power, mill process temperatures and ambient temperature with time at a mill filling of 20% and mill speed of (a) 65%, and (b) 75%

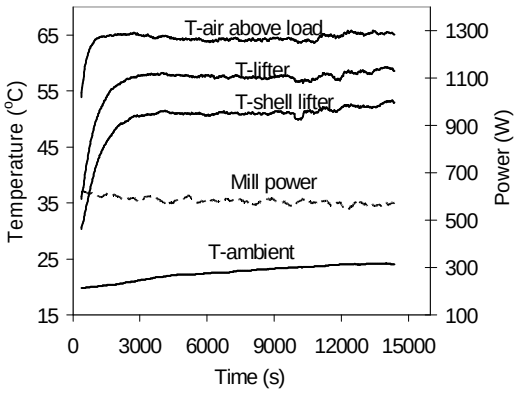

Figure 5.1 (c)

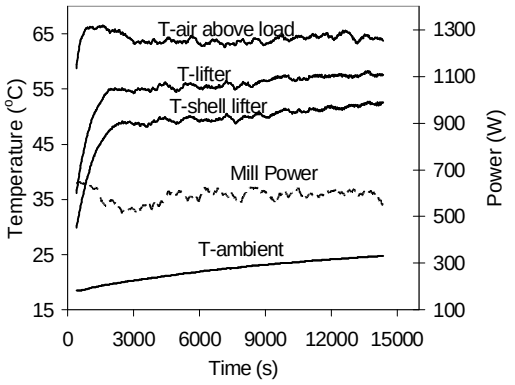

Figure 5.1 (d)

Variation of mill power, mill process temperatures and ambient temperature with time at a mill filling of 20% and mill speed (c) 95%, and (d) 105%. Liner profile: Matimba new liner

The mill filling was then increased to 25% using the same mill speeds and milling time as in the previous experiments. Some of the measured temperatures, mill power and ambient temperature are shown in Figures 5.2 (a) and 5.2 (b):

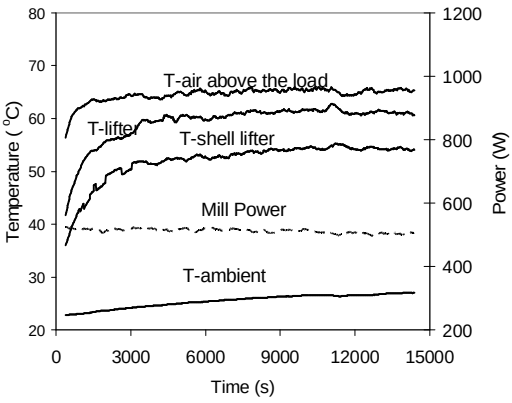

Figure 5.2 (a)

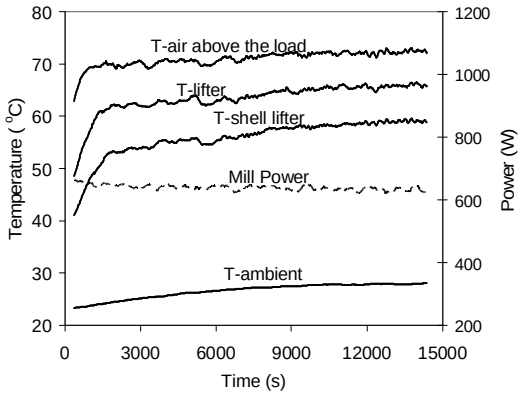

Figure 5.2 (b)

Variation of mill power, mill process temperatures and ambient temperature with time at a mill filling of 25% and mill speed of (a) 75%, and (b) 95%. Liner profile: Matimba new profile

As explained earlier, experiments involving load volumes of 20 and 30 did not involve measuring the temperature of the load. So this data is not available. This was before a new set up to measure the load temperature was introduced.

The mill filling was again increased to 30%. In these experiments, the load temperature was now taken into consideration. The experiments were repeated at speeds of (a) 30% , (b) 50%, (c) 80% and (d) 120%. The following Figures show the variation of mill process temperatures and mill power at a mill filling of 30%.

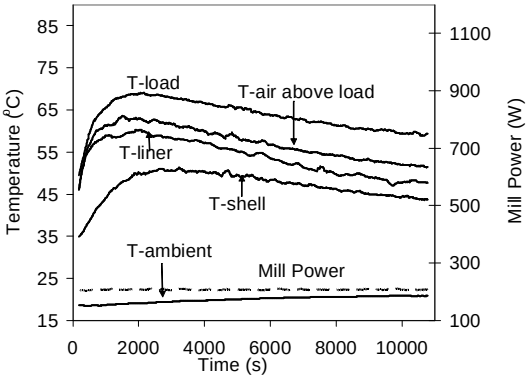

Figure 5.3 (a)

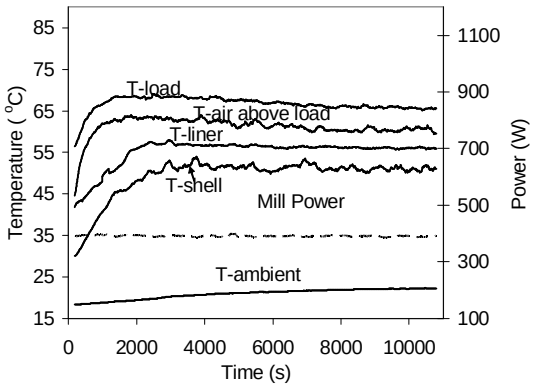

Figure 5.3 (b)

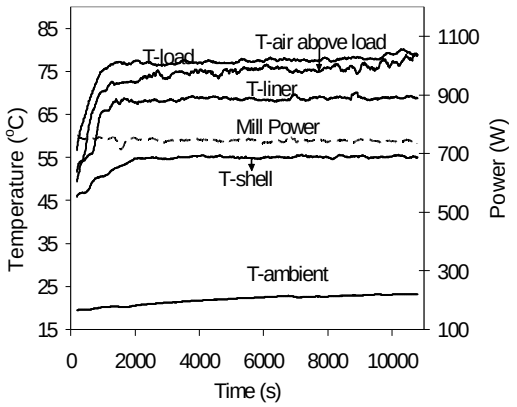

Figure 5.3 (c)

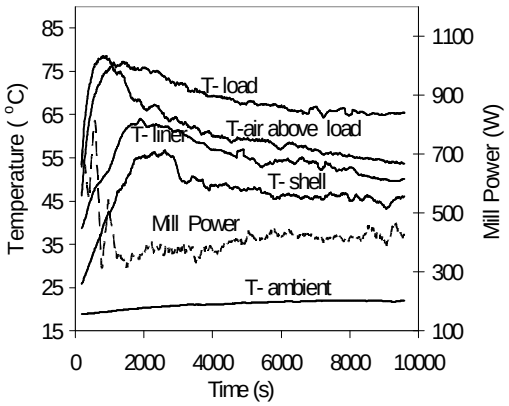

Figure 5.3 (d)

Variation of mill power, mill process temperatures and ambient temperature with time at a mill filling of 30% at varying mill speeds of (a) 30% (b) 50% (c) 80% and (d) 120%. Liner profile: Matimba new liner profile

It can be observed in Figure 5.3(a) that the mill temperatures are decreasing. The reason for this is that the since the mill speed is very low, the mill was losing more thermal energy to the environment than was generated. Hence a drop in the mill process temperatures.

Finally the mill filling was raised to 40% and the measurement of mill power and temperature data are as follows. Variation of mill power, mill process temperatures and ambient temperature with time at a mill filling of 40% and mill speed of (a) 75%, (b) 85% and (c) 105%

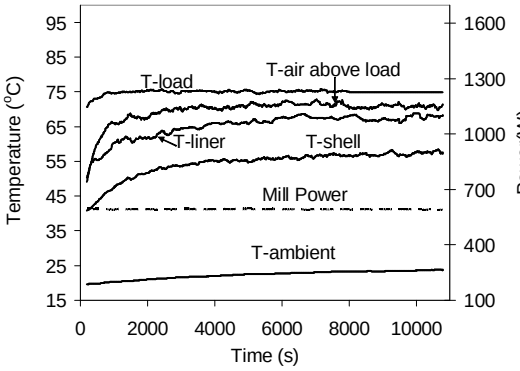

Figure 5.4 (a)

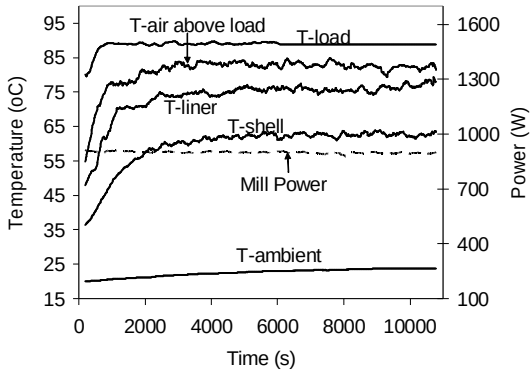

Figure 5.4 (b)

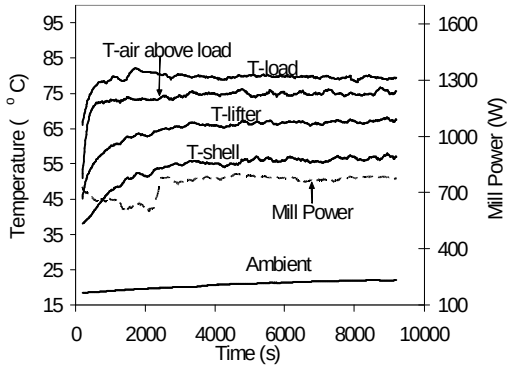

Figure 5.4 (c)

Variation of mill power, mill process temperatures and ambient temperature with time at a mill filling of 40% at varying mill speeds of (a) 75% (b) 85% and (c) 105%. Matimba new liners

5.3 Analysis of the temperature probes data

The mill temperature probe data was meant to measure the temperature of the load, the air above the load, the liner and the shell. The load temperature probe showed a remarkable temperature rise as compared to other temperatures. This is expected as it is measuring a high temperature region in relation to other regions under consideration. The power is transmitted to the load first at the load-liner interface and therefore thermal energy generation takes place in the load. Energy is then transferred from the load to the air above the load and to the liners, and from the load directly to the liner and through to the environment. Generally, the power transmitted to the load is responsible for the temperature increase of the load and therefore the whole system. The load thus transfers energy to the air above the load, the liner, the shell and ambient. Initially both the temperature of the shell behind the liner and shell behind the lifter were measured. It was observed that the temperatures of the shell behind the lifter and that of the shell behind the liner were almost identical. Therefore only one of these was considered, in this case the shell behind the lifter, or simply the mill shell temperature.

The ambient temperature appeared to be almost constant. However, this will vary from day to day. The ambient temperature in this case is vital as it is one of the factors that affect the rate of energy loss from the grinding mill. On a day when the ambient temperature is low, more energy will be leaving the mill due to a higher temperature gradient between the mill and the environment.

It can also be observed from the results that the temperature of the milling system increases with increasing mill speed and load volume. For instance from Figure 5.1(a) to Figure 5.1(d) at a load volume of J=20%, the mill speed is varied from 65 to 105% of the critical. It is observed that as speed increases, there is a corresponding increase in mill process temperatures. However, as the speed reaches supercritical speeds, there is a decrease in mill temperatures. This is evident from Figure 5.3 (d). This is because at supercritical speeds, centrifuging of the load occurs which lead to the reduction of mill diameter and therefore reduces

the active mass of the load. When this happens, power transmitted to the mill and therefore thermal energy generation is reduced. This results in the reduction of the mill temperatures.

5.4 Variation of process temperatures with speed and load volume

Generally mill process temperatures increase with both mill speed and load volume. As the mill speed increases, a higher kinetic energy is transferred to the grinding media which results in more cataracting and therefore a higher energy generation resulting in a higher temperature rise. A higher mill load volume leads to a higher power draw, and hence to a more energy transfer resulting in a higher temperature.

5.5 Dynamic (Transient behaviour) of grinding mill temperature

The transient behaviour of temperature with time for steel balls at room temperature was investigated. In this experiment, the steel balls at room temperature were introduced into the grinding mill. The speed was set at 75% of the critical and a mill filling of 15% was employed. The mill load consisting of steel balls only of size 6-10mm in diameter was run for 1 hour and 30 minutes. The balls were not heated as in the other experiments. Trapezoidal liners with an inclined angle of 45^{o} were used.

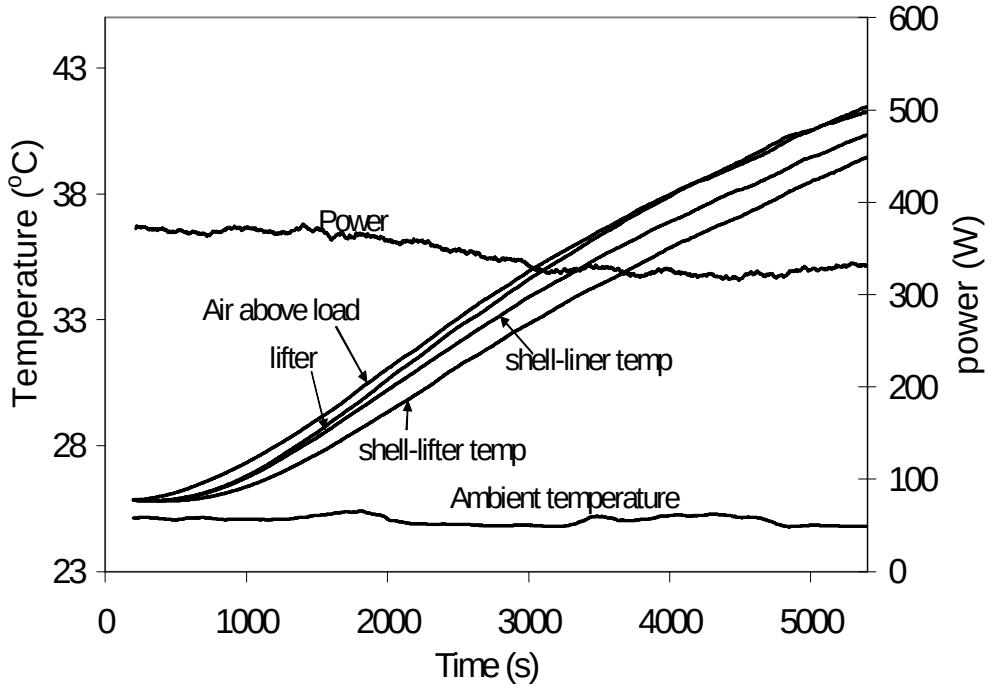

Figure 5.5: Transient variation of mill power and process temperatures with time

The graph shows that the variation of mill power, process temperatures and ambient temperature with time. It is observed that the mill will take a long time to reach a steady state when steel balls are not heated prior to milling. This is because the balls have a lower energy content and therefore it will take a long time for the mill temperatures to be steady.

In order to effectively further enhance the understanding of temperature behaviour in the milling process; a number of other control parameters were investigated. These were ambient temperature and water addition to the mill. Ambient temperature is an important variable in thermal modeling of the grinding mill. The ambient temperature in this case is vital as it is one of the factors that affect the rate of energy loss from the grinding mill. Water addition to the mill and its effect on mill process temperatures and power was also considered. This is given in the following sections, (5.6) and (5.7). For continuous mill operation, adding ore is also another critical factor. If the circuit is closed with a screen/cyclone and has a pebble-crusher recycle, then these two streams returning to the mill also play a part. In addition the presence of ore and water would have a major impact on the

rate of energy transfer inside the mill. For instance, the evaporation of water could reduce the rise in temperature.

5.6 Effect of sudden water addition to mill on mill process temperatures and power

Hot balls at a mill filling of 20% were introduced into the mill. The mill was run at a speed of 65% of the critical. 10 kg of silica powder was added to the mill proving a 100% particle filling the voids between the balls. The ball size used was 6 – 10mm. The grinding mill was then allowed to run for 45 minutes at a steady state temperature after which the mill was stopped momentarily and then 1 liter of cold water was added. The mill was then allowed to run until it came to a new steady state. The internal mill shell was lined with 45^{o} inclined angle Trapezoidal liners. At a point when the mill was stopped, it is observed that the mill power was zero. The process temperatures, ambient temperature and mill power were then observed and measured at a new steady state.

It is observed from Figure 5.6 that addition of cold water to the mill results in a decrease in mill temperatures. It is also observed that there is a decrease in power. This is due to the fact that as water is added to the mill, some portion of the load becomes attached to the walls of the mill. In other words premature centrifuging occurred which resulted in a reduced mill diameter and effective mass of the mill load and therefore a reduction in power drawn by the mill. Packing of the load was observed in the mill liners.

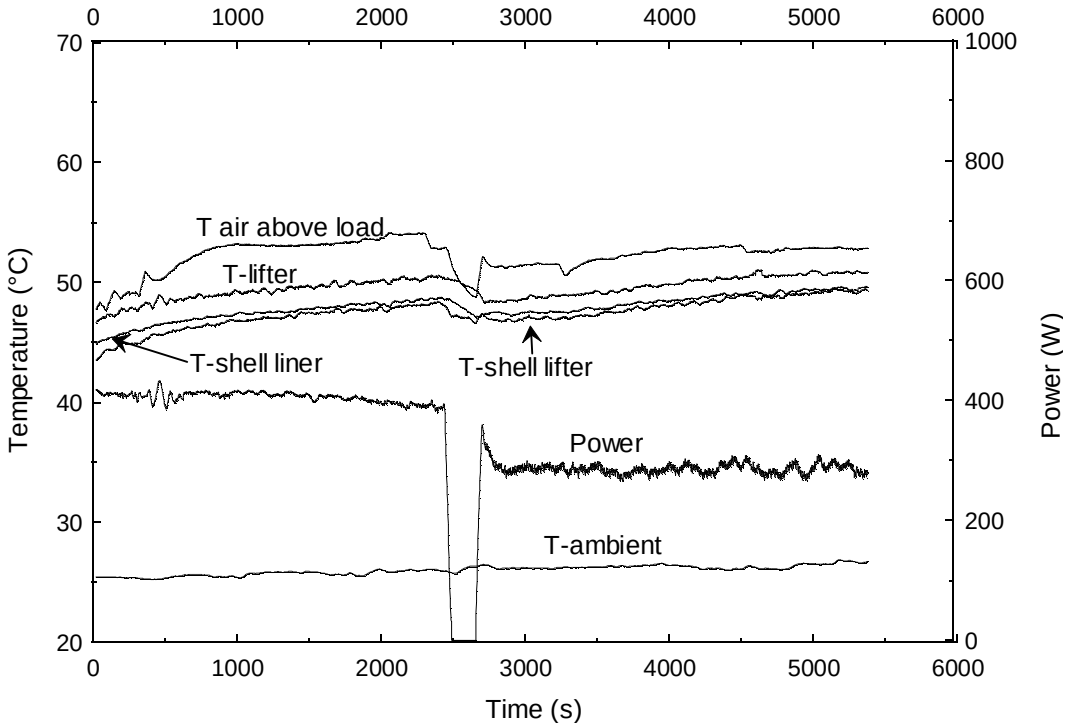

Figure 5.6: Effect of water addition to mill on power and process temperatures

5.7 Effect of change in ambient conditions on mill temperature

Ambient conditions were changed in the grinding mill room and the effect on the mill process temperatures was investigated. To achieve this, the mill grinding room was heated over night by means of a heater. The following day in the morning, grinding media at a mill filling of 30% at room temperature was introduced into the grinding mill with the heater still on and all doors and windows closed. The milling process was carried out for a period of 5 hours at a mill speed of 75% of the critical. The mill shell was lined with new Matimba liner profile. To effect a change in ambient temperature, the heater was switched off and doors were opened after 3 hours of milling to allow fresh air into the mill room. There was sudden change in ambient temperature as evidenced from the results taken.

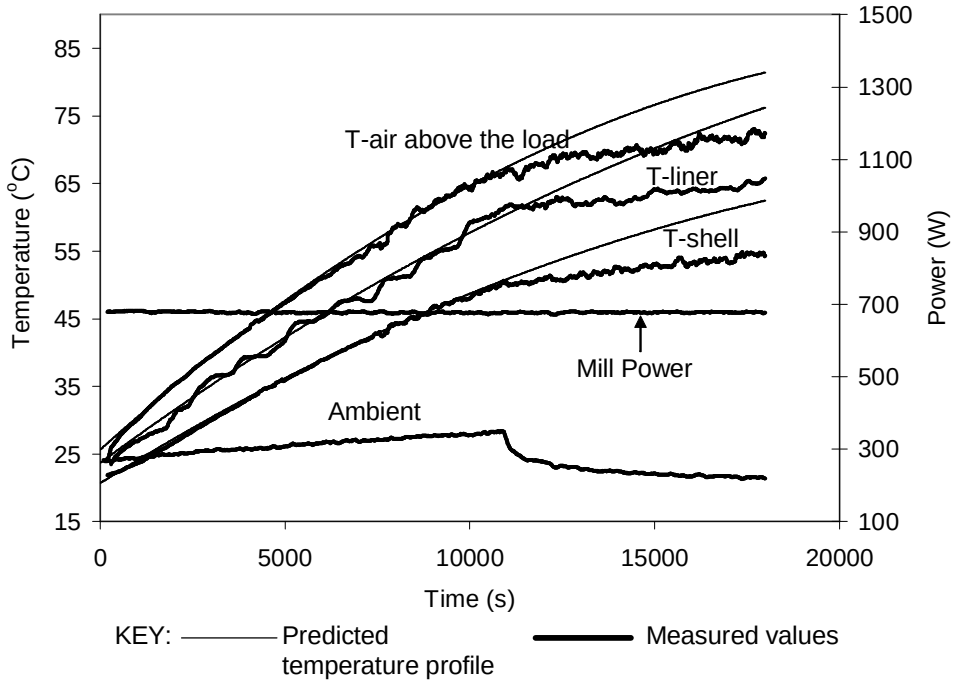

Figure 5.7: Effect of change of ambient temperature on mill process temperatures- Mill filling, 30%: Mill Speed, 75%: t=5 hours

It can be seen from figure 5.7 that as the ambient temperature is decreased, the mill process temperatures increase at a lower rate. The predicted temperature profile is also shown in the figure. More energy is released to ambient due to the increased temperature gradient between the grinding mill and the environment. The environmental temperature is thus an important factor as far as thermal energy loss through the mill shell to the environment is concerned. It can be concluded that variations in ambient conditions affect the rate of energy transfer from the mill to the environment.

5.8 Conclusions

Temperature measurements in the milling process will lead to the understanding of temperature behaviour in milling. Knowledge of temperature behaviour in

grinding mills is as important as knowledge of other mill parameters critical to the operation of the mill.

Temperature results generally show that there is a remarkable difference between the temperatures in each of the regions considered. The effect of mill load and mill speed has also been studied. The study shows that the higher the mill speed, the higher will be the temperature of the milling system. At supercritical speeds, the temperature drops. Likewise, the bigger the mill load, the more pronounced the temperature rise is. Ambient temperature was observed to be almost constant. Although this is constant, it has an effect on the mill process temperature and therefore the energy loss from the system.

Chapter 6

Results of Power and Sound Energy Data

6.1 Results of the Torque data

The torque data was analyzed to determine the net power drawn by the grinding mill. The active charge within the mill is assumed to exert torque acting against the rotation of the mill. The torque of the active charge is calculated from the calibrations and subsequently it's associated power. The sum of all the powers associated with all elements of mass therefore will give the net power draw associated with the entire charge.

Two main variables were investigated in the experiments to determine their effects on mill power and temperature. The Figures have been plotted for mill fillings of 20 and 30% at varying mill speeds.

Figure 6.1 shows the variation of mill net power with mill speed. The mill filling in this experiment was fixed at 20%. The mill speeds employed were 65, 75, 95 and 105% of the critical speed. The corresponding net power was measured from the calibrated torque load beam. It can be observed from the results that as the speed of the mill increases, there is a corresponding increase in net power drawn by the mill. At a speed of 105% however, there seems to be no further increase in the power drawn by the mill. This is attributed to centrifuging of the mill load at this speed. There is a decrease in mill power and this is also evident from the decrease in the temperature of the air above the load as is shown in Figure 5.1 (d) of chapter 5. This behaviour has been explained in chapter 5. It is expected that at much higher supercritical speeds (higher than 105% of the critical), the mill power will decrease even further and so will be the mill process temperatures.

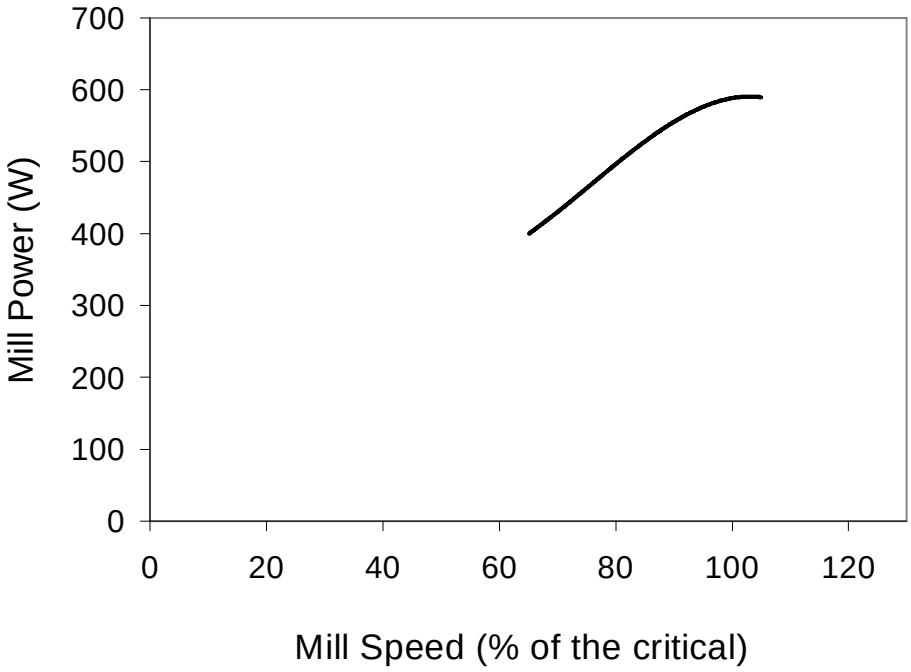

Figure 6.1: Variation of mill power with mill speed at a mill filling of 20%

The behaviour of mill power with mill speed is also observed at a much higher load volume of 30%. This is shown in Figure 6.2.

In Figure 6.2 below, the condition of centrifuging becomes more apparent. In these experiments, the mill filling was maintained at 30%, while the mill speeds were varied: the speeds were: 30, 50, 80 and 120% of the critical speed. At 120% a large portion of the load was centrifuging which resulted in the loss of mill power. When the mill load centrifuges, there is a decrease in the effective mill diameter and a corresponding reduction in the active mass of the load resulting in the loss of mill power. In these experiments, it was also evident from the temperature data. The loss of power entails less thermal energy generation and therefore the decrease in mill process temperatures.

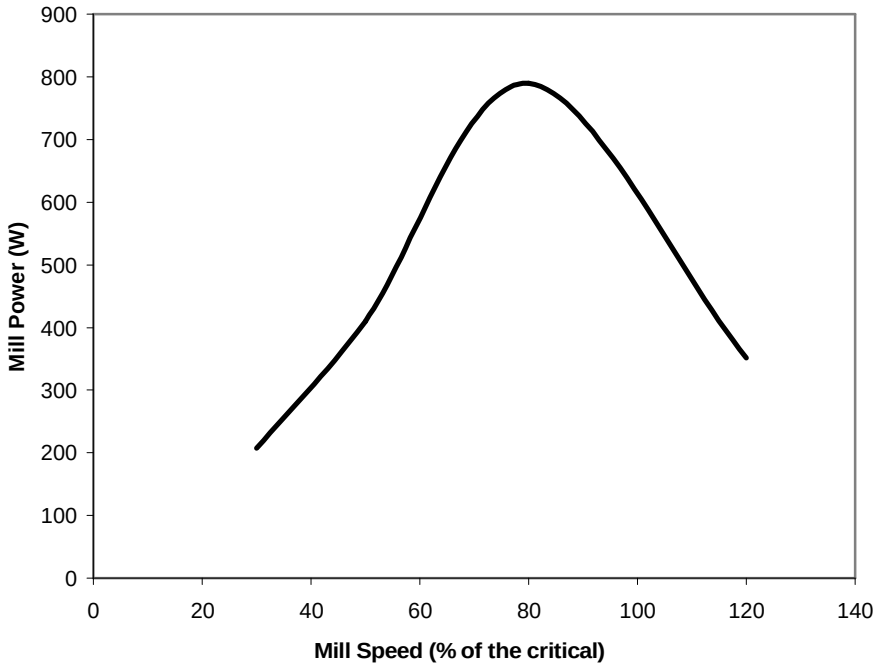

Figure 6.2: Variation of mill power with mill speed at a constant mill filling of 30%

From Figures 6.1 and 6.2, the maximum power at 20% load is approximately 590W. At a load volume of 30%, the maximum power is 790W.

6.2 Results of the Sound energy data

Data collected from the Sound and Vibration Analyzer was analyzed. The measurements were made in units of Decibels. This was then converted to units of energy per unit time integrated over the full surface area of the mill. The measured sound levels are shown in Table 6.1 below. The values tend to increase in intensity with increase in mill speed.

Table 6.1: Variation of sound intensity from the mill with the mill speed

%J=15, %Nc=40	60dB
%J=15, %Nc=65	68dB
%J=15, %Nc=75	74dB
%J=20, %Nc=65	76dB
%J=20, %Nc=75	83dB
%J=20, %Nc=95	87dB
%J=20, %Nc=105	89dB
%J=30, %Nc=30	64dB
%J=30, %Nc=50	70dB
%J=30, %Nc=80	90dB
%J=30, %Nc=120	98dB

The measurement of sound was obtained in the units of decibels (dB). The measured sound showed a small change with mill speed. The energy converted into sound was found to be equal to $0.004 J/s$. Moreover this value was so small that it was considered to be insignificant as compared to other forms of energy considered in this study.

The calculation of the sound energy is given in Appendix E of the Appendix section.

6.3 Conclusions

The amount of energy conversion into sound is far less than the power and the thermal energy loss. It is however important to quantify sound energy so as to determine the extent of the effect it would have on energy lost from the mill.

Chapter 7

Application of the mill temperature models to estimate and quantify parameters

7.1 Introduction: Analysis of steady state results

In this chapter, the temperature behaviour at steady state was observed. Temperature profiles at different mill conditions are presented. The important model parameters are quantified from the steady state models. The variables so determined are the overall heat transfer coefficients which provided an approximation of the energy loss from the system to the environment. The surface wall temperatures of the liners and shell were determined by linear interpolation since the middle temperatures of these regions were known from the measurements. Figures (7.1) and (7.2) show some of the data at steady state temperature distribution at various mill fillings and mill speeds.

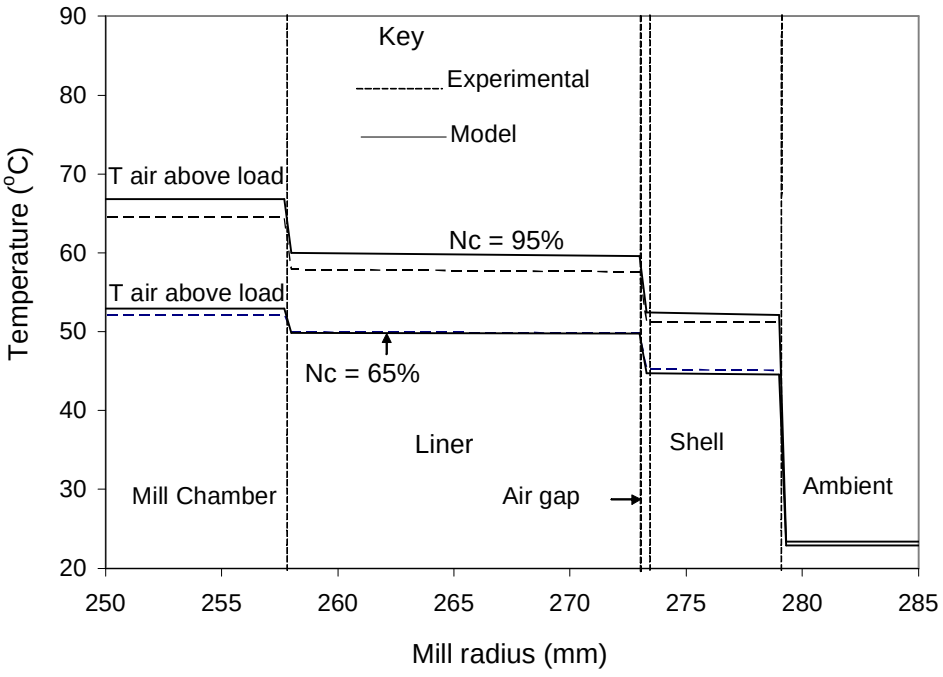

Figure 7.1: Temperature profiles of the grinding mill at different mill speed at a constant mill filling of 20%.

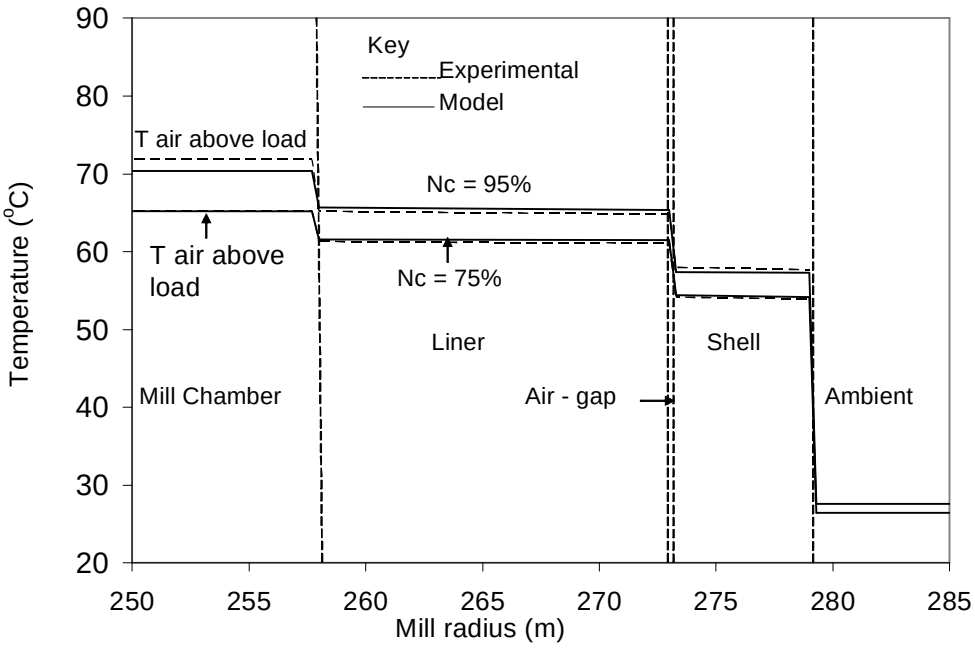

Figure 7.2: Temperature profiles of the grinding mill at different mill speed at a constant mill filling of 25%.

A comparison of temperature profiles at different mill speeds and load volumes shows that when the speed and load volume increase, there is a corresponding increase in the mill process temperature. For instance at a load volume of 20% and speed of 95% of the critical, the temperatures of the air above the load, liner and shell are 64.9, 60 and 52^{o}C respectively. As the load volume is raised to 25% at the same speed of 95%, there is an increase in mill process temperatures to 71.9, 66.7 and 57.4^{o}C for the air above the load, liners and shell respectively. The same is the case with increase in mill speed. A summary of the results at varying mill conditions at steady state is given in Table F1 in Appendix F.

An interesting situation occurs at supercritical speed. As the speed of the mill reaches a supercritical state, there is a significant decrease in the mill power which is marked by a decrease in mill temperatures. This happened due to the

centrifuging of the load at very high speeds. This is evident from the DEM simulations performed as given in section 7.3.

7.2 Analysis of steady state temperature

Steady-state results were analyzed to obtain estimates of the individual heat transfer coefficients and therefore the overall heat transfer coefficient. These were quantified under varying mill conditions (mill speed and mill filling). Figure 7.3 shows a temperature distribution at a mill filling of 30% and a speed of 80% of the critical. Similar figures for other mill conditions are presented in Appendix G.

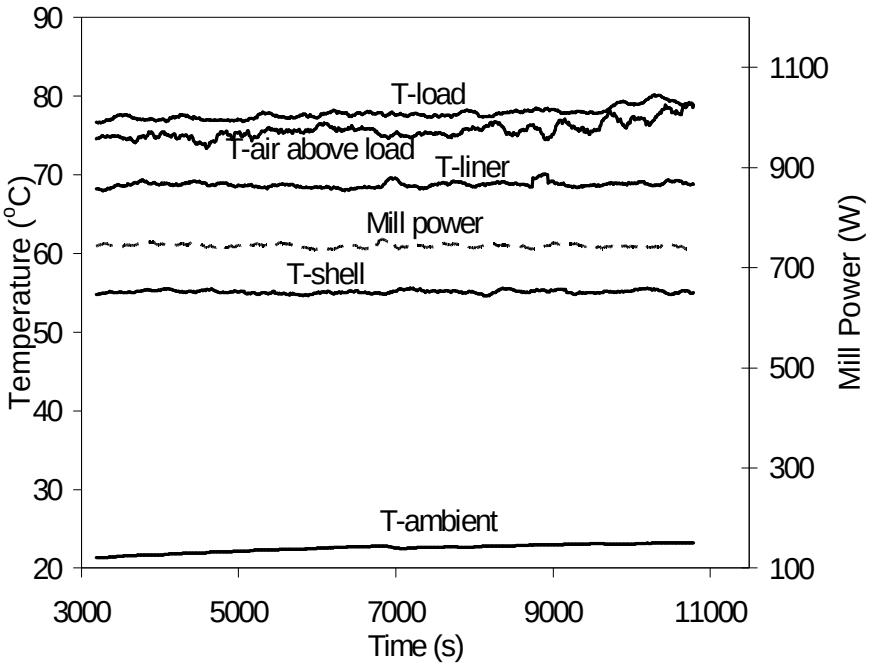

Figure 7.3: Mill Power and Steady state mill process temperature distribution, J=30%, N=80% and t=3 hours

7.3 Quantifying the overall heat transfer coefficients

7.3.1 Model validation

The importance of model validation cannot be over emphasized. Model building is based on approximations and assumptions that necessarily cause the model to be

removed somewhat from reality. Therefore, the model must be checked against the real world to determine its adequacy in making predictions that are accurate enough to be useful. In other words, the measurements of temperature and the overall heat transfer coefficients made in the process are compared to model predictions.

7.3.2 Determination of the ball-air and ball-metal surface heat transfer coefficient

The heat transfer coefficients inside the mill can not be calculated from the steady state energy equations since neither Q_{LD-L}, Q_{LD-AIR} nor Q_{AIR-L} are known. The two paths of energy transfer from the load to the environment are parallel and therefore the steady state energy equations in the inside of the mill can not be solved simultaneously to obtain $hA_{(LD-L)}$, $hA_{(LD-AIR)}$ or $hA_{(AIR-L)}$, from the measurements of P and the mill temperatures, T_{LD}, T_{AIR} and T_L. $h_{ext}A_{ext}$ is however obtained from the measurement of P, T_{S2} and T_{Amb}. To this effect, experiments were performed to determine the experimental heat transfer coefficients from the ball to metal surface and ball to air heat transfer. The heat transfer coefficients obtained from these experiments were employed in the milling experiments to obtain estimates of energy transferred from the load to the liner surface, load to the air above the load and the air above load to the liner surface. Of importance is the determination of the model for the overall heat transfer coefficient from these measurements. The diameter of the ball used in the experiments was 20mm; the mass of steel ball was 0.08kg and its specific heat capacity is 500W/kg ^{o}C.

(a) Ball – metal heat transfer coefficient: To achieve this, a thermistor temperature probe was inserted into a steel ball. The ball was heated to a temperature of 55^{o}C. This was then placed on a massive steel plate (30kg) which was at ambient temperature (24^{o}C). A pile of hot steel balls covered the ball with thermistor. Polystyrene material was then used to cover the hot balls to minimize loss of energy from the set up. The steel ball was kept in contact with the solid plate for 3

hours so as to allow the balls to cool down to ambient temperature. The temperature variation with time was then recorded as given in Figure 7.4 below.

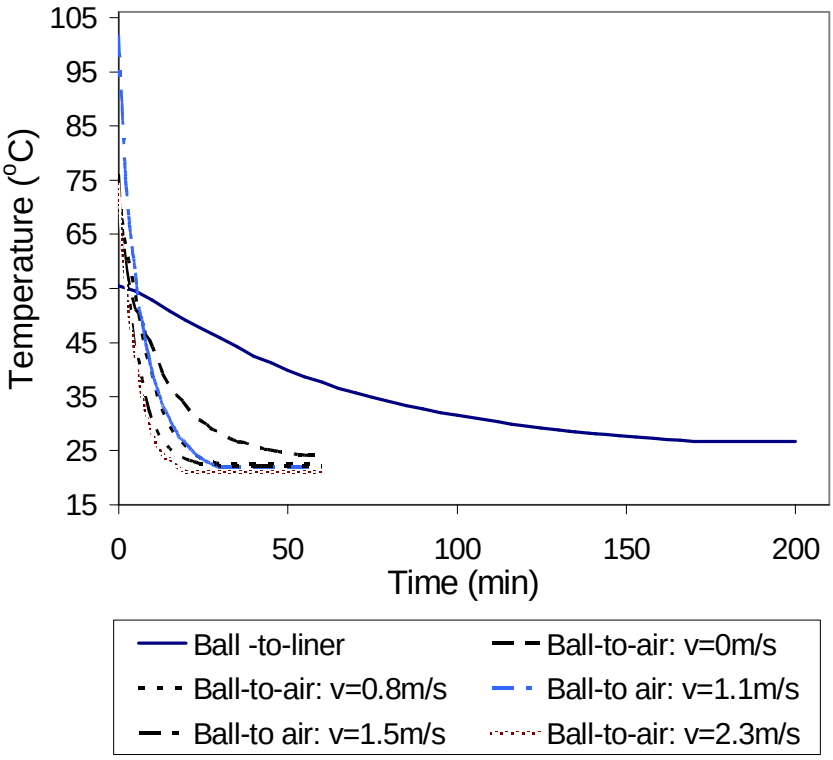

Figure 7.4: Variation of ball temperature with time for ball with thermistor covered in pile of heated balls and for ball swung in air at various velocities

(b) Ball – air heat transfer coefficient: The steel ball with the thermistor inserted in it was again heated to a temperature of 73°C. The steel ball was circulated on a circular path in air at varying speeds for as long as 60 minutes until the ball cooled down to ambient temperature. The following speeds were used in this experiment: 0, 0.8, 1.1, 1.5 and 2.3 m/s. The temperature variation of the ball with time at various velocities is given in Figure 7.4. The data for the ball to air at various velocities could only be obtained for as long as 60 minutes, hence the nature of the graph.

The model governing temperature distribution in a steel ball for the above experiments is given by:

$$m_B Cp_B \frac{dT_B}{dt} = hA(T_{amb} - T_B) \tag{7.1}$$

The solution for T_B is given by:

$$T_B(t) = T_{amb} + (T_{BO} - T_{amb})e^{-\frac{hA}{mCp}t} \tag{7.2}$$

where:

T_B is the temperature of the ball at time t

T_{amb} is the ambient temperature or temperature of steel plate

T_{BO} is the temperature of the ball at $t=0$

h is the heat transfer coefficient and A is the heat transfer area for the ball to the air or from the ball to the metal plate

m is the mass of the ball and C_p is the specific heat capacity at constant pressure

The value of hA is obtained by fitting equation (7.2) to the experimental data in a least squares sense. From equation (7.2), the value of hA computed for the ball to metal surface contact is 0.01W/^{o}K. hA for the ball to air contact varied with velocity of circulation and was found to vary from 0.06 – 0.13W/^{o}K depending on the velocity. The values of h for the ball to air were calculated since the heat transfer area from the ball to the air is known. These values are plotted in Figure 7.5 below. An equation relating the heat transfer coefficient from the ball to the air with the velocity from Figure 7.5 is given by:

$$h_{(ball-air)} = 26.08v + 46.64 \tag{7.3}$$

where: v is the average velocity of circulation. To determine the heat transfer coefficient from the ball to the air in the mill, we instead used the ball velocities obtained from the DEM simulations. Equation (7.3) was used to obtain the ball to

air heat transfer coefficients. The $h_{ball-air}$ obtained are then used to evaluate $hA_{(LD-AIR)}$ and subsequently $hA_{(LD-L)}$ and $hA_{(AIR-L)}$ as will be shown later.

The key is $v_{relative} = v_{par} - v_{air}$. Since v_{air} is not known, we therefore use the average velocity of the particles, v_{avg}. Therefore the heat transfer coefficients of the ball to air are obtained at various mill conditions from equation (7.3).

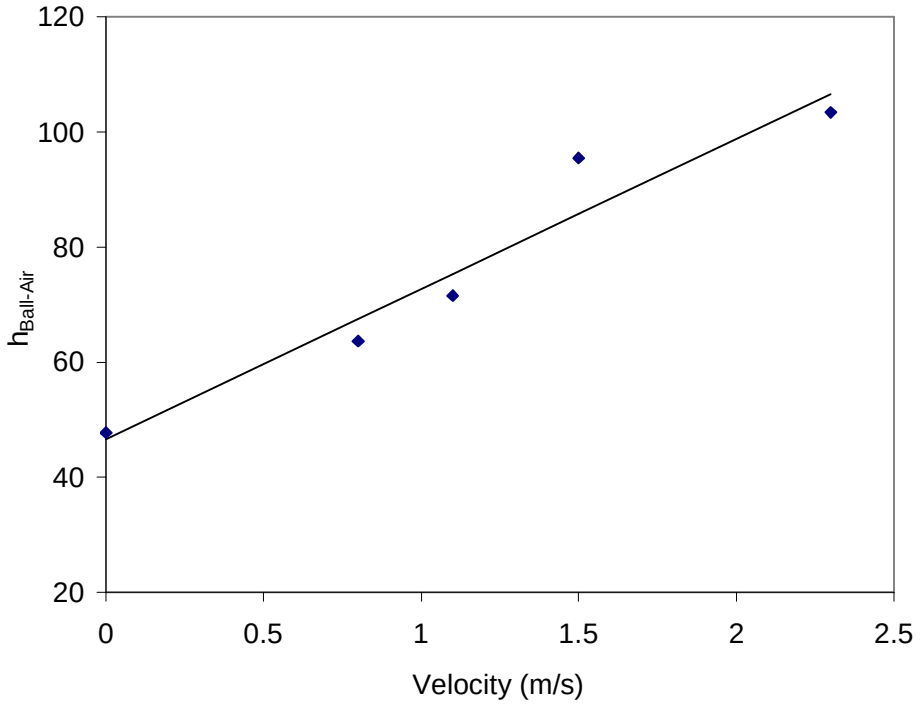

Figure 7.5: Ball to air heat transfer determination: Variation of $h_{Ball-Air}$ with velocity

Discrete Element Method (DEM) computer simulations were performed using Mill Soft 2D program (Rajamani et. al., 1996) to observe mill load behaviour in the grinding mill at varying mill conditions. 2D DEM simulations were employed as 3D DEM was not available at the time of the experiments. Otherwise 3D DEM simulations would have been preferred. Since we were not taking any pictures in the experiments as the front plate was non-transparent, we employed 2D DEM to have an idea of the behaviour of the load in the mill at varying mill conditions. The same mill conditions employed in the milling experiments were applied in the DEM simulations. In addition, from the Discrete Element simulations the ball

velocities and the approximate number of balls in contact with the air above the load and balls in contact with the mill liner surface were determined at various mill conditions. The steady state temperature measurements of the air above the load, the load, the liner surface, the mill shell and the environment were used to estimate the amount of energy leaving the mill via the liner and through the air above the load to the environment.

Discrete element models generally simulate the behaviour of solids by assembly of discrete elements. In the discrete element models, the forces between discrete components are calculated and used to determine the motion of the discrete components. During the simulation process, the simulation time is discretized into small time intervals. The velocities of each discrete component in each time interval are calculated and the positions of these discrete components are updated.

The discrete element method (DEM) was also employed to explain the particle behaviour and hence energy transfers in the mill at different mill operating conditions.

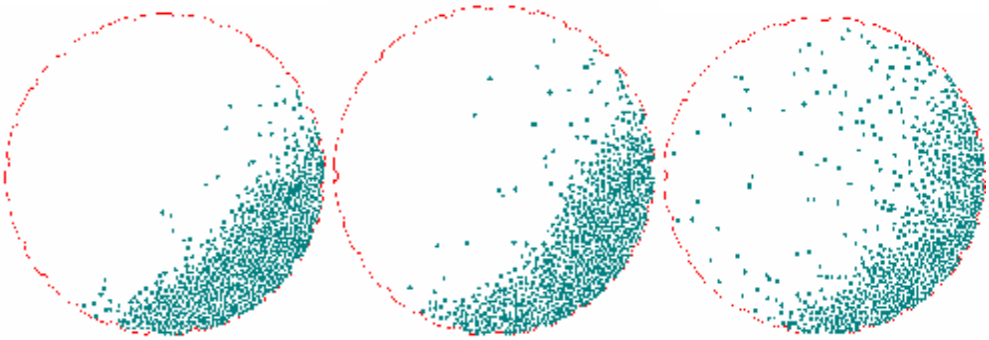

(a) %J=20, N_c =65 (b) %J=20, N_c =75 (c) %J=20, N_c =95

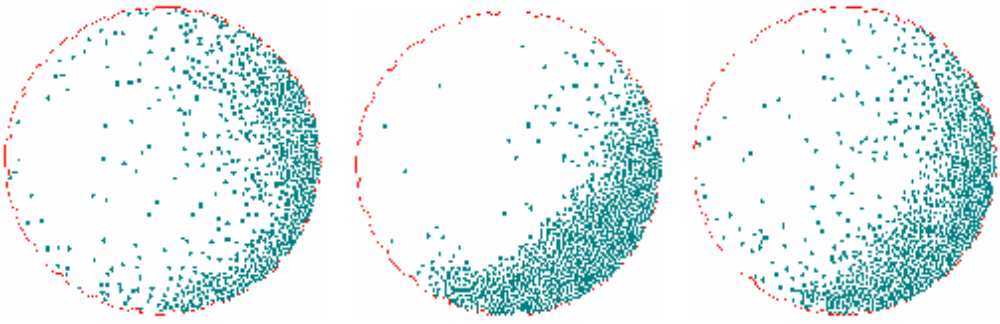

(d) %J=20, N_c =105 (e) %J=25, N_c =75 (f) %J=25, N_c =95

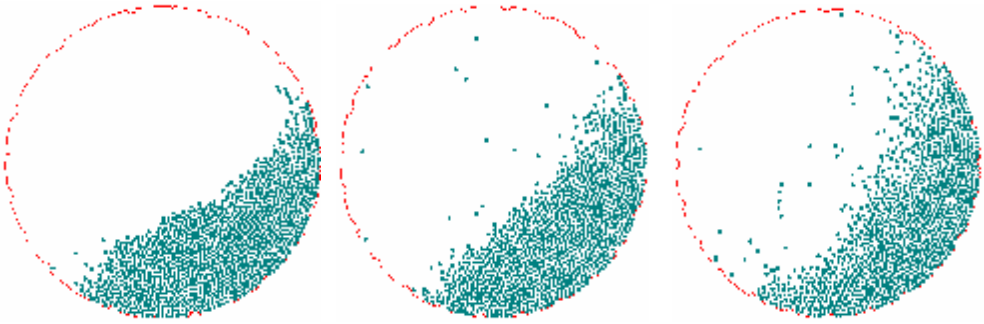

(g) %J=30, N_c =30 (h) %J=30, N_c =50 (i) %J=30, N_c =80

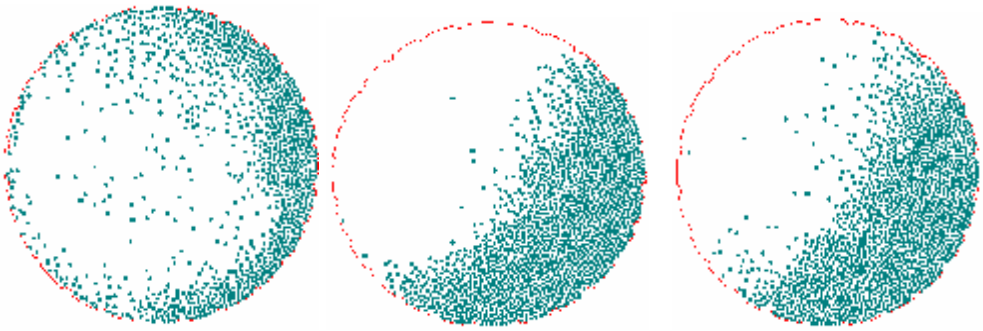

(j) %J=30, N_c =120 (k) %J=40, N_c =75 (l) %J=40, N_c =85

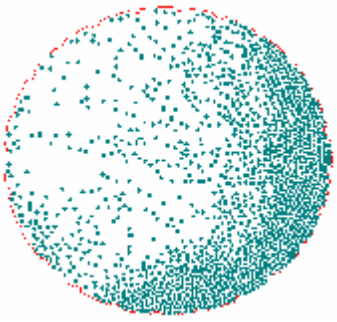

(m) %J=40, N_c =105

Figure 7.6: Behaviour of the load from DEM simulations at varying mill conditions

DEM simulations are presented and the results were analyzed from the Frames. The ball velocities and an approximate number of balls in contact with the air and balls in contact with the metal surface obtained from the simulations are shown in

Table 7.1 and 7.2 respectively. The total numbers of balls in the 2D are also presented in Table 7.3.

It can be observed from Table 7.2 below that as the mill speed increases, the number of balls being thrown off the load (cataracting) increases. This is evident from the DEM simulations in Figure 7.6. The effective heat transfer area is also higher for balls in air as compared to the point contact of the ball to liner surface. At 120% of the critical speed, due to centrifuging, the number of balls in contact with the liners increases appreciably. Difficulties arise in determining the actual number of balls particularly in the case of the balls in contact with the air above the load. The number of balls in contact with the air is more than that in contact with the liner surface.

The ball size distribution available in our pilot mill room and used in the experiments were 6 - 10 and 20mm. 20mm balls sizes were added at higher load volumes since the 6 – 10mm balls only amounted to a load volume of 20%. The 10mm steel ball however constituted about 80% of the load even at higher load volumes. The diameter of the ball used in the DEM simulations was 10mm. Only one ball size distribution of 10mm was used in the simulations. This is because there is poor packing of particles when balls of different sizes are used in the simulations.

Figure 7.7 below shows an example of a profile of a cataracting ball in the grinding mill. The average ball velocities were taken from point A to B as shown in Figure 7.7. The velocities are measured in units of m/s where as the heat transfer coefficients are in W/m^2K.

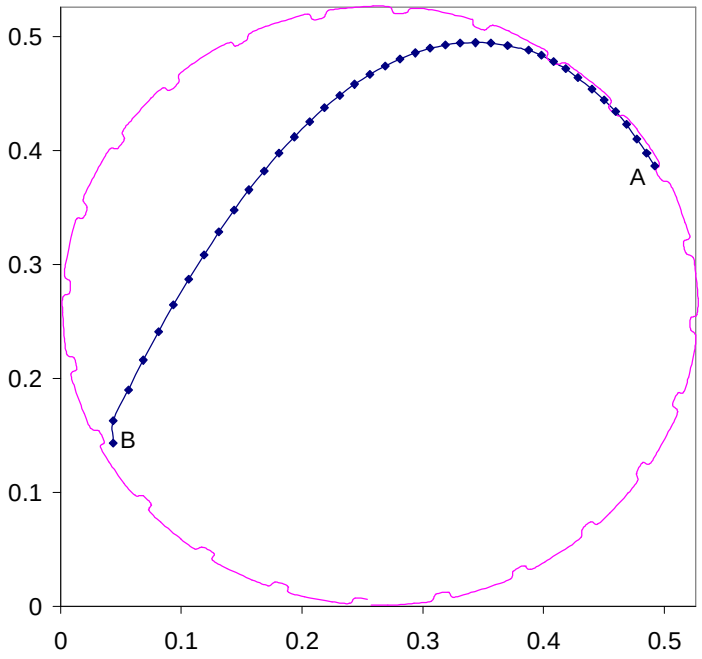

Figure 7.7: Profile of a cataracting ball in a grinding mill.

Table 7.1: Table of DEM velocities and the corresponding values of the heat transfer coefficients from the ball to the air at various mill conditions

Condition	DEM velocities	$h_{ball\text{-}air}$
J20N65	0.846	68.69
J20N75	0.833	68.38
J20N95	1.633	89.22
J20N105	1.660	89.94
J25N75	1.142	76.43
J25N95	1.623	88.96
J30N50	0.616	62.71
J30N80	1.407	83.32
J40N75	1.707	91.16
J40N85	1.011	73.01
J40N105	1.479	85.21

Table 7.2: Number of balls in contact with the air and liner surface from 2D DEM Simulations at varying mill conditions

Load Vol. J(%)	Mill Speed Nc (%)	Ball to liner contact	Ball to air contact
20	65	74	87
20	75	90	115
20	95	94	130
20	105	116	153
25	75	80	120
25	95	119	156
30	50	86	82
30	80	103	140
40	75	106	139
40	85	115	214
40	105	143	265

Table 7.3: Approximate total number of balls in a 2D and 3D Mill

	%J=20	%J=25	%J=30	%J40
Total number of balls in mill from 2D DEM	679	848	1018	1357
Total number of balls in a 3D mill	22000	26796	32155	42873

In order to have an estimate of the total numbers of balls at various mill conditions in a 3D mill as was used in the experiments, the following relationship given in the following equation was used.

$$No_{3D} = No_{2D} \times \frac{No_{(TOTAL)3D}}{No_{(TOTAL)2D}} \tag{7.4}$$

$$No_{(Total)3D} = (Total\ mass\ of\ balls)/(mass\ of\ one\ ball) \tag{7.5}$$

This was necessary as it would be possible to estimate the total number of balls in contact with the air above the load in a 3D mill. The total number of balls from

2D simulations ($No_{(TOTAL)2D}$) were obtained from 2D DEM simulations. The balls that were cataracting and those balls in contact with the region of the air above the load were considered for the ball to air contact.

The product of the heat transfer coefficient for the load to air with the area then obtained from the following relationship:

$$hA_{(LD-AIR)} = h_{(Ball-Air)} \times No_{(ball-air)2D} xArea_{(10\,mmBalls)} \times \frac{No_{(TOTAL)3D}}{No_{(TOTAL)2D}} \qquad (7.6)$$

Equation (7.6) is used to estimate the product of the heat transfer coefficient with its area for the ball to air at various mill conditions.

Since Q_{ext} and $hA_{(LD-AIR)}$ are known, $hA_{(LD-L)}$ and $hA_{(AIR-L)}$ are evaluated from the following steady state energy balance models:

$$Q_{ext} = hA_{(LD-L)}(T_{LD} - T_L) + hA_{(LD-AIR)}(T_{LD} - T_{AIR}) \qquad (7.7)$$

$$hA_{(LD-AIR)}(T_{LD} - T_{AIR}) = hA_{(AIR-L)}(T_{AIR} - T_L) \qquad (7.8)$$

The values of $hA_{(LD-AIR)}$, $hA_{(AIR-L)}$, $hA_{(LD-L)}$, h_{ext} and U_{ext} are given in Table 7.4 below. The external heat transfer area A_{ext} is known.

Table 7.4: Experimental and model values of $hA_{(LD-AIR)}$, $hA_{(AIR-L)}$, $hA_{(LD-L)}$, h_{ext} and U_{ext} at various mill conditions

Nc	J	$hA_{(LD-L)}$		$hA_{(LD-AIR)}$		$hA_{(AIR-L)}$		h_{ext}		U_{ext}	
		Exptal	Model	Exptal	Model	Exptal	Model	Exptal	Model	Exptal	Model
0.5	0.3	22.1	22.3	51.0	51.4	51.3	48.9	22.9	22.6	14.4	14.9
0.65	0.20	23.3	23.0	60.8	61.5	53.9	55.9	24.1	26.1	16.0	16.1
0.75	0.20	24.7	24.5	80.0	78.7	67.0	68.8	27.1	28.2	17.6	17.3
0.75	0.25	25.9	25.6	91.0	91.5	78.9	78.9	29.0	28.2	18.5	17.8
0.75	0.40	28.0	28.1	125.7	125.5	107.0	105.1	28.4	28.2	19.0	18.6
0.8	0.30	27.7	27.3	116.4	115.5	95.7	96.9	31.2	29.2	19.8	18.6
0.85	0.40	29.0	29.7	155.0	155.6	123.5	126.1	32.8	30.2	20.1	19.6
0.95	0.20	26.7	27.1	118.0	118.2	100.0	97.1	30.5	32.1	17.9	19.3
0.95	0.25	28.2	28.4	137.7	137.4	112.5	111.3	30.9	32.1	19.7	19.8
1.05	0.20	28.2	28.3	140.0	140.5	110.0	112.3	32.7	33.9	19.7	20.2
1.05	0.40	33.0	32.5	224.0	223.9	172	171.5	35.4	33.9	21.1	21.4

The values of $hA_{(ext)}$ were obtained from the relationship: $Q_{ext} = hA_{(ext)}(T_{S2} - T_{Amb})$. The rate of thermal energy Q_{ext} is equal to the power P at steady state as the rate of energy conversion into sound is insignificant. The experimental $UA_{(ext)}$ is also evaluated from the energy balance equation. The product of the inside heat transfer coefficients with their areas were modeled individually using equations (3.17), (3.18) and (3.19) of chapter 3 by fitting these models to the experimental data in a least squares sense. The values of *a*, *b*, *c*, *d*, *y*, *z*, k_1, k_2 and k_3 were estimated from the models. The external heat transfer coefficient was also modeled and the values of $\bar{h}_{ext}$ and *x* were estimated. The values of the various coefficients for both experimental and models are tabulated in Table 7.4 above.

The following relative standard deviation was used in an assessment of the goodness of fit of the model to the experimental data.

$$s\,(\%) = \frac{\left[\sum \left(X_{\mathrm{mod}} - X_{\exp}\right)^2 /(^oF)\right]^{0.5}}{X_{Avr,\exp}} x100\% \qquad (7.9)$$

where: ${}^{o}F$ = the number of degrees of freedom = number of experiments – number of parameters. X is the variable under consideration. $X_{Avr,\exp}$, is the average value for the experimental values.

The heat transfer coefficient models with their estimated parameters are now written as.

$$hA_{(LD-AIR)} = k_1 f^a J^b = 381 f^{1.72} J^{0.67} \quad (7.10)$$

$$hA_{(AIR-L)} = k_2 f^c J^d = 279.7 f^{1.45} J^{0.61} \quad (7.11)$$

$$hA_{(LD-L)} = k_3 f^y J^z = 38.1 f^{0.43} J^{0.2} \quad (7.12)$$

$$h_{ext} = A_{ext}\ \bar{h}_{ext}\ f^x = 25.2 f^{0.55} \quad (7.13)$$

The following standard deviation values were obtained for the above models: $hA_{(LD-AIR)}: s = 0.8\%$, $hA_{(AIR-L)}: s = 2.7\%$, $hA_{(LD-L)}: s = 0.9\%$,

And $h_{ext}: s = 5.0\%$.

The model for the overall heat transfer coefficient can then be given by the following:

$$\frac{1}{UA_{(ext)}} = \frac{381 f^{1.72} J^{0.67} + 279.7 f^{1.45} J^{0.61}}{\left[\left(38.1 f^{0.43} J^{0.2} \times 381 f^{1.72} J^{0.67}\right) + \left(\begin{matrix}\left(38.1 f^{0.43} J^{0.2} \times 279.7 f^{1.45} J^{0.61}\right) + \\ \left(279.7 f^{1.45} J^{0.61} \times 381 f^{1.72} J^{0.61}\right)\end{matrix}\right)\right]} + \frac{1}{25.2 f^{0.55}} + 0.021 \quad (7.14)$$

In order to simplify equation 7.14 we explored whether the first term of the right hand side of equation 7.14 can be represented by a simpler model given by:

$$R_{par} = \frac{1}{Kj^{a}J^{b}} \tag{7.15}$$

The parameters *K*, *a* and *b* are found by fitting equation 7.15 to the data from the first term of the right hand side of equation 7.14 with +/- 3.8% standard deviation. The values of *K*, *a* and *b* have been found to be 123, 1.07 and 0.27 respectively. The model then becomes:

$$\frac{1}{UA_{(ext)}} = \frac{1}{123.4f^{1.07}J^{0.27}} + \frac{1}{25.2f^{0.545}} + 0.021 \tag{7.16}$$

The graphs of model and experimental values of $hA_{(LD-L)}$, $hA_{(LD-AIR)}$, $hA_{(AIR-L)}$ and h_{ext} are shown in Figures 7.8, 7.9, 7.10 and 7.11 respectively below:

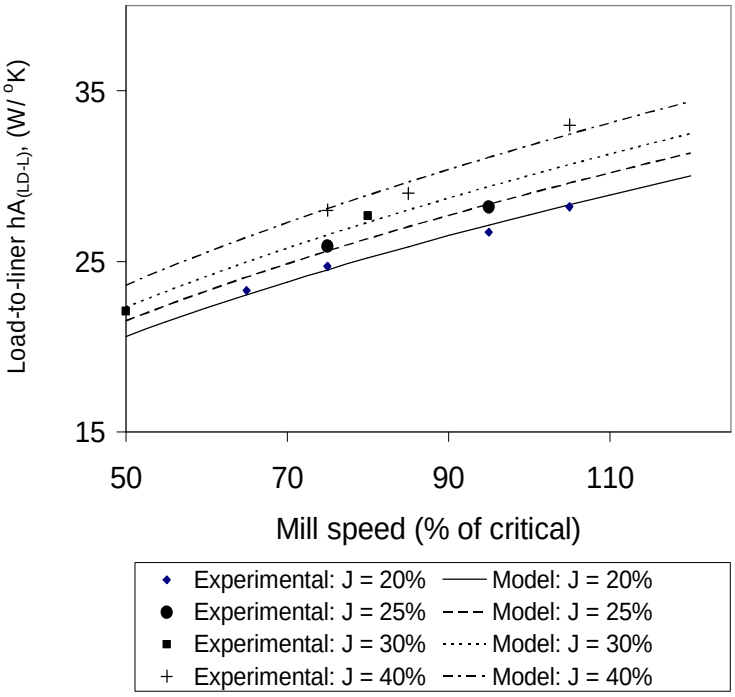

Figure 7.8: Variation of model and experimental values of $hA_{(LD-L)}$ with mill speed

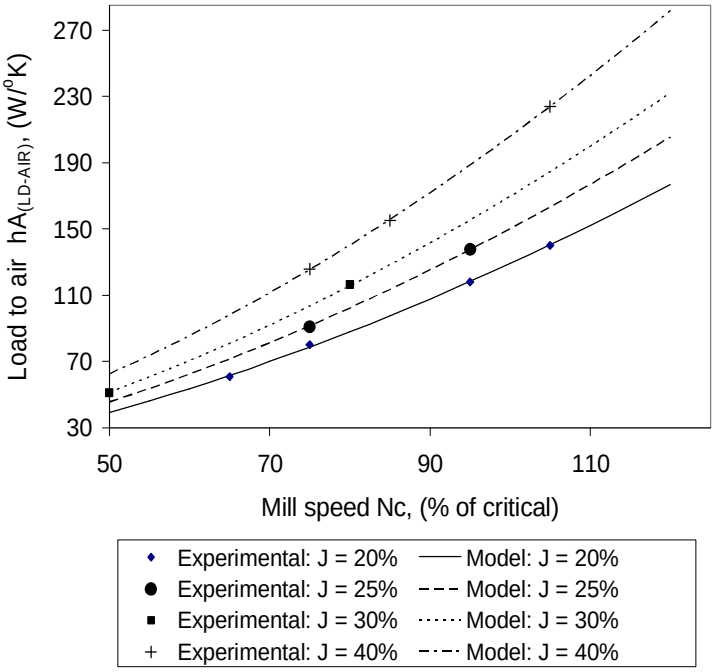

Figure 7.9: Variation of model and experimental values of $hA_{(LD-AIR)}$ with mill speed

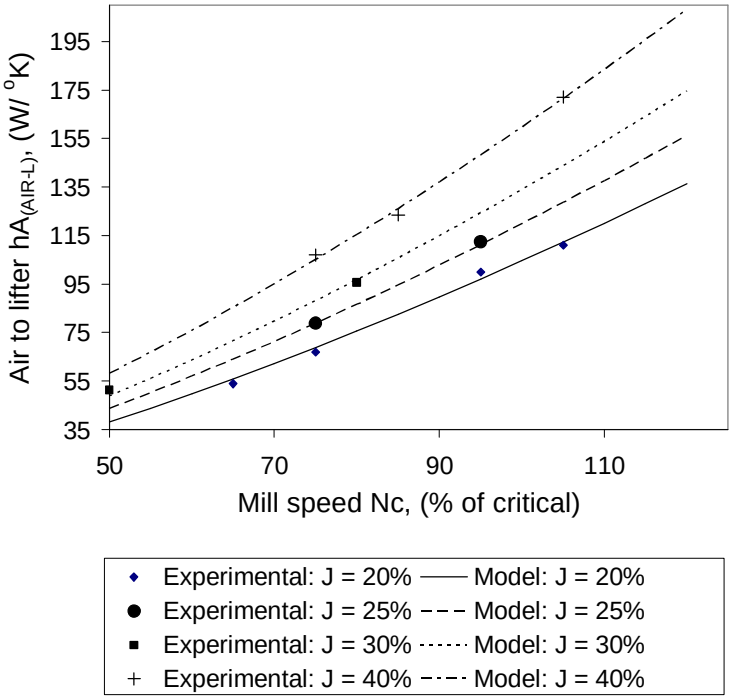

Figure 7.10: Variation of model and experimental values of $hA_{(AIR-L)}$ with mill speed

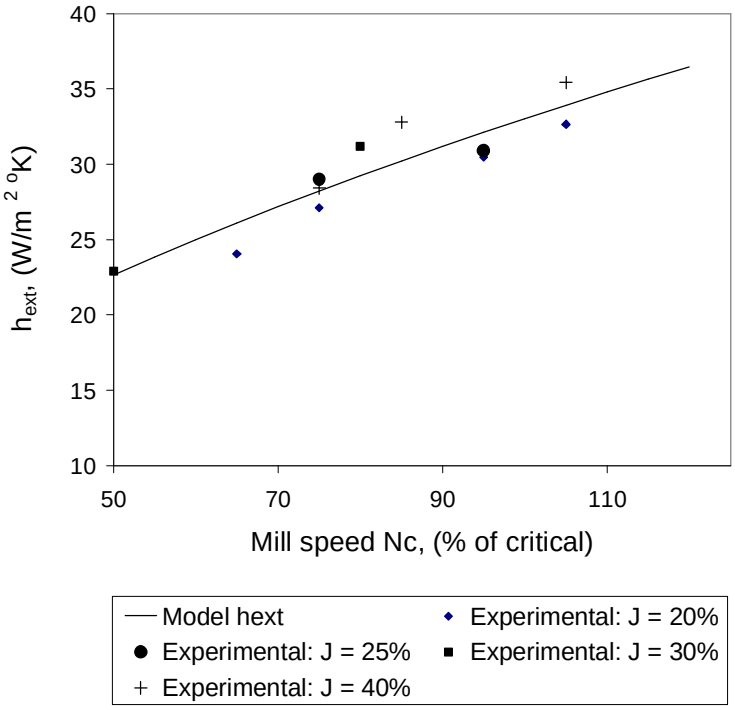

Figure 7.11: Variation of model and experimental values of h_{ext} with mill speed

The models employed in the computation of the energy from the load and air above the load is given in equations (3.4), (3.5) and (3.6) of chapter 3 using the heat transfer coefficients obtained from equation (7.6), (7.7) and (7.8). It can be observed from the results that more energy passes from the load to the air above the load to the liner as compared from the load directly to the lifter path way. These values are given in Appendix F.

Ideally at steady state, $Q_{LD\text{-}AIR} = Q_{AIR\text{-}L}$

In addition, at steady state,

$$Q_{LD\text{-}L} + Q_{A\text{-}L} = Q_L = Q_g = Q_S = Q_{ext} \tag{7.17}$$

The overall heat transfer coefficient can thus be calculated as:

$$Q_{ext} = UA_{(ext)}\left(T_{LD} - T_{Amb}\right) \tag{7.18}$$

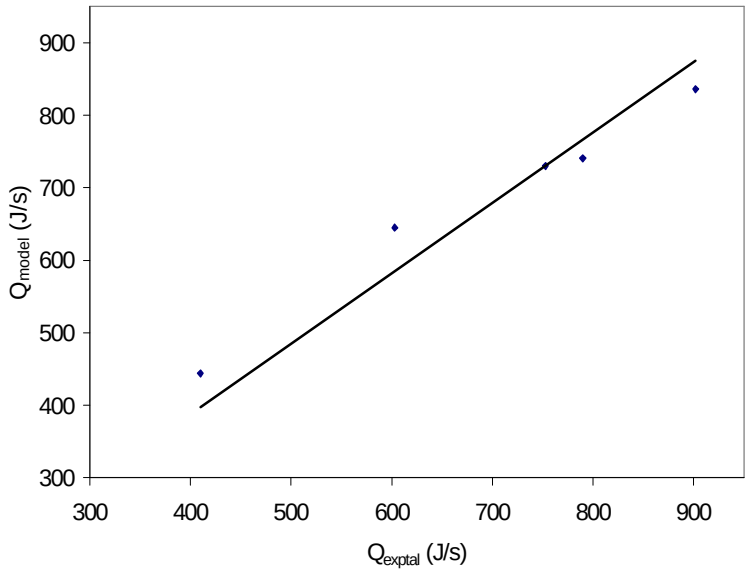

Figure 7.12: Variation of model with various measured rates of energy loss from the grinding mill (Q_{ext})

The steady state measured temperatures for various mill process temperatures were also plotted against the model values as shown in Figure 7.13 below

The maximum % deviation of model from experiment is 9.9 % for Q_{ext} .

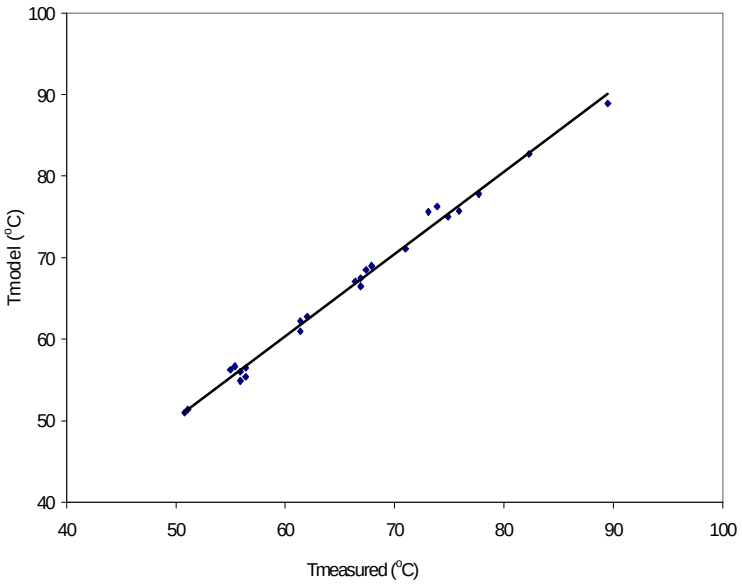

Figure 7.13: Variation of measured with model steady state temperature values

7.3.3 Validation of the overall heat transfer model

Steady state results were analyzed to determine estimates of the overall heat transfer coefficient quantified under varying mill conditions. The experimental and model values for the overall heat transfer coefficients from the energy balance at steady state at various mill speeds and mill load volumes are plotted as given in Figure 7.14. U values obtained in this work range from 14.4 to 21.1W/m^2K.

The overall heat transfer coefficient values are functions of the mill speed, the load volume and the design of the mill liners and shell. Figure 7.14 shows a comparison of model and experimental values of the overall heat transfer coefficient at varying mill speeds. The model values were obtained by fitting the model to the experimental data. The value of the power x obtained in this work has been found to be equal to 0.55. This value compares quite well with the theoretical value of 0.6 to 0.8. Results show that increasing the speed of the mill will increase the overall heat transfer coefficient. It has also been found from the analysis that a large proportion (approximately 55-70%) of the energy is transferred from the load to the liner surface via the air above the load, as compared to the direct load to liner surface path. The heat transfer coefficient from the load to the air above the load is also higher than from the load to the liner surface. This increases as the speed of the mill is increased.

The temperature of the load for the first set of experiments involving load volumes of 20 and 25% was estimated using the heat transfer coefficients obtained from equation (7.6) and the measurement of the temperature of the air above the load. The overall heat transfer coefficients were then obtained for these measurements.

The outside heat transfer coefficient is governed by forced convection due to the speed of the mill and is independent of the mill filling. It can be observed that there is considerable temperature drop at the outside surface of the mill shell as can be seen from the temperature profiles. The inside heat transfer coefficient is a function of both load volume and mill speed. The mill liners and shell offer very

little resistance to the flow of energy. These have a high thermal conductivity. Most of the temperature drop in the mill wall occurs across the air-gap between the liners and mill shell as can be seen from the temperature profiles (Figures 7.1 and 7.2). This is expected as air has a very low thermal conductivity.

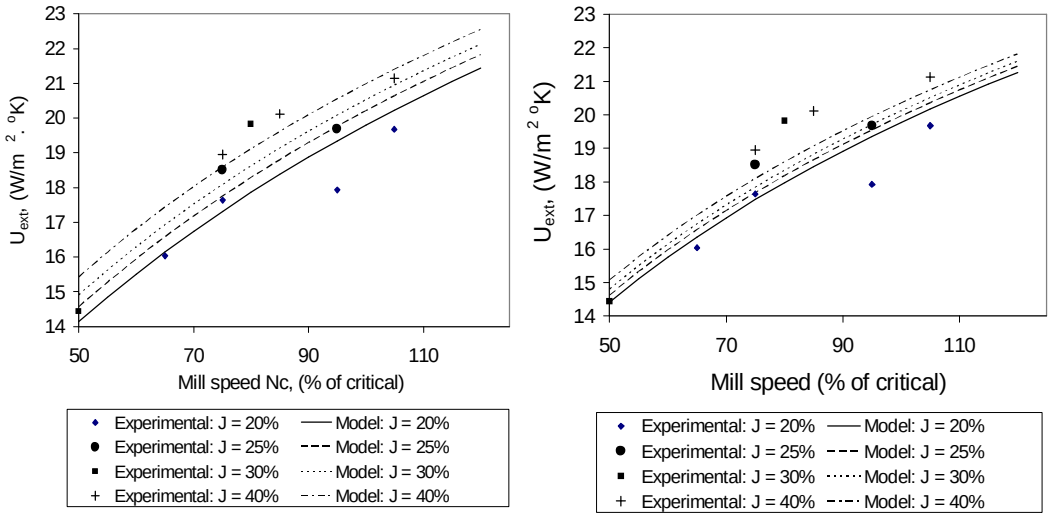

(a) Model equation 7.14 (b) Model equation 7.16

Figure 7.14: Variation of the overall heat transfer coefficient with mill speed

It can be seen from the two graphs that model equations 7.14 and 7.16 are essentially the same. However, equation 7.14 shows a higher increase of U with load volume than equation 7.16. The model generally predicts a very small change in the overall heat transfer coefficient with load volume. The maximum % deviation of model from the experiment is 8% for a load volume of 20% at a mill speed of 95% of the critical.

7.4 Conclusions

The overall heat transfer coefficient has been found to be a function of mill operating conditions, namely, the mill speed, the load volume and the mill liner/shell design. Results show that increasing the speed of the mill will increase the overall heat transfer coefficient. It is anticipated that improved understanding

of temperature behaviour via an energy balance methodology in a milling circuit can be used to control grinding mills. The control can be done by incorporating the energy balance model for the mill into a computer program for process simulation. Due to time constraints of this MSc however, we restricted ourselves to process measurements and model development. Control based on this approach should provide substantial benefits, as temperature measurements can be done cheaply and very accurately, providing reliable information about mill dynamics via an energy balance model for the mill.

Chapter 8

Conclusions and Recommendations

8.1 Introduction

This chapter presents a summary of the findings of the work described in this thesis and the recommendations for further work.

8.2 Summary

In this thesis, the behaviour of temperature in the grinding mill is obtained from an energy balance methodology. A lot of work has been done using mass balances in milling circuits with important measurements being the flow rate and density of the ore stream. In the energy balance methodology, key measurements are the mill process temperatures (load, air above load, liners and mill shell), ambient temperature and mill power. The method employed and experimental work conducted is rigorous and novel. The benefits of energy modeling, compared to mass modeling, are that energy data are more accurately measurable than mass data. The temperature probes are also relatively cheap, easier to calibrate, and are cheaper to maintain, as compared to the flow and density instrumentation used in the mass balances. The use of the energy balance allows one to eliminate (or reduce dependency on) one flowrate measurement.

8.3 Overall findings

Much of the energy consumed in milling is transformed into heat or thermal energy. This is evidenced by a rise in the mill process temperatures; these being the temperatures of the load, the air above the load, the liners and the shell. The temperature rise is affected mainly by the speed of the mill and the volume or mass of the load contained in the grinding mill. Most of this energy is lost as heat from the mill shell, hence the need to model this energy loss.

The behaviour of the balls at different mill speeds and mill fillings and its effect on mill process temperatures and the overall heat transfer coefficient has been studied. The overall heat transfer coefficients at various mill operating conditions

have been quantified from the energy balance models. A model for the overall heat transfer coefficient has been developed. This makes it possible to estimate the energy loss from the mill. This study shows that the overall heat transfer coefficient is a function of mill operating conditions, namely, the mill speed, the load volume and the mill liner/lifter design.

Considerable effort and time has been spent on the formulation of the models and their solutions. This work is an attempt to shed some light on temperature measurement and modeling in grinding mills. It can be stated that the work done in this thesis has made a considerable contribution in the application of the energy balance, particularly in understanding of temperature behaviour in milling as well as use of energy transfer models to determine useful parameters. There is therefore need to take this work further.

8.4 Recommendations for further work

The heat transfer coefficients in the inside of the mill can only be determined upon knowledge of the respective heat transfer areas. These require careful analysis of the particle contact between the particle to air and particle to liner. It is recommended for further work that the heat transfer area A_{LD-L} be determined in order to have accurate knowledge of the inside heat transfer coefficients. For the sake of simulating mills of different sizes, it is recommended that the models for the heat transfer coefficients be written in terms of dimensionless numbers e.g. Reynold's number (*Re*), Nusselt number (*Nu*) and the Prandtl number (*Pr*) in order to explore scale up of this data. Of particular interest is the presentation of the fractional load volume in terms of the Reynold's number.

In this thesis, a non-transparent front plate was employed, and therefore particle motion was not observed at each mill conditions set. DEM simulations were therefore performed using Mill soft Software to predict the behaviour of the load at different mill conditions using the same conditions as in the experiments. It is therefore recommended for further research that the trajectory or motion of the load be observed by using a transparent front plate and then taking the pictures.

The results from the pictures can then be compared to the simulation results using the same conditions as in the experiment. It is further recommended for future work that the analysis be focused on the solutions for the dynamic models and therefore the dynamic state of the system. In this study the dynamic models for temperature behaviour in the mill have been formulated and the solution procedure has been given in Appendix D although this work is not relevant in this research. The analysis can be done by either analytical or numerical methods.

The work was based on a batch pilot plant grinding mill. Power supplied to the mill was considered as the only source of energy going into the mill. Thermal energy loss through the mill shell was considered as the only transfer of energy out of the mill as sound energy was found to be insignificant. In the case of a continuous mill with open ends and feed/discharge streams, the temperature of the feed stream as well as of the discharge stream have to be considered and incorporated into the energy balance in addition to the energy of the cyclone underflow stream which is returned to the mill inlet.

The work done in this thesis comprised of models in 2-dimensions. The mill used is a small batch mill. Therefore the axial temperature change was expected to be very small or negligible. No measurements to verify this were made though. It is therefore recommended for future work that the axial temperature be considered.

Finally the work involved measurement and modelling of temperature in the grinding mill. No control of the mill using temperature measurements and the energy balance was done. However the energy balance model for the mill can be incorporated into a computer program for process simulation and this is therefore recommended for future work. Due to the time limit of this MSc program, mill control using the energy balance could not be done. The importance of this work however is that it has brought to light important information concerning temperature measurement and modelling and the importance of the energy balance in milling. The work will therefore provide reliable information about mill dynamics via an energy balance model for the mill.

REFERENCES

REFERENCES

Radziszewski, P., 1999. Fundamental batch mill model identification, Minerals Engineering, Vol. 12, No. 7, pp 809 – 826.

Stamboliadis, E. Th., 2002. A contribution to the relationship of energy and particle size in the comminution of brittle particulate materials, Minerals Engineering, Vol. 15, pp 707 – 713.

Fuerstenau, D.W., 1999. The effect of ball size on the energy efficiency of Hybrid high-pressure roll mill/ball mill grinding, Powder Technology, Vol. 105, pp 199 – 204.

Tavares, L.M., and King, R.P., 1998. Single-particle fracture under impact loading. International Journal of Mineral Processing, Vol. 54, pp 1 – 28.

Stairmand, C.J., 1975. The energy efficiency of milling processes. Zerkleinern, Dechema Monogr, Volume 79/1549, pp1-17

Herbst, J.A., Pate, W.T., and Oblad, A.E., 1989. Experience in the use of Model Based Control Systems in Autogenous and Semi Autogenous Grinding Circuits. In: SAG 1989. UBC. Vancouver, B.C., Canada. Pp. 669 – 689. First International Conference on: Autogenous and Semiautogenous Grinding Technology.

Serbog, D.E., Edgar, T.F., and Mellichamp, D.A., 1989. Process Dynamics and Control. John Wiley and Sons, Inc.

Herbst, J.A., Pate.W.T., and Oblad, A.E., 1992. Model-based control of mineral processing operations, Powder Technology, Vol. 69, pp21-22.

Incropera, P. I., and Dewitt, P.D., 2002. Introduction to heat Transfer. John Wiley and Sons. pp 13-16.

Van Drunick, W.I., and Moys, M.H., 2002. The use of an energy balance to measure and control the rheology of mill discharge slurry. 2001 SAG conference, Vancouver B.C. Volume II of IV, ISBN 0-88865-794-3, pp304-316.

Van Drunick, W.I., and Moys, M.H., 2003. Online process modeling for SAG mill control using temperature measurements, energy balancing and inferential parameter estimation. 2003 International Mineral Processing Conference.

Austin, L.G., Klimpel, R.R., and Luckie, P.T., 1984. Process Engineering of Size Reduction: Ball Milling, AIME, New York, NY.

Liddell, K.S., and Moys, M,H., (1988). The effect of mill speed and filling on the behaviour of the load in a rotary grinding mill. Journal of South African Institute of Mining and Metallurgy, Vol. 88, no. 2. pp 49 – 57.

Taggart, A.F., 1927. The Handbook of Ore Dressing. School of Mines, Columbia University, John Wiley and Sons Inc.

Moys, M.H., and Skorupa, J., 1992. Measurement of the forces exerted by the load on a liner in a ball mill as a function of liner profile, load volume and mill speed. International Journal of Mineral Processing, Vol. 37, pp 239 – 256.

Van Nierop, M.A., and Moys, M.H., 2001. Axial mixing of slurry in an autogenous grinding mill. International Journal of Mineral Processing. Vol. 65(2002) pp151-164.

Van Nierop, M. A., and Moys, M. H., 1996. Measurement of load behaviour in an industrial grinding mill. Control Engineering Practice, Vol. 5, No. 2, pp 257-262.

Kawatra, S.K., and Eisele. T.C., 1998. Rheological effects in grinding circuits, International Journal of Mineral Processing. No22, pp251-256.

Fuerstenau, D.W., and Abouzeid, A.-Z.M., 2002. The energy efficiency of ball milling in comminution. International Journal of Mineral Processing, Vol. 67, pp 161 – 185.

Zhang, D., and Whiten, W.J., (1996). The Calculation of contact forces between particles using spring and damping models. JKMRC, University of Queensland, Australia.

Cleary, P.W., (2001). Recent Advances in DEM Modeling of Tumbling Mills. Minerals Engineering, Vol. 14, No. 10, pp 1295 – 1319.

Thomas, L.C., 1980. Fundamentals of Heat Transfer, pp12-20.

Coulson, J.M., and Richardson, J.F., 1999. Chemical Engineering Volume 1, Sixth Edition. Fluid Flow, Heat Transfer and Mass Transfer, pp 414 – 416.

Vreedenberg, H.A., 1958. Chemical Engineering Science Volume 9, pp 52 – 60.

Chen, J.C., Grace, J.R., and Golriz, M.R., 2005. Heat transfer in fluidized beds: design methods. Powder Technology, Volume 150, pp 123 – 132.

Coulson, J.M., and Richardson, J.F., 1991. Chemical Engineering Volume 2, Fourth Edition pp 254.

Schack, A., 1965. Industrial Heat Transfer- Practical and Theoretical with basic numerical examples, pp22-24.

Perry., 1973. A Handbook of Chemical Engineering.

Szekely, J., Evans, J.W., and Brimacombe, J.K., 1988. The mathematical and physical modeling of primary metals processing operations. New York: J. Wiley.

Steinhart, J.S., and Hart, S.R., (1968). Calibration curves for the thermistors. Deep-Sea Research, 15, pp 497.

Rajamani, R. K., Songfack, P., Mishra, B.K., Venugopal, R., (1996)/ MillSoft User's Guide Version 1.1, Center For Mineral Technology, 306 WBB, University of Utah, Salt Lake City, UT 84112, USA.

APPENDICES

Appendices

APPENDIX A

Calibration of the Temperature probes: Calibration Equations and Constants

The calibration equation for the temperature probes was obtained from the Steinhart and Hart (1968) equation given by:

$$T = \frac{1}{a + b(\ln R_T) + c(\ln R_T)^3} \qquad \text{(A1)}$$

This equation was used to relate temperature to resistance for the thermistors. a, b and c are constants which are estimated from three measurements of R_T at known temperatures in the range of interest.

From equation (1),

T is the body temperature of the thermistor in ^oK

R_T is the resistance of the thermistor at a temperature T

From the circuit diagram given in section 4.3, the output voltage is given by:

$$V_{out} = V_{in}\left(\frac{1}{1 + R/R_T}\right) \qquad \text{(A2)}$$

The input voltage employed was 12.76V and the fixed series resistor was 100kΩ. The values of the output voltage V_{out} are obtained from the readings from the computer. R_T is easily computed from equation (A2). Once R_T is known, the temperature of the thermistor is obtained from equation (A1).

The circuit was arranged in such a way that temperature channels on the computer indicated almost same output voltages. The thermistor employed has a resistance of 10kΩ at 25^{o}C. To determine the constants a, b and c from experimental measurements, three sets of values of temperature and resistance were obtained.

The values were:

Table A1: Temperature versus Resistance values for the Bead Thermistor

T(^{o}C)	R(Ω)
25	10,000
40	5327
70	1752

Using these values, the three equations in a, b and c is as follows:

$$\frac{1}{298} = a + b\ln(10{,}000) + c(\ln(10{,}000))^3$$

$$\frac{1}{313} = a + b\ln(5{,}327) + c(\ln(5{,}327))^3$$

$$\frac{1}{343} = a + b\ln(1{,}752) + c\ln(\ln(1{,}752))^3$$

This set of simultaneous linear equations can be solved for a, b and c. The values computed for a, b and c is as follows:

$a = 0.001$

$b = 0.000258$, and

$c = -7.76 * 10^{-9}$

Using these values, the temperature from a resistance measurement can be obtained from the following relationship:

$$T^{-1} = 0.00098 + 0.000258\ln(R_T) - 7.76*10^{-9}(\ln(R_T))^3$$

Table A2: Resistance-Temperature characteristics for the thermistors from manufacturer's data and the calculated temperature data

R(Ω)	19900	12490	10000	8057	5327	3603	2488	1752	1255	915.3	678
T(^{o}C)	10	20	25	30	40	50	60	70	80	90	100
T(Calc.)	10.6	20.5	25.5	30.5	40.6	50.8	61	71.4	81.9	92.4	103

The third row represents the calculated temperatures using the calibration equation and constants. The maximum deviation of the calculated from the manufactures temperature data is 5.8% at a resistance of 19900Ω, and the minimum is 1.5% at R=5327Ω. In this work however, the maximum temperature reached was around 88^{o}C.

Calculation of Thermistor Self heating

To obtain the self heating of the thermistors, the following information was available.

(1) R vs. T curve for the thermistor
(2) Dissipation constant (the amount of power it takes a thermistor to raise 1^{o}C). The dissipation constant used in still air was 1mW/^{o}C. The maximum power rating for the thermistor is 0.075W.
(3) Applied voltage

The divider resistance was 94kΩ as shown in Figure 4.2 of chapter 4, and the voltage input was 12.6V. The R vs. T for the thermistor is as shown in Table A2 above. The following procedure is employed to determine the amount of self heating:

(1) First we use the Ohm's Law (V=IR) to determine voltage drop across the thermistor

(2) The next step is to determine the power applied to the thermistor using the equation, $P = \frac{V^2}{R}$. At this point we have to check to be sure that we are not exceeding the power rating of the thermistor which is 0.075W. If the power applied to the thermistor is higher than the maximum power rating, then self heating of the thermistor will occur.

(3) The power applied to the thermistor is known, P_T. The dissipation constant is then used (D_C=1mW/^oC) is now used to figure self heat, using the relationship:

Self heat, $T = \frac{P_T}{D_C}$, (at any temperature)

where:

R_T is the resistance of the thermistor at any given temperature

R is the resistance of the fixed series resistor

V_T is the voltage drop across the resistor, and

I_T is the current passing through the thermistor

P_T is the power applied to the thermistor

Table A3 below shows the calculation of the self heat

Table A3: Calculation of Power applied to the thermistor and the thermistor self heat

T	Therm. R R_T	Fixed series R R	Total R R_T+R	Ohm's Law:V_{in}=12.6 $I_T=Vin/(R_T+R)$	Voltage Drop $V_T=I_T*R_T$	Power applied $P_T=V^2/R_T$	Self Heat $T=P_T/D_C$ (^oC)
20	12490	94000	106490	0.000118	1.478	0.000175	0.17
25	10000	94000	104000	0.000121	1.212	0.000147	0.15
30	8057	94000	102057	0.000123	0.995	0.000123	0.12
40	5327	94000	99327	0.000127	0.676	0.000086	0.09
50	3603	94000	97603	0.000129	0.465	0.000060	0.06
60	2488	94000	96488	0.000131	0.325	0.000042	0.04
70	1752	94000	95752	0.000132	0.231	0.000030	0.03
80	1255	94000	95255	0.000132	0.166	0.000022	0.02
90	915.3	94000	94915.3	0.000133	0.122	0.000016	0.02

An average value of 0.08^{o}C for the self-heating of the thermistor was obtained in the given range.

APPENDIX B

Torque calibration

The following table presents the results obtained from the calibration of the torque load beam.

Table B1: Calibration of the Torque load beam

Mass of Objects	Mass (Kg)	Force (N)	Distance (m)	Torq (Nm)	Voltage (V)
No load	0	0	0.569	0	3.64
Mass of container (Ctn)	0.23	2.3	0.569	1.3087	3.57
Contaner+ M1	2.42	24.2	0.569	13.7698	2.93
Ctn+M1 + M2	4.62	46.2	0.569	26.2878	2.31
Ctn+M1 + M2+M3	6.825	68.25	0.569	38.83425	1.68
Ctn+M1+M2+M3+M4	9.02	90.2	0.569	51.3238	1.05
Ctn+M1+M2+M3+M4+M5	11.21	112.1	0.569	63.7849	0.413
Ctn+M1+M2+M3+M4+M5+M6	13.395	133.95	0.569	76.21755	-0.204
Ctn+M1+M2+M3+M4+M5+M6+M7	15.56	155.6	0.569	88.5364	-0.72

Ctn, M1, M2, M3, M4, M5, M6 and M6 are the masses of the container, mass of load beams 1, 2, 3, 4, 5, 6 and 7.

The torque voltage relationship was achieved in this calibration. The following was the relationship:

$$T = -20.082V + 72.739$$

where:

T is the torque and V is the output voltage.

The net power *P* drawn by the mill is thus computed from the relationship:

$$P = \frac{2pNT}{60}$$

N is the speed of the mill in revolutions per minute.

APPENDIX C

Thermal properties of Substances under consideration

Specific Heat Capacities, density and thermal conductivities of Steel balls, air mild steel and cast steel

Table C1. Thermal properties of substances

Substance	Heat capacity (J/kg.K)	Thermal conductivity (W/m.K)	Density (kg/m^3)
Air	1005	0.027	1.14
Mild Steel	500	50	7800
Cast Steel	500	55	7800

APPENDIX D

Procedure for analytical solution for the dynamic model

This is a solution procedure for the dynamic model although this is not relevant to this study. The dynamic modeling equations given in chapter 3 are a set of linear, ordinary differential equations with constant coefficients, and so we expect to be able to find a general analytical solution for the dynamic response. Although it is a simple matter to solve the equations by using elementary techniques, we followed a matrix approach, which is advantageous for more complex systems such as in this study. The coefficients in the differential equations have elements that are constants but that depend on the particular steady state under investigation.

The Laplace Transform is useful in solving linear ordinary differential equations with constant coefficients. In this situation, power drawn by the mill as well as ambient temperature is assumed to be constant. The various mill process temperatures are functions of time. Therefore all the four first order linear differential equations are solved simultaneously.

The conservation of energy models are written for the important process variables; the mill power, the mill process temperatures and the environmental temperature. These conservation equations are formulated for each of the components relevant to the process. The model developed is then represented in compact matrix notation. The behaviour of the set of process variables T is described by the vector differential equation:

$$\frac{dT}{dt} = f\left(P, T, N, J, t\right) \qquad \text{(D1)}$$

Where:

P is the power drawn by the mill

T is the ambient temperature

N is the speed of the mill-% of critical speed

J is the load volume, and

t is the milling time

The dynamic models are given as follows:

$$m_{LD}C_{pLD}\frac{dT_{LD}}{dt} = P - h_{LD-AIR}A_{LD-AIR}(T_{LD} - T_{AIR}) - h_{LD-L}A_{LD-L}(T_{LD} - T_L) \qquad \text{(D2)}$$

$$m_{AIR}C_{pAIR}\frac{dT_{AIR}}{dt} = h_{LD-AIR}A_{LD-AIR}(T_{LD} - T_{AIR}) - h_{L-AIR}A_{L-AIR}(T_{AIR} - T_L) \qquad \text{(D3)}$$

$$m_L Cp_L\frac{dT_L}{dt} = h_{LD-L}A_{LD-L}(T_{LD} - T_L) + h_{L-AIR}A_{L-AIR}(T_A - T_L) - \frac{k_g A_g}{x_g}(T_L - T_S) \qquad \text{(D4)}$$

$$m_S Cp_S\frac{dT_S}{dt} = \frac{k_g A_g}{x_g}(T_L - T_S) - h_{ext}A_{ext}(T_S - T_{Amb}) \qquad \text{(D5)}$$

The coefficients of the temperatures are constants. These are evaluated at steady state and are called steady state variables. The system given above is a first order linear non homogenous system of differential equations. The system may be written as a matrix differential equation:

$$\dot{T} = AT + b \qquad \text{(D6)}$$

b is the non-homogeneous term.

By setting;

$$T = \begin{bmatrix} T_{LD} \\ T_{AIR} \\ T_L \\ T_S \end{bmatrix},\ A = \begin{bmatrix} a_{11} & a_{12} & a_{13} & a_{14} \\ a_{21} & a_{22} & a_{23} & a_{24} \\ a_{31} & a_{32} & a_{33} & a_{34} \\ a_{41} & a_{42} & a_{43} & a_{44} \end{bmatrix} \text{ and } b = \begin{bmatrix} b_1 \\ b_2 \\ b_3 \\ b_4 \end{bmatrix} \quad \text{(D7)}$$

This is called the normal form (standard form) of the non-homogeneous system. This section uses Laplace transforms to determine the temperature changes of the load, air above the load, the liners and the mill shell for the following initial temperatures:

$T_{LD}(0) = T_{LDi}$

$T_{AIR}(0) = T_{AIRi}$

$T_L(0) = T_{Li}$

$T_S(0) = T_{Si}$

The system is thus called an initial value problem. The ambient temperature and power drawn by the mill are assumed to be constant. The objective is to find the expression for the Laplace transform of each of the variables representing the temperatures of the load, air above the load, the liners and the shell in terms of the initial conditions.

The expression for the dynamic temperature behaviour in the regions under consideration is:

$$m_{LD} Cp_{LD} \frac{dT_{LD}}{dt} = P - h_{LD-AIR} A_{LD-AIR} (T_{LD} - T_{AIR}) - h_{LD-L} A_{LD-L} (T_{LD} - T_L) \quad \text{(D8)}$$

$$m_{AIR} C_{pAIR} \frac{dT_{AIR}}{dt} = h_{LD-AIR} A_{LD-AIR} (T_{LD} - T_{AIR}) - h_{L-AIR} A_{L-AIR} (T_{AIR} - T_L) \quad \text{(D9)}$$

$$m_L Cp_L \frac{dT_L(t)}{dt} = h_{LD-L} A_{LD-L} \left(T_{LD}(t) - T_L(t)\right) + h_{L-AIR} A_{L-AIR} \left(T_A - T_L\right) - \frac{k_g A_g}{x_g} \left(T_L(t) - T_S(t)\right) \quad \text{(D10)}$$

$$m_S Cp_S \frac{dT_S(t)}{dt} = \frac{k_g A_g}{x_g} \left(T_L(t) - T_S(t)\right) - h_{ext} A_{ext} \left(T_S(t) - T_{Amb}(t)\right) \quad \text{(D11)}$$

First we let $mC_{pi} = C_i$, the thermal capacitance of each of the regions i under consideration and then dividing equations (D8) to (D11) by their respective capacitances leaving only the derivative on the left side of the equation:

$$\frac{dT_{LD}}{dt} = \frac{P}{C_{LD}} - \frac{h_{LD-AIR} A_{LD-AIR}}{C_{LD}} \left(T_{LD} - T_{AIR}\right) - \frac{h_{LD-L} A_{LD-L}}{C_{LD}} \left(T_{LD} - T_L\right) \quad \text{(D12)}$$

$$\frac{dT_{AIR}}{dt} = \frac{h_{LD-AIR} A_{LD-AIR}}{C_{AIR}} \left(T_{LD} - T_{AIR}\right) - \frac{h_{AIR-L} A_{AIR-L}}{C_{AIR}} \left(T_{AIR} - T_L\right) \quad \text{(D13)}$$

$$\frac{dT_L}{dt} = \frac{h_{LD-AIR} A_{LD-AIR}}{C_L} \left(T_{LD} - T_L\right) + \frac{h_{AIR-L} A_{AIR-L}}{C_L} \left(T_{AIR} - T_L\right) - \frac{K_g A_g}{x_g C_L} \left(T_L - T_S\right) \quad \text{(D14)}$$

$$\frac{dT_S}{dt} = \frac{K_g A_g}{x_g C_S} \left(T_L - T_S\right) - \frac{h_{ext} A_{ext}}{C_S} \left(T_S - T_{Amb}\right) \quad \text{(D15)}$$

The Laplace transform relations for a variable and its first derivative are as follows:

Laplace transform of $T_{(t)} = T_{(s)}$

Laplace transform of $\frac{dT}{dt} = sT_{(S)} - T_{(0)}$

Taking the Laplace transform of the dynamic models and then combining the coefficients for each temperature variable:

$$\left(s+\frac{h_{LD-AIR}A_{LD-AIR}+h_{LD-L}A_{LD-L}}{C_{LD}}\right)T_{LD(S)}-\frac{h_{LD-AIR}A_{LD-AIR}}{C_{LD}}T_{AIR(S)}-\frac{h_{LD-L}A_{LD-L}}{C_{LD}}T_{L(S)}$$
$$=\frac{1}{C_{LD}}\frac{P}{s}+T_{LDi}$$

(D16)

$$\left(s+\frac{h_{LD-AIR}A_{LD-AIR}+h_{AIR-L}A_{AIR-L}}{C_{AIR}}\right)T_{AIR(S)}-\frac{h_{LD-AIR}A_{LD-AIR}}{C_{AIR}}T_{LD(S)}-\frac{h_{AIR-L}A_{AIR-L}}{C_{AIR}}T_{L(S)}$$
$$=T_{AIRi}$$

(D17)

$$\left(s+\frac{h_{LD-L}A_{LD-L}+h_{AIR-L}A_{AIR-L}+K_gA_g/X_g}{C_L}\right)T_{L(S)}-\frac{h_{LD-AIR}A_{LD-AIR}}{C_L}T_{LD(S)}$$
$$-\frac{h_{AIR-L}A_{AIR-L}}{C_L}T_{AIR(S)}-\frac{K_gA_g}{x_gC_L}T_{S(S)}=T_{Li}$$

(D18)

$$\left(s+\frac{K_gA_g/X_g+h_{ext}A_{ext}}{C_S}\right)T_{S(S)}-\frac{K_gA_g}{x_gC_S}T_{L(S)}=\frac{h_{ext}A_{ext}}{C_S}\frac{T_{Amb}}{s}+T_{Si} \qquad \text{(D19)}$$

The next step is to use Crammer's rule to solve the 4 simultaneous equations. To keep the mathematics organized substitution of the coefficients of $T_{LD(S)}$, $T_{AIR(S)}$, $T_{L(S)}$ and $T_{S(S)}$ is made as follows: $s+a_{11}$, a_{12}, a_{13} and a_{14} corresponding to the coefficients of $T_{LD(S)}$, $T_{AIR(S)}$, $T_{L(S)}$ and $T_{S(S)}$ respectively in the first equation: a_{21}, $s+a_{22}$, a_{23} and a_{24} corresponding to the coefficients of $T_{LD(S)}$, $T_{AIR(S)}$, $T_{L(S)}$ and $T_{S(S)}$ in the second equation: a_{31}, a_{32}, $s+a_{33}$ and a_{34} in the third equation, and finally: a_{41}, a_{42}, a_{43} and $s+a_{44}$ in the fourth equation. The equations can be written in matrix form as given below:

Next substitution is made with b_1, b_2, b_3 and b_4 for the right side of the first, second, third and fourth equations respectively. The compact notation in the

following set of equations; recalling that a_{14}, a_{24}, a_{41} and a_{42} are equal to zero and written in matrix form can be given as:

$$\begin{bmatrix} s+a_{11} & -a_{12} & -a_{13} & 0 \\ -a_{21} & s+a_{22} & -a_{23} & 0 \\ -a_{31} & -a_{32} & s+a_{33} & -a_{34} \\ 0 & 0 & -a_{43} & s+a_{44} \end{bmatrix} \begin{bmatrix} T_{LD} \\ T_{AIR} \\ T_L \\ T_S \end{bmatrix} = \begin{bmatrix} b_1 \\ b_2 \\ b_3 \\ b_4 \end{bmatrix} \text{ or simply } AT = b \qquad \text{(D20)}$$

The solution to the set of equations is written out as follows:

$$T = A^{-1} \bullet b = \frac{adj(A) \bullet b}{\det(A)} \qquad \text{(D21)}$$

The steady state models developed are of value and under consideration in this study as explained before. The parameters under consideration are evaluated at steady state conditions. The dynamic models of the process are equally important and can be used to find the optimal inputs when the objective is to minimize the variance of the outputs of a process. The work in this study is based on a batch pilot mill and therefore the dynamic behaviour of the system is not considered.

APPENDIX E

Determination of the sound energy

Sound intensity is a measure of the sound energy that passes through a given area each second. The energy per second is measured in Watts and thus intensity has units of Watts/m^2.

Sound Intensity Level

Sound intensity is measured using a logarithmic scale, the Decibel abbreviated as dB. It is used to express power but does not measure power. It is in fact a ratio of two power levels. The decibel is equal to one-tenth of a Bel. It is a measuring unit named after Alexander Graham Bel first used in Telecommunications, where signal loss is a function of the cable length.

The decibel scale defined in terms of the sound wave is given by the relation:

$$L_I = 10\log\left(\frac{I}{I_0}\right) \qquad \text{(F1)}$$

where I is the intensity of the sound wave and I_0 is the reference value. The reference value I_0 is the threshold of hearing intensity at 1000 Hz and is 10^{-12} W/m^2. This is the minimum intensity audible to a human being. The intensity decibel scale is called the sound intensity level abbreviated SIL.

Sound energy is energy transferred by waves through a material medium. The formula for sound energy is

$$S_E = I.A.t \qquad \text{(F2)}$$

S_E is measured in Joules

I is the intensity of sound measured in W/m^2

A is the area exposed to the sound energy in m^2

t is the time of exposure in s

The intensity of a sound is related to the sound‘s decibel level. To obtain the intensity of the sound (hence the energy of the sound) from the decibel level, we have to use rearrange equation F1 as follows:

$$I = I_o \log^{-1}\left(\frac{b}{10}\right) \qquad \text{(F3)}$$

In this case, the formula for sound energy becomes:

$$S_E = \left[I_o \log^{-1}\left(\frac{b}{10}\right)\right].A.t \qquad \text{(F4)}$$

Sound energy is not that “energizing”. The combined energy of an entire stadium of screaming fans could barely heat up a cup of coffee.

Sample Calculation from the measurement of sound energy

The highest sound recorded from the mill was at a mill filling of 30 and mill speed, Nc = 120%. The decibel level measured using the Sound and Vibrations Analyzer was 98 dBs. The total area of the mill from which sound was measured was $0.686m^2$. The sound energy in J/s is thus given by:

$$S_E = 10^{-12} * \log^{-1}\left(\frac{98}{10}\right) * 0.686 = 0.004 J/s$$

APPENDIX F

Table F1 shows a summary of the steady state temperature distributions at various mill conditions.

Table F1: Summary of temperatures and various energy values at steady state at various mill conditions

Load Volume	%J = 20				%J = 25		%J=30		%J = 40		
Mill speed	65%	75%	95%	105%	75%	95%	50%	80%	75%	85%	105%
	exptal	exptal	exptal	exptal	exptal	exptal	exptal	exptal	exptal	exptal	exptal
T_{LD} (^{O}C)	56.5	58.8	68.2	63.5	69.1	75	65.6	77.55	74	86.6	77.15
T_{AIR} (^{O}C)	53.0	55.4	64.9	60.6	65.6	71.9	61.3	73.1	70.55	82.4	74.7
T_{L1} (^{O}C)	49.0	51.3	60.9	56.9	61.5	66.9	57	67.7	66.5	77	71.5
T_{L2} (^{O}C)	48.7	51.2	59.6	56.3	59.8	66.5	55.9	67.1	66.4	76.6	69.4
T_{S1} (^{O}C)	44.7	47.7	52.5	49.9	54.4	57.4	50.4	56.9	55.6	62.9	56.2
T_{S2} (^{O}C)	44.6	47.5	52.2	49.7	54.1	57.3	49.8	56.5	55	62.4	55.6
Tamb (^{O}C)	20.9	21.0	20.4	21.0	27.6	26.4	23.7	19.5	24.1	22.3	24.9
Q_{LD-AIR} (J/s)	214.6	273.6	395.3	408.8	323.1	426.9	219.8	516.8	433.7	658.7	551.1
Q_{AIR-L} (J/s)	214.6	273.6	395.3	408.8	323.1	426.9	219.8	516.8	433.7	658.7	551.1
Q_{LD-L} (J/s)	175.4	185.4	194.7	186.2	205.9	228.1	190.2	273.2	169.3	243.3	201.9
Q_{ext} (J/s)	390.0	459.0	590.0	595.0	529.0	655.0	410.0	790.0	603.0	902	753.0